8
METHOD OF CHARACTERISTICS FOR COLUMN CLOSURE WATERHAMMER

Column closure waterhammer (CCWH) may occur when system voids are refilled. The filling water closes the voids and impacts stationary water. The waterhammer pressure developed by the impact is primarily dependent upon the closure velocity. Any effects that change the closure velocity will change the magnitude of the waterhammer.

There are two significant factors that can slow the velocity of the oncoming water column:

- Non-condensable gases act like a cushion as the void pressurizes and closes.
- Steam in the void that does not condense adds to the cushioning effect.

The method of characteristics (MOC) was used to evaluate column closure waterhammer events. Testing has been performed to show the reduction in closure velocity due to void cushioning effects. Input gas cushion boundary conditions for the MOC have been developed by correlating model and test results. It is concluded that the MOC can be used to model non-condensable gas and steam cushioning effects to accurately predict the peak pressure and rise times of CCWH events.

8.1 Objective

The objectives of this section are to:

- Describe how the Method of Characteristics (MOC) was used to simulate CCWH events.
- Describe how the method was benchmarked against textbook examples and test data.
- Demonstrate the validity of input boundary conditions determined from the test results.

8.2 MOC Description

The MOC used to simulate the CCWH events is described in Reference [6] and briefly in the following subsections. A pipeline is divided into an even number of segments (called reaches) for ease of solving the MOC equations. The solution is based on a one-dimensional representation of the piping system. Some limitations relate to the representation of system elements such as reservoirs, valves, series and branching pipelines, minor losses, etc.

8.2.1 Development of Finite Difference Equations

MOC allows the partial differential equations for momentum and continuity to be converted to ordinary differential equations. The ordinary differential equations may then be solved using a finite difference method to describe the magnitude and propagation of a waterhammer pressure. The simplified equations of motion and continuity as derived by Wylie in Reference [6] are:

$$g\frac{\partial H}{\partial x}+\frac{\partial V}{\partial t}+\frac{f}{2D}V|V|=0 \qquad \text{8-1}$$

$$\frac{\partial H}{\partial t}+\frac{C^2}{g}\frac{\partial V}{\partial x}=0 \qquad \text{8-2}$$

The MOC reduces these two partial differential equations into four ordinary differential equations, written as

$$\frac{g}{C}\frac{dH}{dt}+\frac{dV}{dt}+\frac{fV|V|}{2D}=0 \quad \text{when} \quad \frac{dx}{dt}=+C \qquad \text{8-3, 8-4}$$

and

$$\frac{-g}{C}\frac{dH}{dt}+\frac{dV}{dt}+\frac{fV|V|}{2D}=0 \quad \text{when} \quad \frac{dx}{dt}=-C \qquad \text{8-5, 8-6}$$

The ordinary differential equations are integrated to obtain the following two finite difference equations (the derivation is described in Reference [6]), which apply to right- and left-traveling characteristics, respectively:

$$H_{x,t}=H_{x\text{-}\Delta_x,t\text{-}\Delta_t}-B(Q_{x,t}-Q_{x\text{-}\Delta_x,t\text{-}\Delta_t})-RQ_{x,t}|Q_{x\text{-}\Delta_x,t\text{-}\Delta_t}| \qquad \text{8-7}$$

and

$$H_{x,t}=H_{x+\Delta_x,t\text{-}\Delta_t}+B(Q_{x,t}-Q_{x+\Delta_x,t\text{-}\Delta_t})+RQ_{x,t}|Q_{x+\Delta_x,t\text{-}\Delta_t}| \qquad \text{8-8}$$

The characteristic impedance B and the resistance coefficient R are defined as:

$$B=\frac{C}{gA} \qquad \text{8-9}$$

and

$$R=\frac{f\cdot\Delta x}{2gDA^2} \qquad \text{8-10}$$

The subscripts on the head H and flow Q terms indicate the position x and time t. The Δx and Δt subscripts indicate the change in position and time for the upstream/downstream nodalization. The nodalization is shown in Figure 8-1. If the pressure and flow are known at a time (t - Δt) for positions upstream (x - Δx) and downstream ($x + \Delta x$) then the pressure and flow at time t and position x may be solved using Equation 8-7 and Equation 8-8.

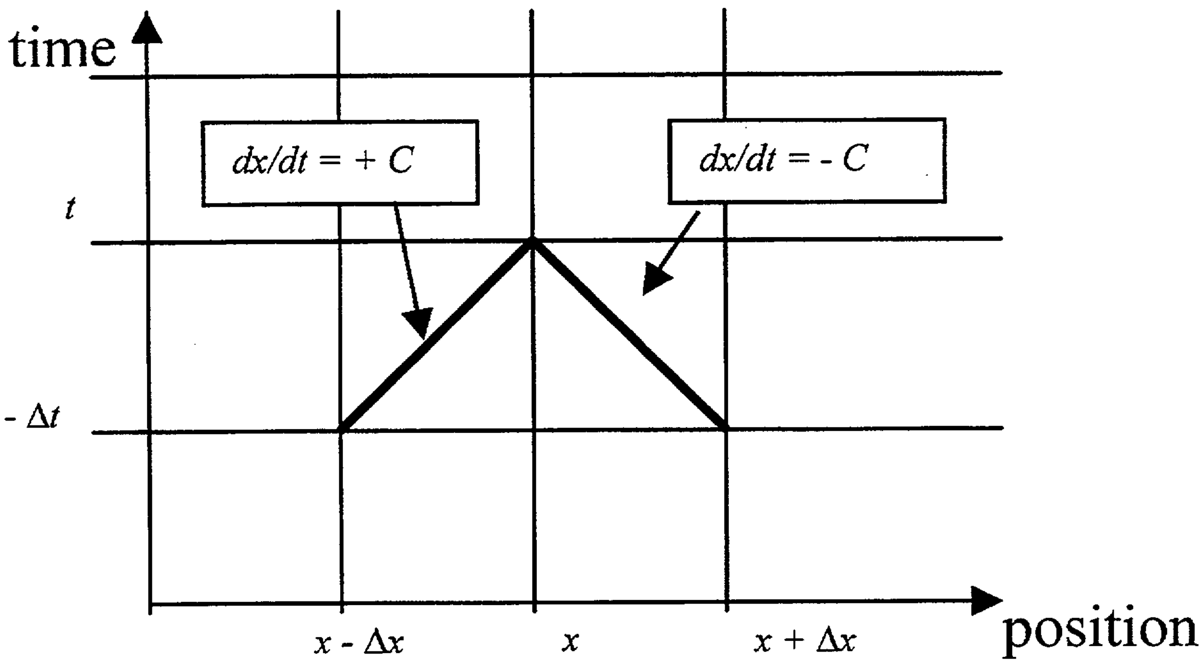

Figure 8-1
Characteristic Lines in the x-t Plane

By establishing appropriate initial and boundary conditions, the characteristics of a pressure disturbance may be obtained throughout a piping system. Wylie provides Fortran coding for this solution method in Reference [6].

8.2.2 Discrete Gas Cavity Model

Wylie's "discrete free-gas cavity model" distributes small pockets of gas through the system to act as small compressible nodes during the calculation (described in detail in Chapter 8 of Reference [6]). For the SW systems of interest, small vapor/air bubbles would be distributed in the system and it could reduce the magnitude of the waterhammers. The discrete gas cavity model was used to represent the TBR CCWH testing configuration (see Appendix D of Reference [6]). It became apparent after modeling the test configurations and imposing a variety of void distributions through the system that small voids introduced only a second order effect. The dominant effect was the gas in the main void. Analyses with gas only in the main void provided results that were very close to the test results.

8.2.3 Air Compression

The main void was simulated as an internal boundary condition. The compression of air and the condensation of steam in the void were represented as described below.

The void pressure was obtained by Dalton's law as the sum of the partial pressures of steam and air, or:

$$P_v = PP_{air} + PP_{stm} \tag{8-11}$$

The mass of air in the void remained constant during compression, since there was no mass transfer of air to the water. The air partial pressure was calculated at any given time step from the void size at that time and the void size and air partial pressure at the previous time step. A polytropic process was assumed, for which the air partial pressure at time t was obtained from:

$$PP_{air@t} = PP_{air@t-\Delta t}\left(\frac{Vol_{t-\Delta t}}{Vol_t}\right)^{\gamma} \tag{8-12}$$

8.2.4 Steam Condensation

The mass of steam in the void was not constant since condensation could occur. The steam mass was converted to water at a rate equal to the rate of steam condensation. Steam condensation is a complex process. A simplified method that proved to be relatively accurate is described with the help of Figure 8-2. Important assumptions are described below:

- The steam was assumed to remain saturated at a quality of 100%. In actuality, the steam quality may become superheated if the condensation rate is extremely slow relative to the compression of the steam. By assuming that the steam remained saturated, it condensed more readily. More rapid condensation is conservative since it provides less steam cushioning.
- The condensing surface temperature was assumed to remain constant at the initial void temperature. The surface temperature will increase during the transient since heat will be added to the surface. Holding the surface temperature at its initial value would be conservative since the condensation rate decreases with increasing surface temperature. The actual surface temperature is expected to decrease, promoting condensation, as cold water in the center of the pipe pushes forward and hot water is left behind near the outside of the pipe.
- The hA term was assumed to remain constant during the void closure. This assumption is supported by experimental observations and analytical arguments, to be discussed later. Moreover, it appears that the condensation heat transfer coefficient h itself is relatively constant, and that the steam condenses on a fixed water surface area A. The time-dependent piping surface area was ignored. Twice the available flow area was assumed for the surface area of a given configuration. The condensation rate of steam on water is expected to be at least an order of magnitude greater than the condensation rate of steam on the pipe wall for the same temperatures. It was recognized, though, that the available surface area for the piping may be greater than that for the water. To check the appropriateness of the assumption, simulations were run with both the water surface and the pipe surface available. With both surfaces available, accurate correlation between the test data and program outputs could not be achieved. Simulating steam condensation on a fixed water surface area correlated best with the test data and therefore, that assumption was considered appropriate.

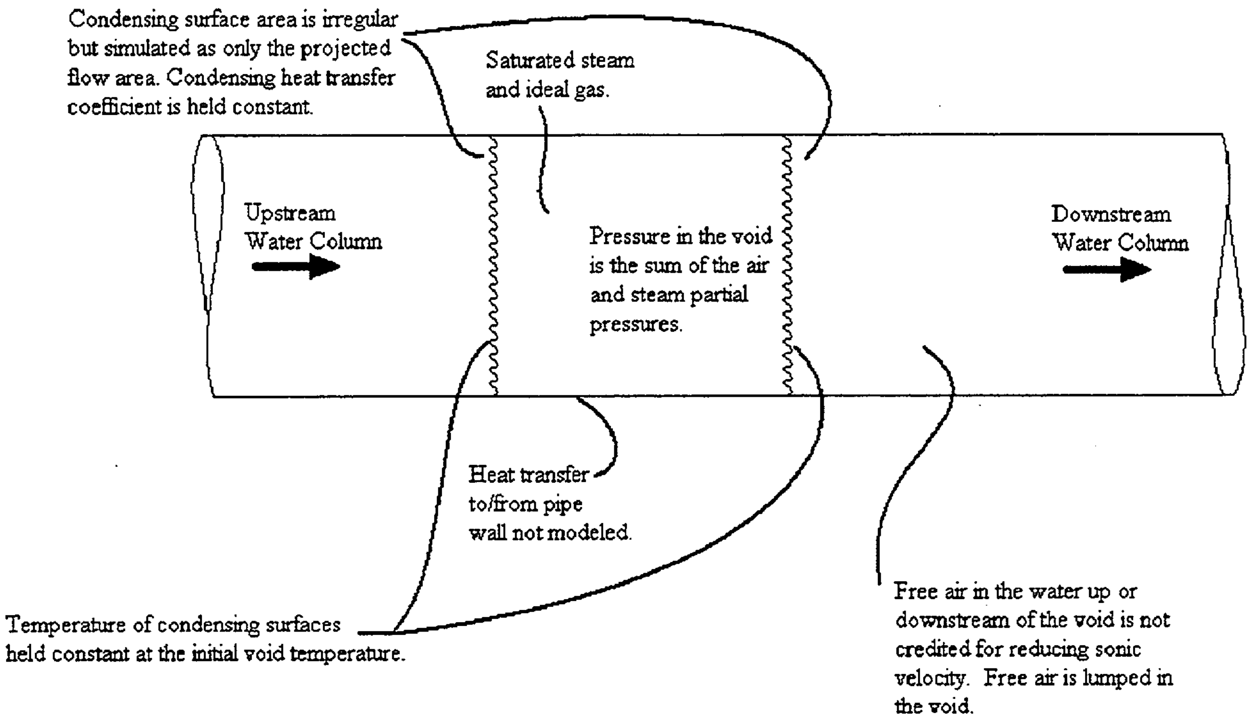

Figure 8-2
Void Simulation

The steam temperature and partial pressure at time t was found from steam tables for the specific volume at time (t - Δt). For small time steps the error introduced by this approximation was negligible. The steam condensation rate was calculated from:

$$m'_{stm} = \frac{h \cdot A \cdot (T_{stm} - T_s)}{h_{fg}} \qquad \text{8-13}$$

By knowing the condensing rate at each time step, the total steam mass was calculated. The ratio of void volume to steam mass gave the specific volume. The steam pressure and temperature were then taken from steam tables for the specific volume at that time step. The total pressure in the void represented the initiating waterhammer pressure pulse. The total void pressure was found by adding the steam and air partial pressures using Equation 8-11.

The balance of the MOC simulation was coded as described by Wylie [6] for the discrete free-gas cavity model. The supply pressure boundary condition was variable considering the potential for pressure drop in the air supply line. The return pressure was fixed at atmospheric conditions in the vented receiver tank. The boundary conditions were easily changed to simulate either the actual plant conditions or the text book examples described in the next section on benchmarking.

8.3 Code Benchmarking

The MOC code was checked against textbook examples and test data. Both are described below.

8.3.1 Textbook Benchmarking

The MOC coding was checked to ensure that it simulated wave propagation and pressure generation by comparing it against three examples from Reference [6]. Examples 8-1, 8-3, and 8-5 from Reference [6] were coded and results are shown in Figure 8-3, Figure 8-4, and Figure 8-5. These figures correspond to Reference [6] Figures 8-5, 8-7, and 8-10, respectively. Although the textbook figures are not reproduced here, the figures shown are nearly identical to those in the book. From a comparison of the text solutions and the figures below, it was concluded that the coding was correctly formulated.

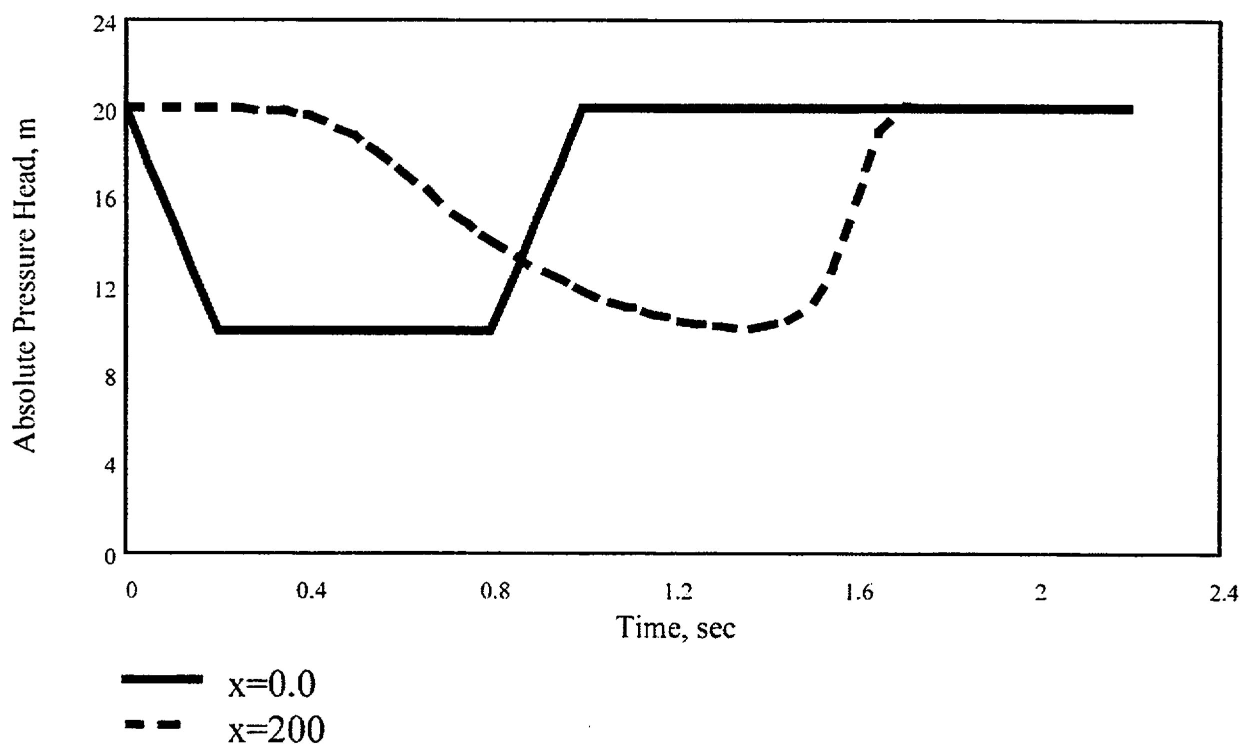

Figure 8-3
MOC Code Simulation of Wylie Example 8-1

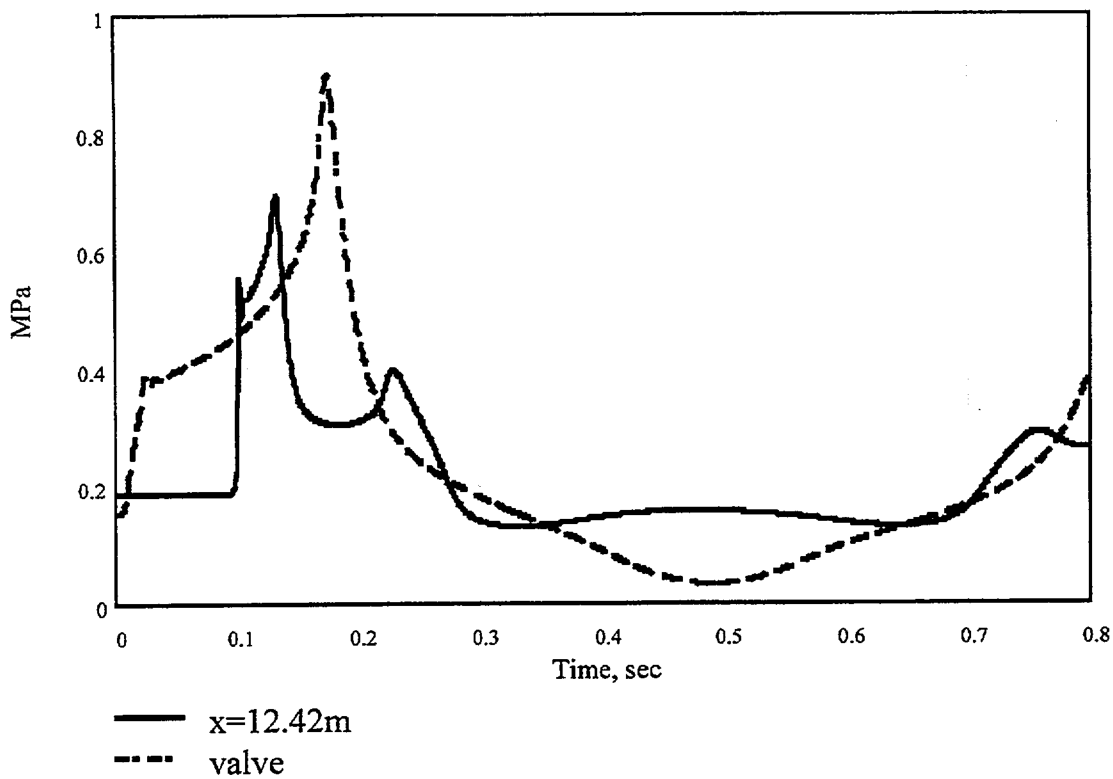

Figure 8-4
MOC Code Simulation of Wylie Example

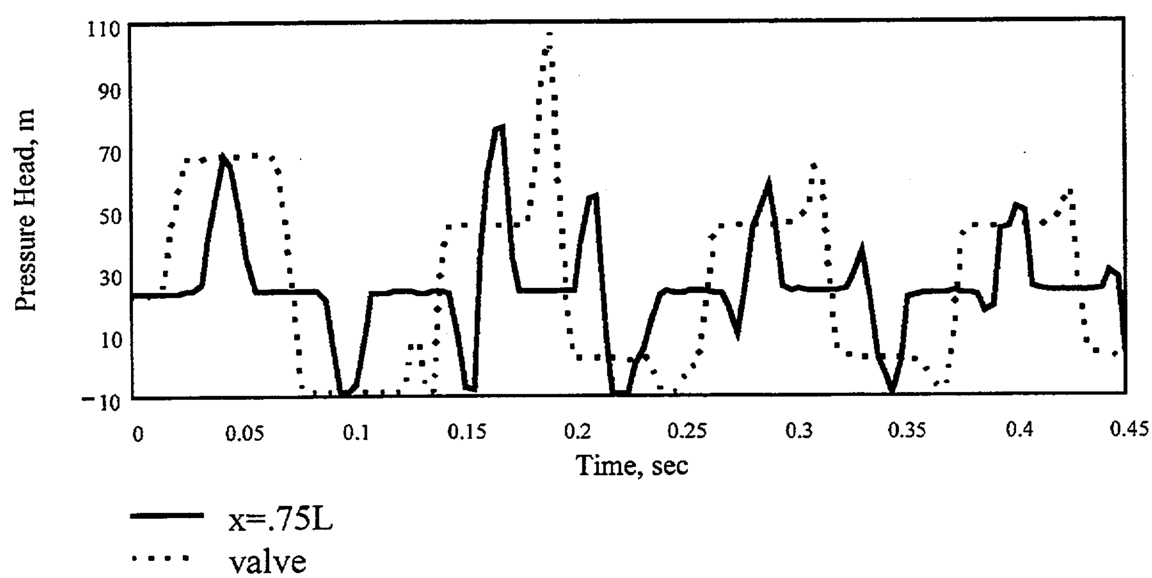

Figure 8-5
MOC Code Simulation of Wylie Example

8.3.2 Test Benchmarking

Column closure waterhammer testing as described in Section 10 was simulated using the MOC code. The particular geometry and test conditions were input for each test and the code was run. The MOC outputs are very similar to the test conditions once the air concentration and the condensing heat transfer coefficient are appropriately specified . These two variables have a significant influence on the pulse shape, duration, and magnitude.

A relative amount of air was known to be in the void for the different tests. Tests were performed with deaerated and normal water. The amount of air expected to be in the void was determined by considering the amount of water that was heated during the testing as follows:

- For configuration 2a, the heated length of water was 72 inches. Water dissolved air concentration was varied from 5 to 50 mg/L and, based on the 3- to 5-minute boiling time, 100% of the air was assumed to collect in the void.
- For configuration 2b, the heated length was 127 inches. Water dissolved air concentration was varied from 5 to 50 mg/L and, based on a brief boiling time, it was assumed that 40% of the dissolved air collected in the void.

The condensing heat transfer coefficient was determined by comparing the analysis results to the test results. Condensing heat transfer coefficients on the order of 10^3 to 10^4 BTU/hr·ft^2·°F are expected. Reasonable results were achieved by fixing the condensing heat transfer coefficient at a value no greater than 64,000 BTU/hr·ft^2·°F and assuming that the steam was condensing on a water surface equal to twice the pipe flow area. It is recognized that a bubbly contorted interface between the water and void causes a much greater surface area than the pipe flow area. Sensitivity to the *hA* term is evaluated in Section8.3.3.

Test configuration 2b was simulated first. Section 10.1 describes the CCWH test configurations. The appropriate condensing heat transfer coefficient was determined by using different values in the analysis until good results were achieved. Outputs from the code were selected at points that matched the pressure transducer locations. These are shown in Figure 8-6.

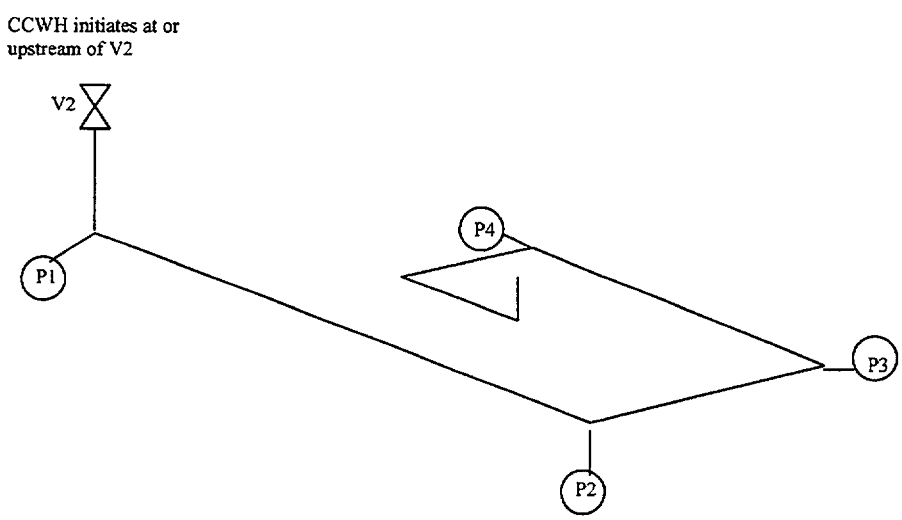

Figure 8-6
Transducer Locations – Test Configurations 1, 2a, and 2b

The approach used to benchmark the code and establish the appropriate condensing heat transfer coefficients is described below:

1. The 70-psi driving pressure, 20-ft driving column, test configuration 2b (see Section 10.1.2) was input with the following variations:

- A realistic air mass (60 mg) was input with unrealistically high heat transfer (hA >> 2625 BTU/hr·°F). This resulted in a test shape that resembled the test data but had a significantly larger magnitude. This comparison is shown in Figure 8-7 and Figure 8-8. P1, P2, P3, and P4 correspond to the transducer locations shown in Figure 8-6.
- An unrealistically high air mass was input with an unrealistically high heat transfer. This resulted in a pressure pulse shape and magnitude that did not match the test data. The duration of the pulse was longer and the magnitude was larger. This comparison is shown in Figure 8-9 and Figure 8-10.
- An unrealistically low air mass and a reasonable hA product were input. This resulted in a pulse shape that did not match the test data and had a slightly higher magnitude. Although the magnitude could be reduced to match the test data by increasing the condensing resistance, the shape would still not match. This comparison is shown in Figure 8-11 and Figure 8-12.
- Lastly, the expected air mass (60 mg) and realistic condensing heat transfer (hA = 2625 BTU/hr·°F) were input. This resulted in a pulse shape and magnitude that matched the test data. This comparison is shown in Figure 8-13 and Figure 8-14. This run showed that a fixed hA term of 2625 BTU/hr·°F provided a remarkably good representation of the transient.
- Figure 8-13 and Figure 8-14 correspond to test number "5" for this configuration. Tests "1" through "4" were also plotted against the simulation for the 70-psi driving pressure and 20-ft column. These plots are shown in Figure 8-15, Figure 8-16, Figure 8-17, and Figure 8-18.

2. The 20-psi driving pressure, 20-ft driving column, test configuration 2b was input:

All inputs were fixed as described for the final 70-psi driving pressure case Figure 8-13 and Figure 8-14 except that the driving pressure was changed to 20 psi). The outputs are shown in Figure 8-19 and Figure 8-20. This run shows that using a fixed hA term results in close simulation of the transient. There is nearly an identical match between the test data and code output for these conditions.

- Figure 8-19 and Figure 8-20 correspond to test number "10" for this configuration. Tests "6" through "9" were also plotted against the simulation for the 20-psi driving pressure and 20-ft column. These plots are shown in Figure 8-21, Figure 8-22, Figure 8-23, and Figure 8-24.

3. The 45-psi driving pressure, 3-ft driving column, test configuration 2a (see Section 10.1.2) was input:

- Approximately half the air mass was assumed to be in the void compared to the configuration 2b testing. This is expected since the amount of water that was heated was less in this case. The condensing heat transfer coefficient was at 2625 BTU/hr·°F as in cases 1 and 2 above.

The outputs are shown in Figure 8-25 and Figure 8-26 and correspond to test number "5" for this configuration.

- Tests "1" through "4" were also plotted against the simulation for the 45-psi driving pressure and 36" column. These plots are shown in Figure 8-27, Figure 8-28, Figure 8-29, and Figure 8-30.

4. The 45-psi driving pressure, 17-ft driving column, test configuration 1 was input:

- The condensing surface temperature was reduced here since in this configuration the water is initially isolated from the steam. The water temperature was considered to be 150°F and an *hA* term of 738 BTU/hr·°F was assumed. A lower condensing heat transfer coefficient is reasonable since it is inversely proportional to the temperature difference raised to some exponent [22]. Here the temperature difference is greater than the previous cases so a decrease in the coefficient is appropriate. The amount of air corresponded to the amount of air in a mass of normal tap water equivalent to the mass of steam (approximately 0.008 mg). The results are shown in Figure 8-31 and Figure 8-32.

Five tests from test configuration 2b were arbitrarily chosen to be plotted against the MOC code results for deaerated and normally aerated water. The results are shown in Figure 8-33 and Figure 8-34 for the 20-psig and 70-psig driving pressure cases respectively. To generate these plots, the air mass in the void for the tests was assumed to be equal to the calculated air mass used in the MOC run. These plots demonstrate that the pressure pulse predicted with the MOC code is appropriate for normal and deaerated conditions and that the waterhammer pressure is reduced with increasing air concentrations in the void.

Figure 8-7
Realistic Air Mass & High Heat Transfer, P1 & P2
(Test Configuration 2b, 70 psig, Normal Water, psi=psig

Figure 8-8
Realistic Air Mass & High Heat Transfer, P3 & P4
(Test Configuration 2b, 70 psig, Normal Water, psi = psig)

Figure 8-9
High Air Mass & High Heat Transfer, P1 & P2
(Test Configuration 2b, 70 psig, Normal Water, psi = psig)

Figure 8-10
High Air Mass & High Heat Transfer, P3 & P4
(Test Configuration 2b, 70 psig, Normal Water, psi = psig)

Figure 8-11
Low Air Mass & Realistic Condensing Heat Transfer, P1 & P2
(Test Configuration 2b, 70 psig, Normal Water, psi = psig)

Figure 8-12
Low Air Mass & Realistic Condensing Heat Transfer. P3 & P4
(Test Configuration 2b, 70 psig, Normal Water, psi = psig)

Figure 8-13
Realistic Air Mass & Realistic Condensing Heat Transfer, P1 & P2
(Test Configuration 2b, 70 psig, Normal Water)

Figure 8-14
Realistic Air Mass & Realistic Condensing Heat Transfer, P3 & P4
(Test Configuration 2b, 70 psig, Normal Water)

Figure 8-15
Test No. "1", Configuration 2b, 70 psig, Normal Water, 20 ft Column

Figure 8-16
Test No. "2", Configuration 2b, 70 psig, Normal Water, 20 ft Column

Figure 8-17
Test No. "3", Configuration 2b, 70 psig, Normal Water, 20 ft Column

Figure 8-18
Test No. "4", Configuration 2b, 70 psig, Normal Water, 20 ft Column

Figure 8-19
Realistic Air Mass & Realistic Condensing Heat Transfer, P1 & P2
(Test Configuration 2b, 20 psig, Normal Water, psi = psig)

Figure 8-20
Realistic Air Mass & Realistic Condensing Heat Transfer, P3 & P4
(Test Configuration 2b, 20 psig, Normal Water, psi = psig)

Figure 8-21
Test No. "6", Configuration 2b, 20 psig, Normal Water, 20 ft Column (psi = psig)

Figure 8-22
Test No. "7", Configuration 2b, 20 psig Normal Water, 20 ft Column (psi = psig)

Figure 8-23
Test No. "8", Configuration 2b, 20 psig, Norm Water, 20 ft Column (psi = psig)

Figure 8-24
Test No. "9", Configuration 2b, 20 psig, Normal Water, 20 ft Column (psi = psig)

Figure 8-25
Realistic Air Mass & Realistic Condensing Heat Transfer, P1 & P2
(Test Configuration 2a, 45 psig, Normal Water)

Figure 8-26
Realistic Air Mass & Realistic Condensing Heat Transfer, P3 & P4
(Test Configuration 2a, 45 psig, Normal Water)

Figure 8-27
Test No. "1", Configuration 2a, 45 psig, Normal Water, 36" Column

Figure 8-28
Test No. "2", Configuration 2a, 45 psig, Normal Water, 36" Column

Figure 8-29
Test No. "3", Configuration 2a, 45 psig, Normal Water, 36" Column

Figure 8-30
Test No. "4", Configuration 2a, 45 psig, Normal Water, 36" Column

Figure 8-31
Realistic Air Mass & Realistic Condensing Heat Transfer, P1 & P2
(hA = 738 BTU/hr·°F) (Test Configuration 1, 45 psi, Normal Water)

Figure 8-32
Realistic Air Mass & Realistic Condensing Heat Transfer, P3 only
(*hA* = 738 BTU/ hr·°F) (Test Configuration 1, 45 psi, Normal Water)

Figure 8-33
Configuration 2b Air Sensitivity

Figure 8-34
Configuration 2b Air Sensitivity Comparison

8.3.3 *hA* Sensitivity

Heat transfer affects the steam cushioning of the closing velocity during a CCWH event. The condensing heat transfer coefficient and condensing surface areas used to simulate the test data will not be identical to those in actual plant configurations. The most significant reasons for differences in *hA* between testing and plant conditions are differences in pipe size, air content, temperatures, and flow. These effects are conservatively addressed by the constant *hA* model and are described in detail below.

8.3.3.1 Pipe Size

The testing showed that simulating heat transfer to/from the pipe wall during the closure process was unnecessary. This does not mean that some heat transfer is not occurring, rather that the constant *hA* approach provides an acceptable simulation method. The piping wall will absorb heat if the steam temperature goes above the pipe temperature. Conversely, if the steam temperature falls below the pipe wall temperature then the pipe wall will add heat to the steam. The pipe wall provides a stabilizing effect while the void is closing. As the void closes and a significant pressure rise begins to occur, typically the void is quite small. Since the heat transfer coefficient for steam to metal is much less than the heat transfer coefficient for steam to water, the heat transfer from the steam to the piping is less significant than the heat transfer to the water at this stage. As a result, the dominant influence is heat transfer between the steam and the water.

By definition, the heat transfer rate is

$$q = \int_{A_S} q'' \, dA_S$$

Assuming a uniform surface temperature and an average convection coefficient h for the entire surface, this equation reduces to

$$q = \Delta T \cdot h \cdot A$$

The area, A, is defined for this study as the cross sectional pipe area for the water/steam interface regions. Therefore, when the void is closing between two water columns,

$$A = 2 \times \frac{\pi D^2}{4}$$

Using the defined area, the average convection coefficient h_{test} = 64,000 BTU/hr·ft^2·°F was determined from the test data.

In reality, the actual interface between the steam and water is not a clean, sharp wall as shown in Figure 8-35. Rather, the interface may be characterized as irregular, "fingers" of water extend into the steam and a surface area greater than that of just the water flow area results. By defining a fixed area equal to twice the cross-sectional area of the pipe, the convection coefficient h encompasses this irregular surface. The depth of the jagged surface, or "fingers," is not expected to vary significantly with pipe size in the 2" to 16" range, as it is primarily a function of the flow velocity. There will be more surface irregularity at higher velocities. However, the total surface area available for heat and mass transfer will change proportionally with the pipe flow area. Using the test data heat transfer coefficient of 64,000 BTU/hr·ft^2·°F and multiplying by twice the water flow area appears to be representative for cases where the void is closing between two water columns. If the void is closing between a water column and a closed end such as a valve or fitting, then only the cross sectional area of the decelerating column would be simulated as the condensing surface area.

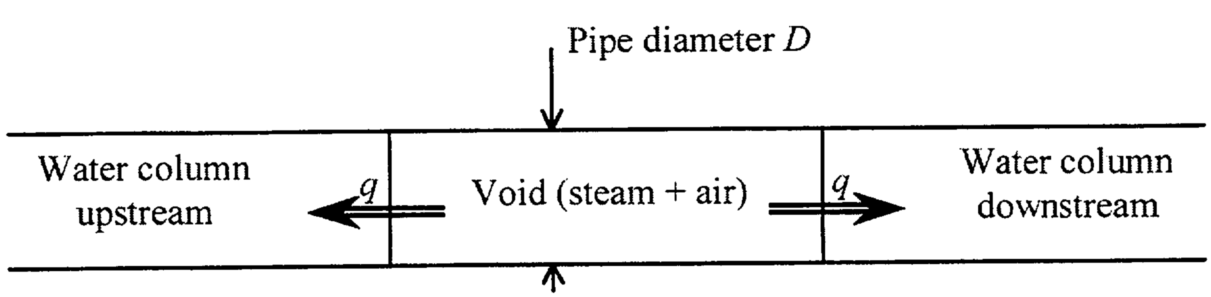

Figure 8-35
Definition of the Convection Rate Between Steam and Water

The heat transfer coefficient for the given pipe flow area was determined from test data. Figure 8-36 presents MOC simulations for three test configurations and driving pressures combinations. The effect of varying h (x-axis) can be seen in the resulting waterhammer peak pressure magnitudes (y-axis) for each simulation. Plotted with the simulations are the test data peak waterhammer pressures (open symbols). From this plot, the range of h values that would produce the test waterhammer pressures can be determined. It can be seen that the h values that produce waterhammer pressures matching the test data fall in the range of 48,000 to 67,000 BTU/hr·ft^2·°F.

All the final MOC and Rigid Body Model (RBM) analyses were performed with h_{rec} = 72,000 BTU/hr·ft^2·°F. This value was chosen to provide conservatism relative to that determined by the testing. Figure 8-36 shows that for all test configurations, the measured waterhammer pressure peak falls below the MOC pressure peak computed h_{rec} = 72,000 BTU/hr·ft^2·°F. The sensitivity of the hA term is discussed further in Section 8.3.4.

Figure 8-36 indicates that for heat transfer coefficients beyond the recommended value (h_{rec} = 72,000 BTU/hr·ft^2·°F), the waterhammer pressure peak magnitude dependence on h is reduced (the slope of every curve is decreasing and tends towards zero). The reason for this is that as h is increased, the column closure becomes less dependent on the heat transfer at the steam/water interface, and the event becomes more inertially dominated. Figure 8-36 shows that for values of h that are 25% larger than the largest h that corresponds to the test data (h = 67,000 BTU/hr·ft^2·°F), that is with h = 84,000 BTU/hr·ft^2·°F, the waterhammer pressures would be larger than that determined using h_{rec} by 15 to 22%.

Figure 8-36
Pressure Peak Magnitude vs. *h* for Different Test Configurations

Further discussion of the pipe diameter relationship is provided in Section 8.3.6.

8.3.3.2 Flow Rate

The *hA* term was insensitive to velocity for the column closure waterhammers created in the test program. A fixed *hA* term of 2625 BTU/hr·°F resulted in good correlation between the test data and simulations for both the 20-psig and 70-psig driving pressures in configuration 2b. The 20-psig driving pressure case had a minimum velocity of approximately 13 ft/sec. The 70-psig driving pressure cases had closure velocities of as high as approximately 30 ft/sec, approximately 2.3 times the 20-psig driving pressure cases.

One method of calculating a condensing heat transfer coefficient is to apply the Reynold's analogy. The Reynold's analogy for a condensing heat transfer coefficient [23] is:

$$h = \frac{f}{8} \cdot \rho \cdot C_p \cdot V$$

In this equation, the condensing heat transfer coefficient is directly proportional to the velocity (neglecting any friction factor dependence on velocity). The condensing heat transfer coefficient for a 70-psig driving pressure test should then be approximately twice that of a 20-psig driving pressure test. For the test simulations, the *hA* term was not changed for the different closure velocities but good correlation with the test data was obtained. As described in the "air content" discussion below, there was apparently enough air in the void to prevent significant variation of *hA*. The *hA* dependence is then considered negligible for the flow range of concern by extrapolating to lower velocities (~ 5 ft/sec to ~ 30 ft/sec).

A consideration of the variation of the condensing surfaces as a function of water column closing velocity relates to this heat transfer. A higher closing velocity would require greater deceleration of the water column or slug as void pressure increases. This would tend to produce greater irregularity of the condensing surfaces (Figure 8-2), especially for the closing column of water. Heat transfer would be expected to increase with the increased surface irregularity. As noted above, the 20-psig driving pressure cases had a prototypical velocity of approximately 13 ft/sec while the 70-psig driving pressure cases had closure velocities of approximately 30 ft/sec. Since the CCWH testing used higher velocities than prototypical, larger surface areas would result and hA would be larger than what would be expected in the plants for prototypical velocities. The test results are therefore conservative and would provide a bounding value of hA for the in-plant conditions.

In summary, the *h* term is likely to be constant or increasing with velocity. The *A* term is likely to increase with velocity, as surface irregularity will increase with the increased deceleration required to stop a higher velocity water column. Therefore, using an *hA* term that provides good correlation at prototypical or higher than prototypical velocities will produce conservative results in actual plant situations.

8.3.3.3 Air Content

Air will be concentrated at the water/steam interface. The air provides an insulating effect and tends to reduce the heat transfer rate. A value of hA = 2625 BTU/hr·°F (64,000 BTU/hr·ft^2·°F with condensation on twice the available flow area) was found representative of the test configuration 2b, normally involving aerated water tests. In these tests, there was a relatively low concentration of air in the void (approximately 60 mg in a 6.1-liter void in a 2" pipe). The controlling factor is the concentration of air in the air/steam mixture when the void finally closes.

Most of the heat transfer will be occurring at the jagged water/steam interface. If the concentration of the air at the interface for the plant conditions is similar to the concentration of air for the test conditions, then the test condition heat transfer coefficient may be applied. A minimum mass of air that needs to be concentrated in the void to apply the test data may be calculated using the ideal gas law. The minimum air required is calculated from the following equation and plotted in Figure 8-37.

M_{plant} = minimum mass of air to apply h = 64,000 BTU/hr·ft^2·°F and twice flow area when calculating hA

M_{test} = mass of air in test configuration (60 mg)

ID_{plant} = inside pipe diameter for plant configuration

ID_{test} = inside pipe diameter for test (2")

Figure 8-37
Minimum Air Required to Use h = 64,000 BTU/hr·ft^2·°F

8.3.3.4 Temperature

The fourth factor that can influence *hA* is the water and steam temperatures. The condensing surface temperature is fixed at the initial void temperature in the simulations. Fixing the condensing surface temperature at the initial void temperature simulates a thermal layer that remains throughout the closure process. This is conservative, since the condensing surface temperature will increase as condensation transfers heat to the water, although mixing of the fluid layer will transfer this heat through the liquid. At higher initial void temperatures, the p_{SAT} pressure is greater and the condensation rate is reduced such that the simulation will over predict the peak pressure. At lower temperatures, there is a limit where the simulation may under predict the peak pressure as discussed below.

The sensitivity of the *hA* term to temperature was investigated using an MOC simulation for test configuration 2b with normal air and a 20-psig driving pressure.

At lower temperatures, there is little difference down to a temperature of 200°F. Simulations of Configuration 1 testing indicated that a lower *hA* term was appropriate for lower water temperature cases. The simulation method is considered appropriate down to a temperature of approximately 200°F. At void temperatures less than 200°F, steam cushioning should not be included.

hA Sensitivity Summary:

Factor	*Limitation*
Flow	Velocity range from ~ 5 ft/sec to ~ 30 ft/sec
Pipe Size	None; multiply 64,000 BTU/hr·ft^2·°F by the sum of the projected area of the upstream and downstream water columns to calculate *hA* (if closure occurs on a closed end such as a valve or fitting, then only credit condensation on the upstream water column area).
Air Content	$M_{air} > (60\text{ mg})\times(ID/2")^2$
Temperature	When Void Temp ≥ 200°F, consider air and steam cushioning. When Void Temp < 200°F, consider air cushioning only.

If the conditions for a particular plant fall within the limits tabulated above, then the condensation process may be simulated by fixing the condensing heat transfer coefficient at 64,000 BTU/hr·ft^2·°F. The condensing surface area should be twice the available flow area for the condensing surface area. If plant conditions fall outside the limits described, then additional plant specific justification may be required to apply the fixed *hA* approach.

For steam and air cushioning, a heat transfer coefficient of 64,000 BTU/hr·ft^2·°F was determined in the MOC validation as an appropriate and conservative value to match the test data. This heat transfer coefficient was conservatively increased 12.5% to 72,000 BTU/hr·ft^2·°F for the development of the RBM curves. This higher coefficient is conservative since it implies that steam is consumed faster and therefore provides less cushioning.

8.3.4 hA Sensitivity on the RBM Curves

To further assess the effect of variation in the heat transfer coefficient on the waterhammer parameters, h was varied from 72,000 BTU/hr·ft²·°F (h_{rec}) to 84,000 BTU/hr·ft²·°F (25% above the largest h_{test}) in the Rigid Body Model equations. RBM curves were prepared for air and steam cushioning.

In the following figures, a new set of curves (computed for h = 84,000 BTU/hr·ft²·°F) was added to the ones already present in the original figures (computed for h = 72,000 BTU/hr·ft²·°F). All the original curves can all be found in Appendix A of the User's Manual. Several curves were selected to demonstrate the influence of hA variation.

Figure 8-38 was taken from Figure A-34 in the User's Manual. It shows that the cushioned velocity calculated using an unrealistically high h value (h = 84,000 BTU/hr·ft²·°F) increases by approximately 1% the initial velocity for the low K case (low pipe resistance model). The change is less for the other cases.

Similar results can be observed for a 10" pipe on Figure 8-39, which was taken from Figure A-45 in the User's Manual. In this case, the cushioned velocity determined using the high h value increases by approximately 2% of the initial velocity for the low K case. The change is less for the other cases.

Figure 8-38
4" Pipe, Air and Steam Cushioning, Initial Velocity 10 fps, *Lwo* = 400 ft

Figure 8-39
10" Pipe, Air and Steam Cushioning, Initial Velocity 20 fps, *Lwo* = 400 ft

The third case evaluated is shown in Figure 8-40 (taken from Figure A-46 in the User's Manual). In this case, the cushioned velocity determined using the high h value increases by approximately 3 to 4% of the initial velocity for the $K = 10$ case. For higher values of K, the influence of h is, again, much smaller.

Figure 8-40
16" Pipe, Air and Steam Cushioning, Initial Velocity 10 fps, *Lwo* = 100 ft

These evaluations for changes in *h* are performed for a variation in *h* that is 25% above the largest value determined by test. It is performed to show that the change in the waterhammer pressures is not particularly sensitive to changes in *h*. If the value of *h* were changed by an additional 25%, the increase would be less than for the initial 25% increase since the peak pressure versus *h* curve flattens out for increasing values of *h* (see Figure 8-36).

8.3.5 MOC Comparison Against Test Data

The geometry and conditions for the test configurations described in Chapter 10 were input in the MOC Model. A comparison of testing results (from Chapter 10) and MOC runs to model the specific test conditions is shown below in Table 8-1.

Table 8-1
MOC Comparison Against Test Data

The MOC code was shown to be representative of the effects of air, steam, and wave propagation when compared against the test data, and the effects of air and steam pressurization in the void were found to be accurately modeled.

8.3.6 Evaluation of the Effect of Pipe Area

The pressure resulting from the closure of a gas void between two water columns is determined from a solution to the fluid flow equations with a compressible gas boundary condition. The gas void is composed of both non-condensable gas and saturated steam, which may undergo condensation on the water interfaces.

Basic flow equations are employed to show that in most FCU cases, the pipe friction effect on water flow is negligible, for which the governing water motion equations are essentially one-dimensional, and independent of the flow area (or pipe diameter). Non-condensable gas compression is also independent of the pipe area. However, heat transfer to both the pipe walls and the water interfaces determines removal of the steam by condensation.

Heat transfer to the pipe wall is expected to be negligible relative to condensation on cold water interfaces, since the vapor formation itself is a direct result of heating through the pipe wall. Therefore, axial heat transfer is dominated by the water surfaces, which are idealized as semi-infinite slabs with a constant temperature applied to the surface, and with water at the surface undergoing continual replacement by turbulent transport. Therefore, the heat transfer to the water is assumed to occur as a uniform heat flux, which also is independent of pipe flow area.

It appears that water motion, gas and steam state properties, and condensation heat transfer only depend on the length scale in the flow direction, but not on the flow cross-sectional area or pipe diameter. It follows that the observed experimental tendency of the *hA* product to remain constant is supported for 1:1 length and state property scaling. That is, the area *A* cancels from all the equations, and simplified condensation modeling shows that the condensing coefficient *h* is influenced by the axial length and thermodynamic state properties, but not the pipe diameter.

8.4 Fluid Flow Equations

The mass conservation and momentum equations for one-dimensional flow in uniform area pipes with friction and slanted from the horizontal are given by

$$\frac{\partial P}{\partial t}+V\frac{\partial P}{\partial x}+\frac{\rho\cdot C^2}{g}\frac{\partial V}{\partial x}=0 \qquad \text{8-14}$$

$$\frac{\partial V}{\partial t}+V\frac{\partial V}{\partial x}+\frac{g}{\rho}\frac{\partial P}{\partial x}+\frac{f}{D}\frac{|V|V}{2}+g\sin\theta=0 \qquad \text{8-15}$$

Equation 8-14 and Equation 8-15 are normalized for waterhammer flows by introducing the non-dimensional variables,

$$V^*=\frac{V}{V_{\max}};\qquad P^*=\frac{P-P_i}{\left(\frac{\rho\cdot C\cdot V_{\max}}{g}\right)};\qquad x^*=\frac{x}{L};\qquad t^*=\frac{C}{L}t \qquad \text{8-16}$$

which yields

$$\frac{\partial P^*}{\partial t^*}+\left(\frac{V_{\max}}{C}\right)V^*\frac{\partial P^*}{\partial x^*}+\frac{\partial V^*}{\partial x^*}=0 \qquad \text{8-17}$$

$$\frac{\partial V^*}{\partial t^*}+\left(\frac{V_{\max}}{C}\right)V^*\frac{\partial V^*}{\partial x^*}+\frac{\partial P^*}{\partial x^*}+\left(\frac{V_{\max}}{C}\right)\frac{fL}{D}\frac{|V^*|V^*}{2}+\frac{gL\sin\theta}{V_{\max}C}=0 \qquad \text{8-18}$$

The non-dimensional variables and their first derivatives have an order of magnitude equal to 1. Also, the Mach number, V_{max}/C, of liquid flows is relatively small so the convective (second) terms of Equation 8-17 and Equation 8-18 can be neglected. Unless the friction parameter *fL/D* is about as large as a reciprocal Mach number, the friction term in Equation 8-18 also can be neglected. The final elevation term of Equation 8-18 is negligible in most cases. It follows that the fluid flow equations for FCU systems can be written as follows without introducing significant errors:

$$\frac{\partial P}{\partial t} + \frac{\rho \cdot C^2}{g}\frac{\partial V}{\partial x} = 0 \qquad \text{8-19}$$

$$\frac{\partial V}{\partial t} + \frac{g}{\rho}\frac{\partial P}{\partial x} = 0 \qquad \text{8-20}$$

Equation 8-19 and Equation 8-20 are independent of the pipe diameter or flow area.

8.5 The Gas Pocket

The gas pocket with total pressure

$$P = P_g + P_a \qquad \text{8-21}$$

and volume $\forall$ contains both steam and non-condensable gas, with internal energies for steam

$$U_g = e_g(T)M_g \qquad \text{8-22}$$

and for non-condensable gas:

$$U_a = \frac{1}{k-1}P_a\forall \qquad \text{8-23}$$

The mass of steam contained in the void is given by:

$$M_g = \rho_g\forall = \frac{1}{v_g}\forall \qquad \text{8-24}$$

It is assumed that the vapor is nearly saturated so that a heat transfer rate q from the void to the water interfaces results in a vapor mass condensation rate m'_{gf}, given by

$$m'_{gf} = \frac{q}{h_{fg}} \qquad \text{8-25}$$

Heat transfer from the void results in the formation of saturated water at a rate given in Equation 8-25, which transfers out of the void at saturated water enthalpy, h_f. The outflow energy rate from the void is composed of the expansion work rate, the heat transfer, and the condensed water transfer, or

$$\dot{out} = P\frac{d\forall}{dt} + q + m'_{gf}h_f = P\frac{d\forall}{dt} + q\left(1 + \frac{h_f}{h_{fg}}\right) = P\frac{d\forall}{dt} + q\frac{h_g}{h_{fg}} \qquad 8\text{-}26$$

It follows that energy conservation for the void is given by

$$P\frac{d\forall}{dt} + q\frac{h_g}{h_{fg}} + \frac{d}{dt}(U_g + U_a) = 0 \qquad 8\text{-}27$$

The void volume can be written as

$$\forall = Az \qquad 8\text{-}28$$

where z is its length. If the enthalpy expression,

$$h_g = e + p \cdot v \qquad 8\text{-}29$$

and the convection heat transfer rate

$$q = h \cdot A \cdot \Delta T \qquad 8\text{-}30$$

are employed, Equation 8-27 can be written as

$$\frac{k}{k-1}P\frac{dz}{dt} - \frac{1}{k-1}P_g\frac{dz}{dt} + \frac{z}{k-1}\frac{dP_a}{dt} + \frac{z}{v_g}\frac{de_g}{dT}\frac{dT}{dt} + \frac{P_g v_g}{h_{fg}}h \cdot \Delta T = 0 \qquad 8\text{-}31$$

If it can be shown that the condensing heat transfer coefficient h does not depend on flow area, Equation 8-31 is independent of the pipe flow area. The variables are total pressure P, vapor pressure P_g, non-condensable gas pressure P_a, the void temperature T, and the void length z. If P_g is the vapor saturation pressure at T, and P_a is obtained from the perfect gas law, then

$$P_g = P_{sat}(T) \qquad 8\text{-}32$$

and

$$P_a = \frac{M_a R_a T}{\forall} = \frac{\rho_{ai}\forall_i R_a T}{\forall} = \rho_{ai}\frac{z_i}{z}R_a T \qquad 8\text{-}33$$

then Equation 8-31 becomes a function of the dependent variables, T and z, to be used as a boundary condition in a solution of the fluid flow, governed by Equation 8-19 and Equation 8-20

If the heat transfer coefficient is shown not to be flow area dependent, then the observed tendency for the hA product to remain constant in piping of a given diameter would extend to pipes of other diameters. The dependence of the heat transfer coefficient on flow area will be addressed next.

8.6 Condensing Heat Transfer Coefficient

Heat transfer to a water interface is similar to that of semi-infinite slab with a constant temperature boundary, for which

$$q = \frac{\kappa \cdot A}{\sqrt{\pi \cdot \alpha \cdot t}} \Delta T \qquad \text{8-34}$$

except that cool water continues to replace that near the condensing surface by flow inside the moving water column, as it advances and deposits water on the pipe wall. If the time period to replace surface water is Δt, the average heat transfer rate during this time is approximated by

$$q = \frac{1}{2} \frac{\kappa \cdot A}{\sqrt{\pi \cdot \alpha \cdot \Delta t}} \Delta T \qquad \text{8-35}$$

If the surface water heating takes place in a film of thickness δ, cool water would be transported to the surface by the axial turbulent fluctuating velocity component V' approximately in the time interval Δt, given by

$$\Delta t = \frac{\delta}{V'} \qquad \text{8-36}$$

If the heat transfer rate of Equation 8-35 is expressed as a convection equivalent, it follows that

$$q = h \cdot A \cdot \Delta T = \frac{1}{2} \frac{\kappa \cdot A}{\sqrt{\pi \cdot \alpha \cdot \frac{\delta}{V'}}} \Delta T \qquad \text{8-37}$$

If an idealized linear temperature gradient exists in the film of thickness δ, the heat transfer rate can be written as

$$q = \frac{\kappa}{\delta} \cdot A \cdot \Delta T = h \cdot A \cdot \Delta T \qquad \text{8-38}$$

Equation 8-37 and Equation 8-38 can be combined to yield the film thickness as

$$\delta = \frac{4 \cdot \pi \cdot \alpha}{V'} \qquad 8\text{-}39$$

with a corresponding heat transfer coefficient

$$h = \frac{\kappa}{\delta} = \frac{\kappa \cdot V'}{4 \cdot \pi \cdot \alpha} \qquad 8\text{-}40$$

Note that if the turbulent velocity is independent of the pipe diameter, the heat transfer coefficient h also is independent of the pipe size.

Saturated steam condensing on cold water at 100°F, with $\kappa = 0.364$ BTU/hr·ft²·°F, $\alpha = 0.00588$ ft²/hr, and a turbulent average velocity component of about $V' = 2$ fps, or about 1/10 of the 20-fps water column velocity, gives a value of

$$h = 36{,}000 \text{ BTU/hr·ft}^2\text{·°F}$$

Condensing heat transfer coefficients on the order of 64,000 BTU/hr·ft²·°F were observed in the experiments. The simple model described here for condensation heat transfer h, while not refined enough to accurately predict experimental values, appears to be sufficiently close to conclude that h is not dependent on the pipe diameter.

8.7 Overall Conclusion

Experiments were run at full-scale thermodynamic state properties and flow lengths in pipes of constant diameter. It was observed that the condensing heat transfer parameter hA was relatively constant, and apparently independent of pipe diameter. This analysis shows that for waterhammer modeling in the water and a void compression boundary condition involving both non-condensable gas and condensing steam, flow area A cancels from the governing equations, and the condensing coefficient h is independent of flow area.

9
RIGID BODY MODEL FOR COLUMN CLOSURE WATERHAMMER

A simplified Rigid Body Model (RBM) has been developed to assist in the prediction of realistic column closure velocity and waterhammer in plant conditions. This RBM conservatively predicts the peak pressure and rise times of CCWH events, and RBM analytical results have been compared to the test results and MOC solutions.

The primary difference between the RBM and MOC methods is that the RBM treats the mass of water closing a void as a rigid body while the MOC allows for wave propagation effects. The RBM method independently considers the possible added impact of reflected waves. This simplified method provides a more direct solution to the range of variables expected in actual power plants, and allowed the tabularized solutions that are provided in the User's Manual to be prepared.

9.1 Objective

The objectives of this section are to:

- Describe the Rigid Body Model (RBM) used to simulate the CCWH events.
- Describe how the RBM was benchmarked against MOC examples and test data.
- Describe the methods for simulating the pressure pulse magnitude, rise time, and duration using the RBM.

9.2 Theory

The following section describes the theory for the prediction of column closure waterhammer pressure pulses.

9.1.1 Waterhammer Pressure Pulse Magnitude

Figure 9-1 shows an example of a water column closure event similar to those created in the testing. When advancing water traveling at velocity V closes a steam void and impacts stagnant water, a pressure pulse, ΔP, will travel back through the fluid, changing the fluid momentum. The pressure pulse is the "communication" of the decelerated water at the front of the advancing column as it runs into the stagnant water, and the traveling water behind the front that "piles up."

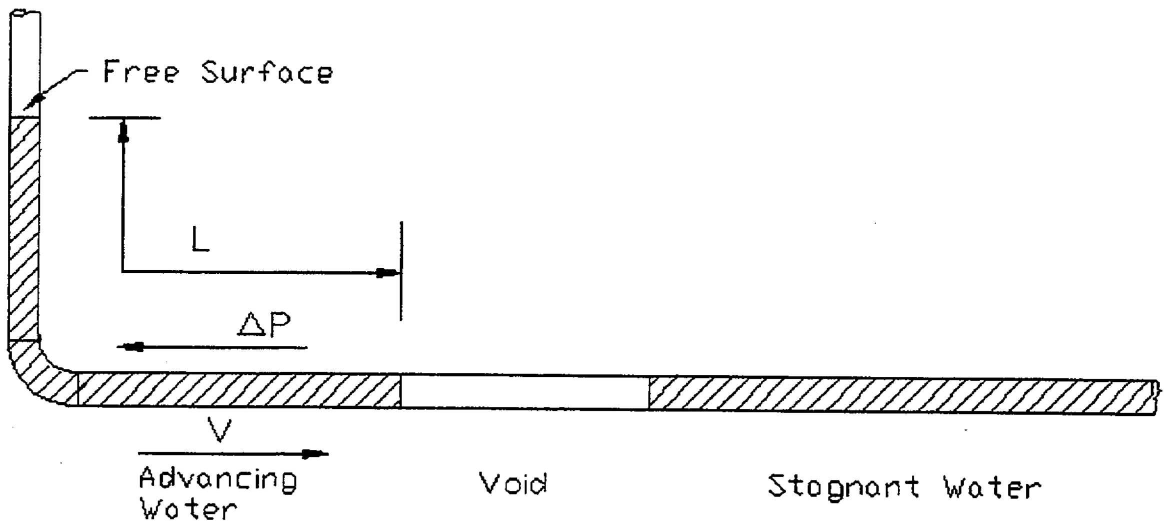

Figure 9-1
Example Column Closure Waterhammer Event

The magnitude of a waterhammer pressure pulse can be predicted using the Joukowski equation as described previously.

$$\Delta P = k \cdot \rho_L \cdot C \cdot \Delta V$$

The terms in the equation are as described with the exception of the velocity change. As a first approximation, the entire velocity of the advancing water can be assumed to be reduced to zero at impact ($\Delta V = V$). However, the downstream column may also be accelerated by pressure in the void, and the upstream column slowed, as the void compresses. These effects, referred to as "cushioning," reduce the relative velocity and therefore the waterhammer magnitude.

9.2.2 Pressure Pulse Shape

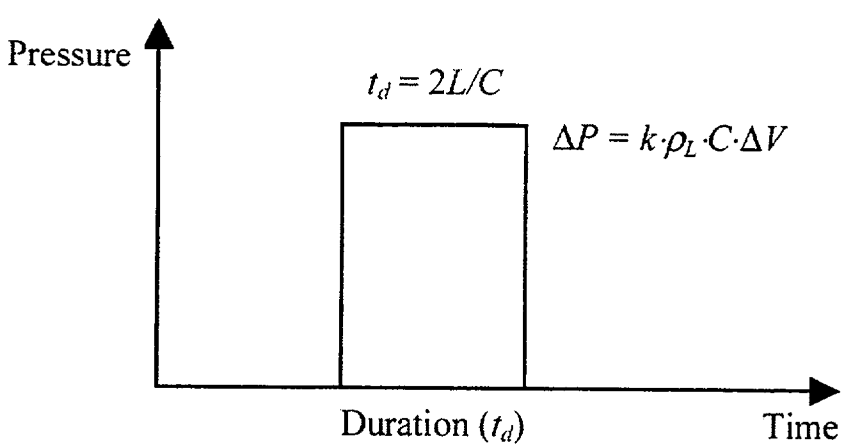

Figure 9-2
Idealized (Square) Pressure Wave

Theoretically, a waterhammer event produces a square wave with a duration t_d based on the water-solid length L through which the wave travels to a reflecting surface and back. For a wave traveling at the sonic velocity C, the duration can be calculated as follows and is shown in Figure 9-1 above:

$$t_d = 2L/C$$

The length of the water column L used to calculate the duration is usually taken as the length back to the nearest free surface as shown in Figure 9-1. The free surface is not able to maintain an elevated pressure, and a rarefaction wave is reflected back through the fluid, reducing the pressure to its value before the transient.

In reality, the analytical square wave model is modified due to several phenomena that are displayed graphically in Figure 9-3. The leading edge of the waveform does not have an instantaneous rise, but has a finite "rise time" over which the pressure magnitude increases from the steady state value to the elevated transient pressure. The initial pressure increase can be attributed to the increase in void pressure as the void compresses due to non-condensable gas or slow steam condensation rates that can contribute to the increase of pressure in the void before column closure. The rise time is particularly important to the structural loading of the piping, since loads are dependent on the slope of the rise.

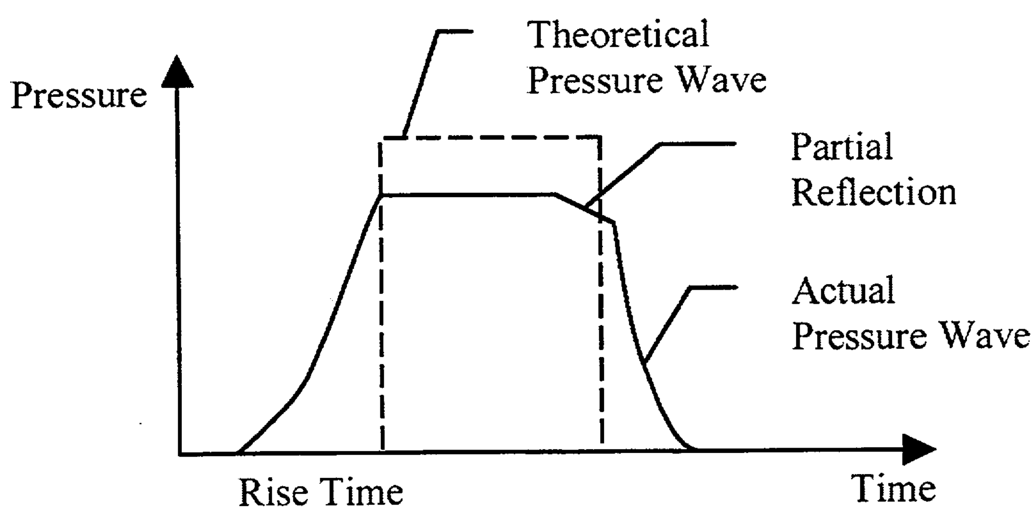

Figure 9-3
Actual Pressure Wave Comparison

The leading and trailing edges of the wave may also be influenced by partial reflections from changes in direction and small voids in the water. The reflection effects may even reduce the maximum pressure attained by the pulse, if rarefaction waves arrive back at the pulse initiation location before the pressure rise is completed. This is described in more detail in Section 9.3.4.

The combination of these "real world" effects can produce a wave that is more trapezoidal than the theoretical square wave. In some cases, a relatively long rise time and short duration will create a triangular pulse.

It is proposed that an appropriate analytical model for the pressure pulse be based on a trapezoidal shape. This simplified form captures the pressure pulse magnitude, duration, and rise time in a more realistic manner than a simple square wave or a triangular wave.

In developing a trapezoidal pulse model, the area of a square wave is conserved, despite the alterations that reduce the peak value and spread the rise and fall times. This means that a square wave, having a height equal to the waterhammer pressure determined using the Joukowski equation and a width equal to $2L/C$, can be used as a starting point. This is shown in Figure 9-4. The area of the square wave should be maintained when the pressure magnitude, duration, and rise or fall times are adjusted.

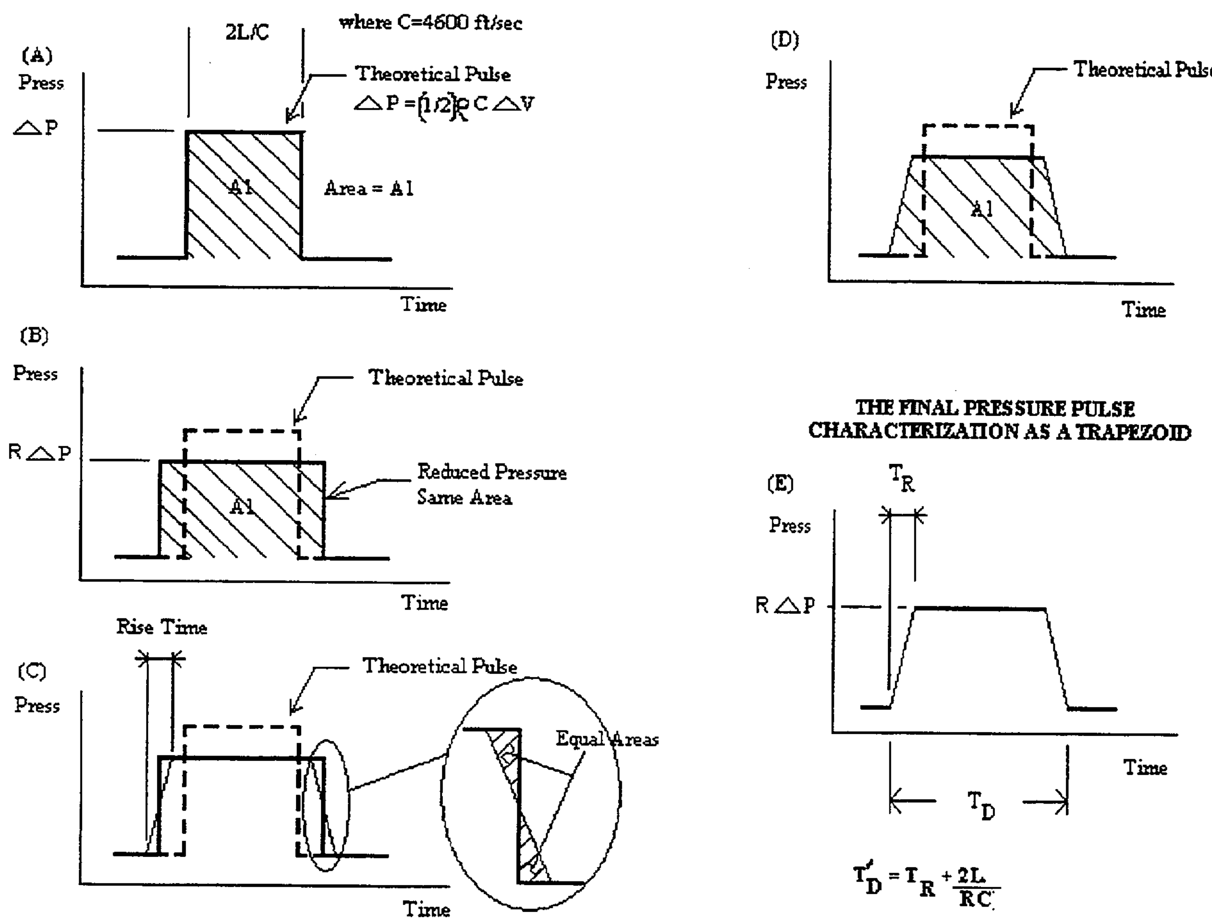

Figure 9-4
Modified Pressure Wave Shape

The area under the pressure-time (P-T) plot is constant for a specific set of conditions because of the momentum equation. The area under the P-T curve (multiplied by the pipe cross sectional area, A) equals the pressure impulse required to cause the momentum change in the fluid. Mathematically,

$$F = m \cdot a = m \cdot dv/dt$$

$$\int F \cdot dt = \int m \cdot dv$$

Since $F = P \cdot A$

$$A \cdot \int P \cdot dt = m \cdot \int dv \qquad \text{(impulse = momentum change)}$$

Therefore, if the peak pressure magnitude is lowered due to cushioning, the duration must increase to maintain the area to satisfy conservation of momentum.

9.2.3 Cushioning and the Effects of Non-Condensables

The Joukowski equation shows that waterhammer magnitude can be reduced by lowering the closure velocity of the water column. Velocity reduction can occur in real column closure events by pressurization of the steam void. The effect of void pressure is to slow the oncoming water column and accelerate the downstream column. As stated previously, this is referred to as "cushioning." Relative velocity is reduced and the peak waterhammer pressure is reduced. Additionally, the "slower" increase in the pressure as the void compresses provides significant additional rise time to the pulse shape. This lowers waterhammer pressure and increases the pulse duration. In some cases, sufficient air mass can result in the refilling water columns not coming into contact and, therefore, not creating a true waterhammer. In these cases, a pressure pulse caused by the gas compression will occur, and this pulse will travel through the piping system.

Pressurization of the void can be caused by two primary effects. These are:

1. compression of released non-condensables that have accumulated in the void, and
2. slow condensation of steam that has accumulated in the void.

9.3 Analytical Modeling

9.3.1 Rigid Body Model Description

The CCWH may be simulated by considering a rigid body as shown in Figure 9-5 below.

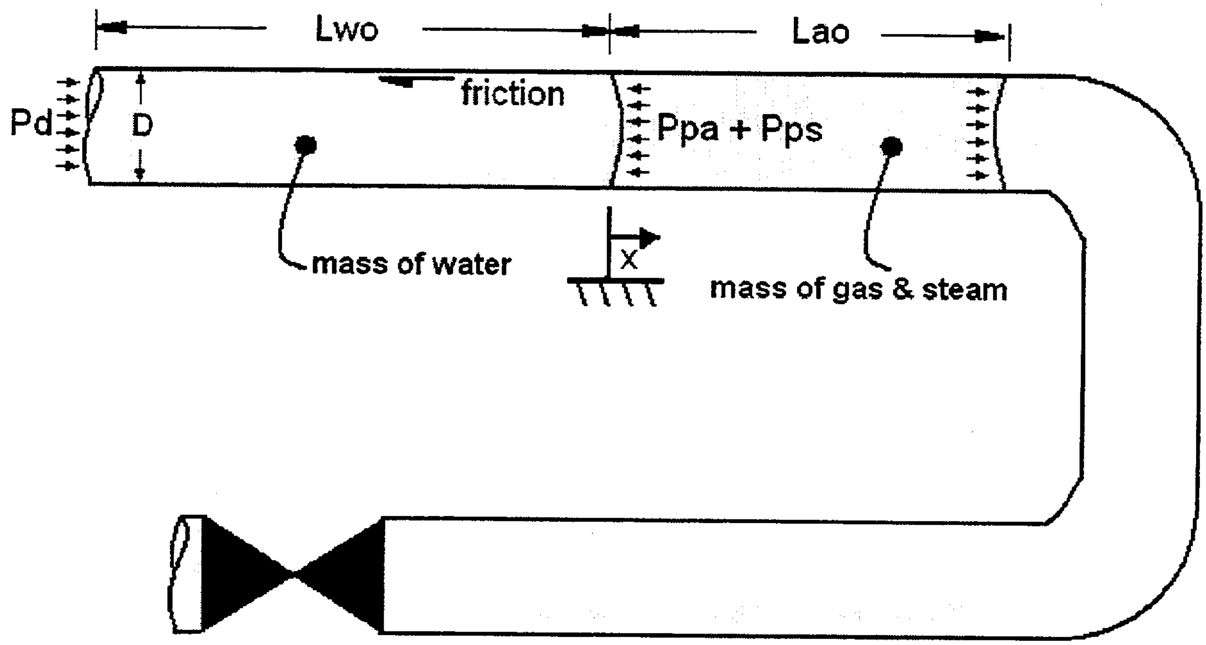

Figure 9-5
Steam/Gas Cushioning Model (downstream column does not move)

The following assumptions are made for this rigid body model:

1. One dimensional model – faces remain planar.
2. Heat transfer occurs from the void to the water, but not to the pipe walls.
3. Velocity of moving slugs of water depends on driving pressure and pressure buildup in gas and steam-filled void.
4. Peak waterhammer pressure is related to Joukowski equation.

The conservatism of these assumptions is described below.

The forces acting on the water slug are summed below:

$$m \cdot a = Pd \cdot A - Ppa \cdot A - Pps \cdot A - friction \qquad \text{9-1}$$

The frictional force is written as:

$$friction = \rho \cdot \frac{f(Lw_o + x)}{2 \cdot D \cdot g} \cdot V^2 \cdot A \qquad \text{9-2}$$

The mass of water that is accelerating into the void is:

$$m = \rho \cdot (Lw_o + x) \cdot A \cdot \frac{1}{g} \qquad \text{9-3}$$

The partial pressure of the gas in the void assumes that the gas acts ideally. The gas is assumed to have a polytropic exponent of 1.3. An exponent of 1 would indicate an isothermal process while an exponent of 1.4 would indicate an isentropic process. The process is expected to be between isothermal and isentropic. An exponent of 1.3 was used in the MOC benchmarking and provided a good correlation between testing and analytical predictions. The air partial pressure is then represented as:

$$Ppa = Ppa_o \left(\frac{La_o}{La_o - x} \right)^{\gamma} \text{ where } \gamma = 1.3 \qquad \text{9-4}$$

The acceleration and velocity terms are given by:

$$a = \frac{d^2 x}{dt^2} \qquad \text{9-5}$$

$$V = \frac{dx}{dt} \qquad \text{9-6}$$

By combining terms, the force summation may then be rewritten as:

$$\rho \frac{(Lw_o + x)}{g} \frac{d^2 x}{dt^2} = Pd - Ppa_o \left(\frac{La_o}{La_o - x} \right)^{\gamma} - Pps - \rho \frac{f(Lw_o + x)}{2 \cdot D \cdot g} \left(\frac{dx}{dt} \right)^2 \qquad \text{9-7}$$

All of the terms here are relatively easy to define except for the steam partial pressure. Steam partial pressure was determined by evaluating the steam condensation. The steam condensation rate was found using the following assumptions:

- Steam was assumed to remain saturated at a quality of 100%.
- Condensing surface temperature was assumed to remain fixed at the initial temperature. For the simulations performed in this report, the surface temperature was fixed at the initial void temperature.
- Steam was assumed to condense only on the available water surface area, the piping surface area was ignored. This is consistent with the conclusion developed in the MOC evaluation.
- The combined *hA* term developed as part of the MOC evaluation in Section 8 was used.

By assuming that the steam remains saturated, the steam partial pressure may then be considered to be a function of the specific volume of the steam. An approximate curve fit of the saturation pressure as a function of steam specific volume was developed using MathCad [33] and the ASME steam tables [25]. The ASME data and curve fit are shown in Figure 9-6. While the curve fit is not an exact solution, it is sufficiently accurate as shown in the comparison to test data (see Section 8.3). The curve fit is accurate for pressures up to approximately 1,000 psia.

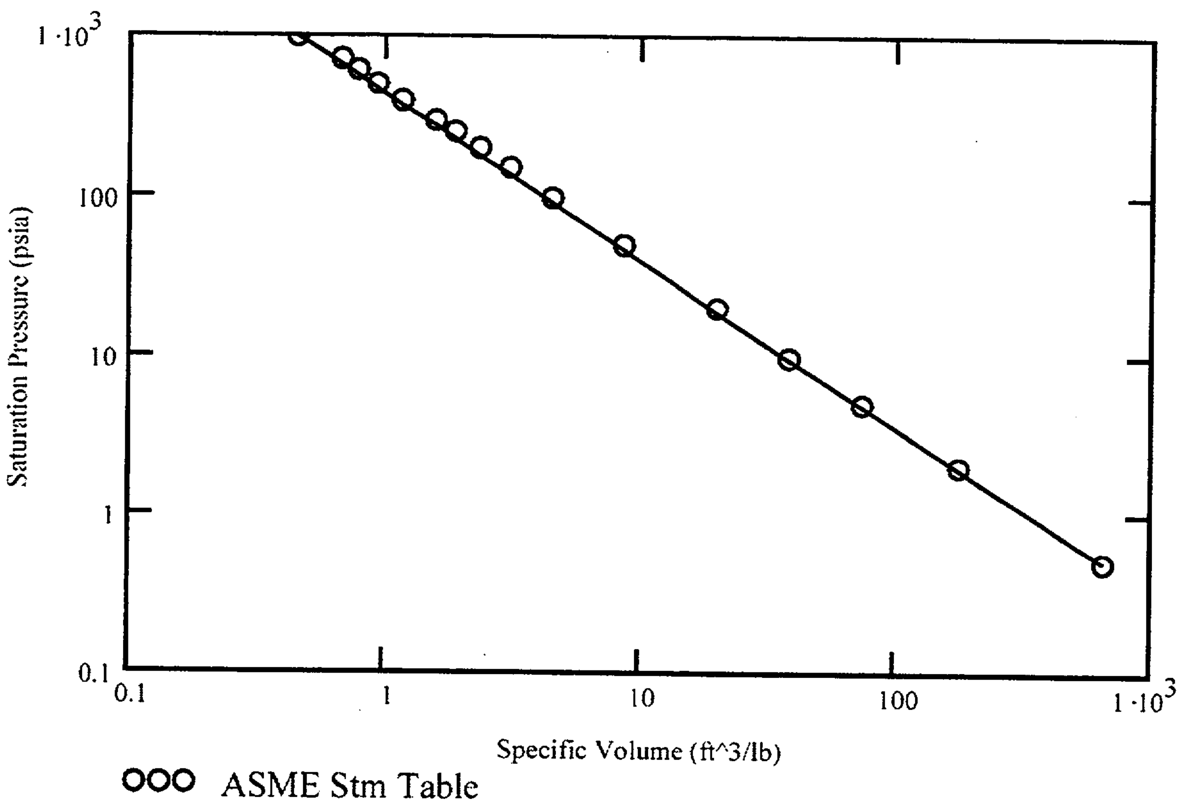

Figure 9-6
Saturation Pressure vs. Steam Specific Volume Curve Fit

The specific volume is the ratio of steam volume to steam mass. The steam partial pressure P_{ps} may be written in terms of the void length La, the flow area A, and the mass of steam in the void m_s:

$$P_{ps} = 10^{2.633 - 1.045 \cdot \log\left(\frac{La \cdot A}{m_s}\right)} \qquad 9\text{-}8$$

The steam mass in the void is reduced as the steam condenses on the available cold surfaces. By considering a heat balance at the condensing surface, the steam condensation rate may be written:

$$\frac{dm_{stm}}{dt} = h_{cds} \cdot A_{cds} \cdot (T_s - T_{stm}) \cdot \frac{1}{h_{fg}} \qquad 9\text{-}9$$

where

T_s = the initial temperature of the condensing surface

In order to relate the force balance differential equation (Equation 9-7) with the heat balance differential equation (Equation 9-9), a relationship between the steam temperature and pressure is needed. By assuming that the steam remains saturated, the temperature can be solved for as a function of the steam pressure. Again a curve fit of ASME Steam Table data was performed using MathCad. The steam table data and curve fit are shown in Figure 9-7. While the curve fit is not an exact solution, it is sufficiently accurate as shown under shown in the comparison to test data (see Section 8.3).

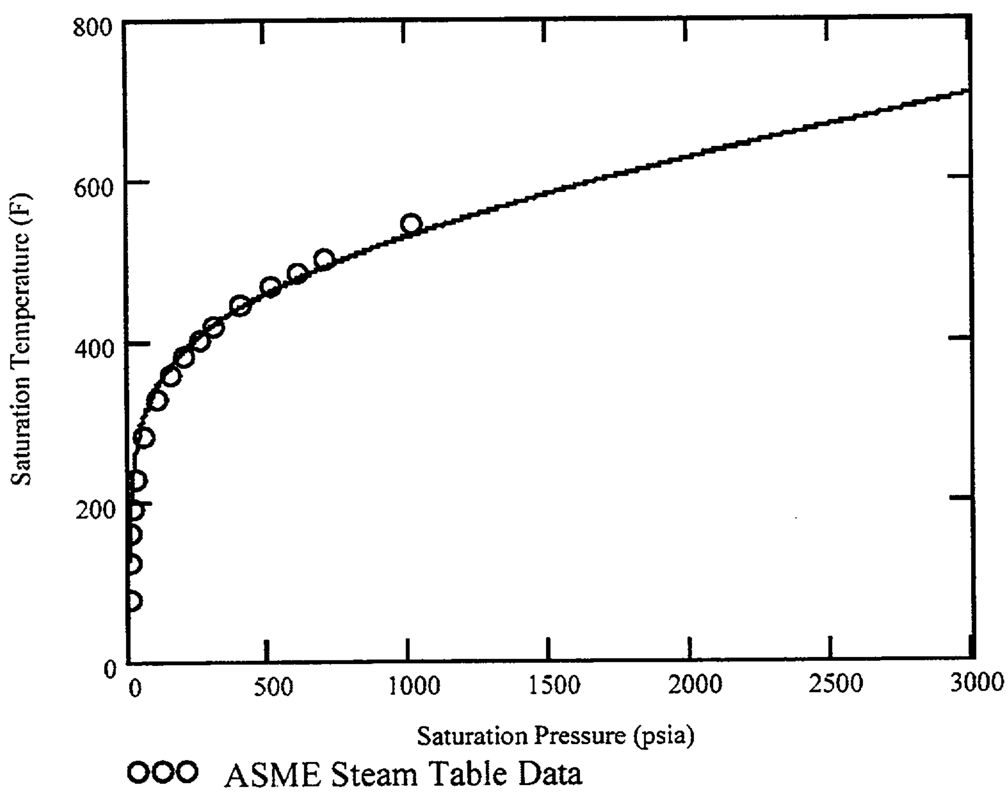

Figure 9-7
Saturation Temperature vs. Pressure Curve Fit

The curve fit equation for saturation temperature T_{sat} as a function of saturation pressure P_{sat} is used to define as the steam condition inside the void ($T_{sat} = T_{stm}$):

$$T_{stm} = 46.042 + 0.055 \cdot P_{sat} + 10.489 \cdot \exp\left(\frac{1}{P_{sat}}\right) + 60.483 \cdot \ln(P_{sat}) \qquad 9\text{-}10$$

In Equation 9-10, temperature is in terms of °F and pressure is in terms of psia. A solution engine that implements a fourth order Runge-Kutta method was applied to solve the simultaneous equations.

A typical set of inputs to the model for two cases is shown in Table 9-1. Case 1 presents a model with both gas and steam cushioning. Case 2 presents a model with gas cushioning only. It should be noted that the steam cushioning was eliminated in the model by setting the steam pressure to a constant value. This method was later changed to eliminate the condensation term and use a constant steam partial pressure of 14.7 psia to simplify the model. Also note that a condensing heat transfer coefficient of 72,000 BTU/hr·ft²·°F was used instead of the 64,000 BTU/hr·ft²·°F determined by use of the MOC code. This increase of approximately 12% was added to provide additional conservatism on the rate of condensing steam in the void. If the steam condenses more rapidly, the pressure pulse will be larger.

Table 9-1
Typical Rigid Body Model Inputs

Input	Case 1	Case 2	Description
P_d	13 psig	65 psig	Driving pressure [fixed]
T_{void}	212°F	212°F	Initial void temperature
T_s	212°F	212°F	Condensing surface temperature [fixed]
x_o	0 ft	0 ft	Initial displacement of accelerating slug
v_o	0 ft/sec	0 ft/sec	Initial velocity of accelerating slug
D	16"	4.5"	Inside pipe diameter [fixed]
wall	0.844"	0.337"	Pipe wall thickness [fixed]
Lwo	100 ft	100 ft	Initial length of accelerating water column
Lao	100 ft	50 ft	Initial length of void
f	0.067	0.25	Friction factor from: $friction = fL/D(V^2/2g)$
m_{air}	4000 mg	1000 mg	Mass of air concentrated in the void [fixed]
ρ	62 lb/ft³	62 lb/ft³	Water density [fixed]
h_{fg}	1150 BTU/lb	1150 BTU/lb	Latent heat of vaporization [fixed]
C	4428 ft/sec	4549 ft/sec	Sonic velocity of water
γ	1.3	1.3	Polytropic expansion coefficient for gas
Hz	4000 Hz	4000 Hz	Solution frequency
h	72,000 BTU/hr·ft²·°F	constant steam pressure	Condensing heat transfer coefficient
A	2 x 1.396 ft²	2 x 0.11 ft²	Condensing surface area

At approximately 7.5 seconds, the final void closure occurs with a resulting peak in pressure. For this configuration, the resulting pressure could achieve an unrealistically high value since water compressibility is not simulated in the above equations. The limit on the void pressure is defined by the Joukowski equation. When this limit is imposed on the solution outputs and the time scale is reduced, then the final pressure output is as shown in Figure 9-8.

Figure 9-8
Case 1 Void Pressure (psig) vs. Time (sec)

At approximately 4.7 seconds, the final void closure occurs in Case 2 with a resulting peak in pressure. Similarly to Case 1, the resulting pressure could achieve an unrealistically high value since water compressibility is not simulated in the above equations. The pressure is limited to that calculated using the Joukowski equation and the pressure output is shown in Figure 9-9.

The solution method described above provides appropriate predictions of waterhammer pressures and rise times for cases where rarefaction wave effects are not significant. If a negative rarefaction wave returns to the initiation point before the pulse peaks then the RBM simulation results in an over-prediction of the peak pressure.

Figure 9-9
Case 2 Void Pressure (psig) vs. Time (sec)

9.3.2 Rise Time Prediction

The rate of pressure increase during the waterhammer event can have a significant effect on the peak pressure pulse magnitude and on the unbalanced loads in piping segments. The peak pressure will be reduced by reflections from area expansions if the rise time is long compared to the pressure wave transit times to area change locations. Unbalanced loads on piping will be reduced if the distance occupied by the rising pressure wave is long relative to the length of a piping segment.

Pressure pulse rise time is affected by the driving pressure, relative lengths of the water column and void, rate of condensation, and amount of gas in the void. The rigid body model was used to predict the pressure pulse rise times. They are plotted in Figure 9-10 for several parametric variations, using only air cushioning. To simplify this prediction, a conservative bounding function was devised to fit the predictions based on the impact velocity. The impact velocity was chosen as the independent variable because it integrates the net effects of the driving pressure, lengths, condensation, and gas.

The bounding function that was developed is based on the rise time being inversely proportional to a function of impact closure velocity *V*. The constant for the function was developed from comparison to RBM results for a range of cases (Figure 9-10) and to actual test data (Figure 10-8 in Chapter 10) and is presented as Equation 9-11.

$$t_r = 0.5 \cdot V^{-1.3} \qquad \text{9-11}$$

It can be seen that significant margin exists between the bounding curve and many of the individual RBM rise time predictions. Bounding the individual RBM runs on the "low side" of the curve results in a more rapid rise time, which will be conservative for evaluation of piping systems.

Figure 9-10
Rise Time vs. Impact Velocity

9.3.3 Duration

A method is described here to define the pressure pulse duration. A pressure wave will travel from the origination point, through the piping system, and reflect as a partial rarefaction wave as it passes area changes. Free surfaces will provide 100% reflection. The net effect of many partial reflections from area changes will be to eventually return the pressure pulse to the system pressure. The time it takes for the pressure pulse to return to the system pressure is the pulse duration.

The approach described herein uses a value of 90% of the pulse reflected back to the origination point to define the return of the pressure to its undisturbed state. Stated in terms of the transmission coefficient (*Tau* or τ, see also Section 12), which is the ratio of the transmitted pulse to the incident pulse, 90% reflection would produce a transmission coefficient of 10%. The distance the pulse travels to reduce the transmitted pulse by 90% can be converted to pulse duration by knowing the velocity of the traveling pulse, which is the sonic velocity. The value of 10% transmission has been selected based on the test program modeling. In the test program, the rise time for a particular pressure pulse was defined as the time from 10% of the peak value to the peak. The lower 10% of the pressure pulse was found to not significantly affect the pulse duration.

To find the pulse duration, τ is calculated for each successive area change moving away from the initiation point until τ is less than 0.1. The distance L_{dur} is defined as the length of piping that defines the pulse duration. The pulse duration t_d is then calculated from:

$$t_d = 2 \cdot \frac{L_{dur}}{C} + t_r \qquad \text{9-12}$$

A trapezoidal representation is used to define the pressure pulse. The entire pulse is shown in Figure 9-11 below. The total duration for the trapezoidal pulse is calculated as the time it takes the pulse to travel to the $\tau = 10\%$ location and back plus the rise time (half the rise time on the front end and half on the back end).

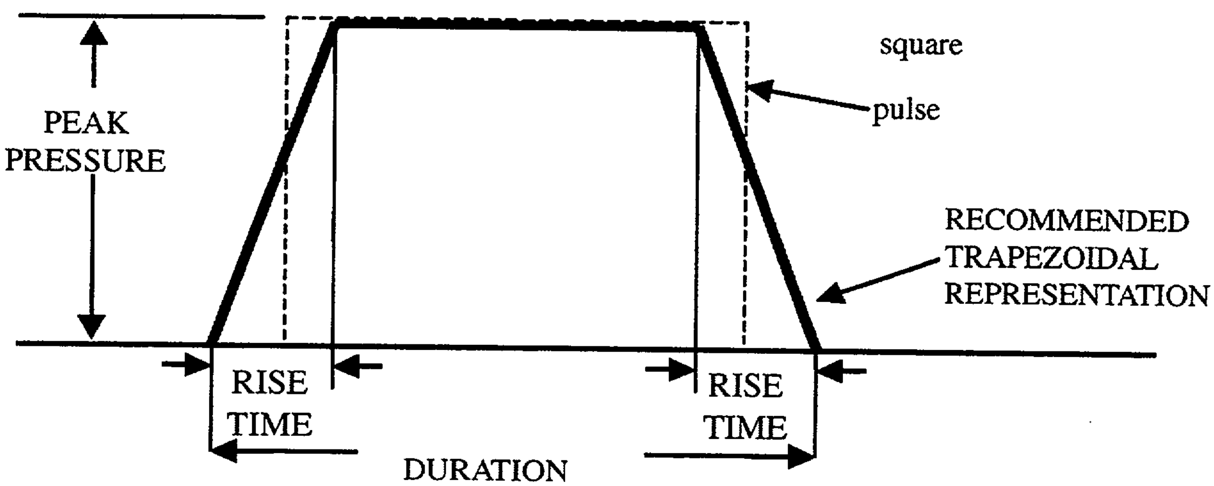

Figure 9-11
Duration Definition and Trapezoidal Representation

9.3.4 Peak Pulse "Clipping"

The peak pressure pulse may be affected positively or negatively by reflections. A method of evaluating the effects of reflections on the pressure pulse magnitude is described below.

During a column closure event, the pressure rises as the void closes. This rising pressure travels upstream and downstream from the closure location. As the pulse encounters area changes, a reflected wave travels back toward the closure location. The reflected wave will add to the pressure it encounters. If the reflection comes from an expansion, then it will have a negative magnitude and cause the oncoming pressure to be reduced. The peak pressure will be "clipped" if the reflection reaches the closure location before the pressure peaks. Similarly, if the pressure wave encounters a reduction in area while it is rising in magnitude, then a positive wave is reflected and the peak pressure may be increased.

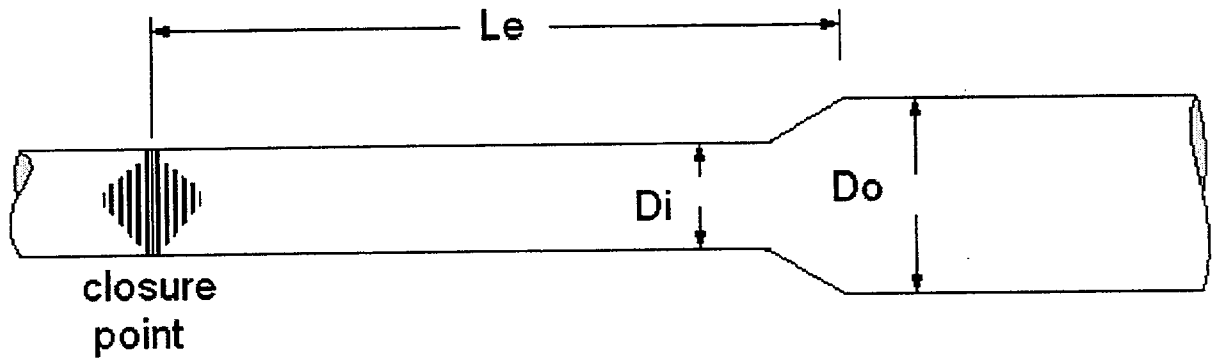

Figure 9-12
Pressure Peak Clipping Due to Reflection

The transmission coefficient associated with the reflection point of concern is defined as:

$$\tau = \frac{P_{trans} - P_{sys}}{P_{inc} - P_{sys}}$$

The calculation of transmission coefficients τ based on piping geometry is provided in Section 12. The transmitted and reflected pressures associated with the interaction at the area change are defined as:

$$P_{tran} = \tau \cdot (P_{inc} - P_{sys}) + P_{sys}$$

$$P_{ref} = (\tau - 1.0) \cdot (P_{inc} - P_{sys}) + P_{sys}$$

When the reflected pressure reaches the point of pulse initiation then the new pressure that propagates from the closure point will be (written as a function of time):

$$P_{new}(t) = P_{inc}(t) + P_{ref}(t - 2L_{ref}/C)$$

where:

$P_{new}(t)$ = the new pressure at the closure point at time t

$P_{inc}(t)$ = the pressure at the closure point without considering reflections at time t

$P_{ref}(t - 2L_{ref}/C)$ = the reflected pressure from the area change at time $t - 2L_{ref}/C$

L_{ref} = the distance from the initiation point to the reflection of concern

In terms of only the incident pressure and the transmission coefficient, the new pressure at the initiation point is:

$$P_{new}(t) = (\tau - 1) \cdot P_{inc}(t - 2L_{ref} / C) + P_{inc}(t) \quad 9\text{-}13$$

For trapezoidal shaped pulses, the equation for P_{new} was solved for a series of transmission coefficients and a pulse with a 0.0125-sec rise time. The ratio of the peak interaction pressure P_{new} to the peak incident pressure P_{inc} was plotted as a function of the length between the closure point and the reflection point. The plot is shown in Figure 9-13, and the figure presents a graphical solution to a specific case of the general solution presented in Table 9-2.

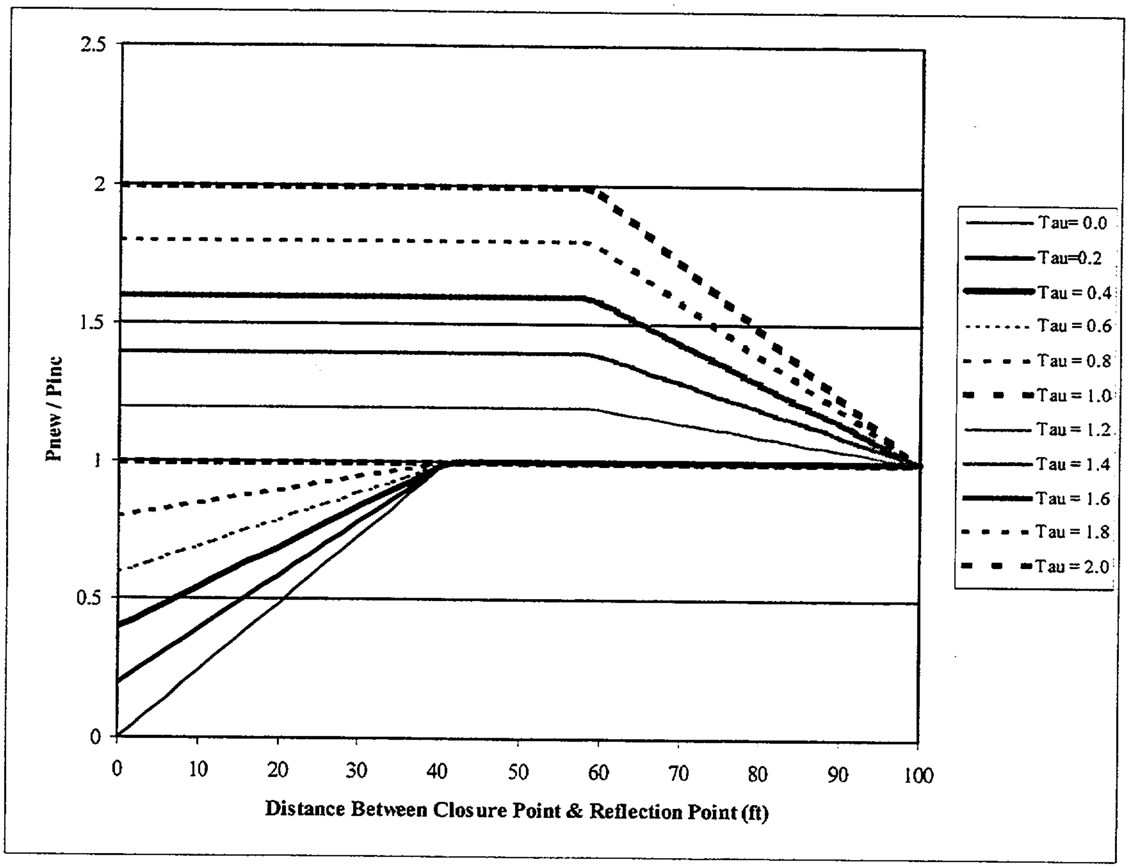

Figure 9-13
Peak Clipping

(Note: This chart applies to 10" pipe, t_r = 0.0125 sec, 100 ft = (duration × $C/2$), trapezoidal shape; equations in this section may be used to determine pressure interaction ratio for other trapezoidal shaped pulses.)

As expected, P_{new} is less than P_{inc} for cases where:

- The pulse is incident upon a larger area ($\tau < 1$).
- The distance between the reflection point and the initiation point is smaller than the distance the pulse can travel in half the rise time.

Also as expected, P_{new} is greater than P_{inc} for cases where:

- The pulse is incident upon a smaller area (τ>1)
- The distance between the reflection point and the initiation point is smaller than the distance the pulse can travel over half its duration.

The relationships provided in Table 9-2 may be used to determine the percent increase or decrease in the pressure pulse as a result of reflections from area changes for any trapezoidal pulse:

Table 9-2
Reflection Effects

Transmission Coefficient & Reflection Length	Pressure Interaction Ratio
$\tau < 1$ and $0 < Le < t_r \cdot C/2$	$\frac{P_{new}}{P_{inc}} = \frac{1-\tau}{t_r \cdot C/2} \cdot Le + \tau$
$\tau < 1$ and $t_r \cdot C/2 < Le$	$\frac{P_{new}}{P_{inc}} = 1$
$\tau > 1$ and $(t_d - t_r) \cdot C/2 < Le < t_d \cdot C/2$	$\frac{P_{new}}{P_{inc}} = \frac{1-\tau}{t_r} \cdot (2Le/C - t_d) + 1$
$\tau > 1$ and $Le < (t_d - t_r) \cdot C/2$	$\frac{P_{new}}{P_{inc}} = \tau$
$\tau > 1$ and $(t_d) \cdot C/2 < Le$	$\frac{P_{new}}{P_{inc}} = 1$

9.4 Model Benchmarking

9.4.1 Comparison Against Method of Characteristics

The rigid body model was compared against the MOC to validate the rigid body model's ability to predict the peak waterhammer pressure and the rise time associated with the waterhammer. In order to provide an appropriate comparison, it was necessary to ensure that the cases being studied would not be influenced by rarefaction waves while the pressure pulse was developing. The case simulated is shown in Figure 9-14.

Numerous cases were run to compare the MOC and RBM solutions as shown in Table 9-3. Two specific cases are described in detail, and these correspond to the Case 1 and Case 2 problems described previously (see Table 9-1). Figure 9-15 and Figure 9-16 show the pressure transient from the RBM and from the MOC code for Cases 1 and 2 respectively. The MOC code inputs included a long length of piping (> 500 ft) downstream of the void with a closed end. This prevented the downstream water from moving during the closure and prevented rarefaction waves on the downstream side of the void from interfering with the pulse magnitude.

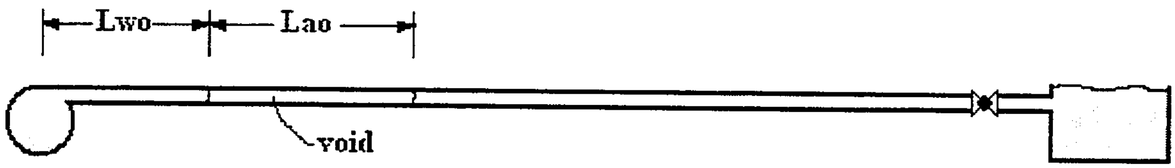

Figure 9-14
RBM / MOC Comparison Configuration

Figure 9-15
Case 1 RBM / MOC Comparison

The RBM peak pressure for Case 1 is quite close to the peak pressure from the MOC code. The start times for these transients were arbitrary. The difference in magnitude between the RBM and MOC predictions is more pronounced in Case 2. The time for the pressure to rise to its peak value (rise time) is longer in Case 2 than Case 1. The pressure in Case 2 is clipped by rarefaction waves returning from the free surface before the pressure peaks.

Figure 9-16
Case 2 RBM / MOC Comparison

Similar runs were performed for other configurations with 4" and 16" piping. The driving pressures, void sizes, and air contents were varied to cause different pressure pulse characteristics. If the rise time is short relative to the time for the pulse to reach the free surface and return then reflection effects will be small. Inputs were therefore selected to cause short rise times.

Summaries of the results of the RBM and MOC code comparison are provided in Figure 9-17 and Figure 9-18. Figure 9-17 compares the peak pressure magnitude for these two methods. Figure 9-18 compares the rise time. A summary of the inputs/outputs for these runs is shown in Table 9-3.

Figure 9-17
RBM / MOC Pressure Comparison (psig)

Figure 9-18
RBM / MOC Rise Time Comparison (sec)

It is apparent from Figure 9-17 that the rigid body model over-predicts the peak void pressure when compared with the MOC code. The differences between the MOC and RBM runs are explained by the following:

1. Even though the conditions were selected in an effort to minimize reflections, some reflections still occurred. For the 100-ft long void cases, the pressure takes approximately 0.09 sec to travel from the closure point and return. For the 50-ft long void scenarios, the pressure transit time is approximately 0.07 sec. Five of the ten runs have a difference in peak pressure greater than 5%. Of those five cases, at least three have some clipping due to reflections. There may be clipping effects in others runs that are not identified here because of the numerical approximation technique used to define the rise time. This clipping accounts for a majority of the differences between the MOC and RBM simulations.

2. The RBM applied curve fit approximations for water properties while the MOC code interpolated values from steam tables. The RBM curve fits tended to under predict the steam saturation pressure at low pressures by 1 or 2 psi. This provided a slightly greater differential pressure when the slug began accelerating. The differences in steam properties also contribute to the differences between the MOC and RBM models.

The RBM simulation provides a conservatively high prediction of the peak waterhammer pressure pulse when compared against the MOC simulation for these conditions where the reflections reduce the pulse magnitude.

The codes also differ in their prediction of rise time. This is because of the numerical method used to approximate the rise time for the MOC code pressure pulse. It is apparent from Figure 9-15 and Figure 9-16 that both codes result in similar pulse slopes. The rigid body model results in shorter rise times than the MOC code. A short rise time is typically conservative since there is less time for reflections to occur and to clip the peak pressure. In addition, short rise times make the pulse approach a square wave shape. Square wave shapes result in larger dynamic loads on the system and are therefore conservative when compared against triangular or trapezoidal shaped pulses.

Table 9-3
Summary of RBM / MOC Comparison Runs

9.4.2 Comparison to Test Data

For configuration 2a, the rigid body model was run with the conditions of the two driving air pressures and for dissolved oxygen concentrations ranging from 0 to 10 ppM. The RBM predictions are presented as open triangles and open circles for the 30-psig and 45-psig driving air pressures, respectively. Linear curve fits to the model prediction data are presented as dashed lines with the linear equation towards the right side of the plot. The method used to predict the mass of dissolved air in the void for configuration 2a (see Chapter 10 for description and test data) considers all the dissolved air released from the piping from the valve to the steam void (approximately 6' of 2" pipe for configuration 2a). This water would be heated to the boiling point and held there for several minutes. By this method, approximately 17 mg of air was calculated to be released into the void for every 1 mg/L of dissolved oxygen in the water.

It can be seen that the RBM generally represents the test data, but more closely captures the behavior for the water column driven by the 30-psig pressure. The differences in the analytical model predictions and the test data are due to the difficulties in determining exactly how much air is in the void and the effects of reflected waves which are not accounted for in the RBM. Void air content varies with the mass of water boiled and condensed, and the concentration of dissolved air in the water. The water dissolved air concentration and void size were controlled, but the void size was set by boiling more than was required and condensing back to a desired size. This contributed to variability in the actual void air concentration and scatter in the 2a test data. The RBM lines on Figure 9-19 show conservative peak pressures except for two data points.

Figure 9-19
Effects of Non-Condensables – Configuration 2a

For configuration 2b, the rigid body model was run with the conditions of the two driving air pressures and for dissolved oxygen concentrations ranging from 0 to 10 ppM. The RBM predictions are presented in Figure 9-20 as open triangles and open circles for the 20-psig and 70-psig driving air pressures, respectively. Linear curve fits to the model prediction data are presented as dashed lines with the linear equation towards the right side of the plot. The method used to predict the air release for configuration 2b was to consider the same piping from the valve to the steam void (approximately 10' of 2" pipe for configuration 2b), but to only release 40% of the dissolved air from the mass of water in these pipe sections. This was justified by the test procedure that brought this water to the boiling point for only enough time for the void to form in the top horizontal pipe. The air release was an appropriate value based on other testing to estimate air release in a system brought to the saturation point. By this method, approximately 12 mg of air was calculated to be released into the void for every 1 mg/L of dissolved oxygen in the water. It should also be noted that the configuration 2b water column (the mass of water used to close the steam void) was approximately 30 feet in length and that of configuration 2a was only 9 feet. The combination of the small air amount in the 2b void and the much larger water mass accelerated into the void – compared to configuration 2a – greatly reduced the effects of air in the steam void. It can be seen that the configuration 2a waterhammer is affected by the amount of air in the water and therefore in the void, while the configuration 2b model is not significantly affected. However, the RBM presents a reasonable and conservative model of the test data.

Figure 9-20
Effects of Non-Condensables – Configuration 2b

9.4.3 Rigid Body Model Comparison Against MOC and Test Data

The test configurations were analyzed in the rigid body model and the MOC model. In all cases, the RBM over-predicted the pressure pulse magnitudes. A comparison of testing and RBM runs and MOC analysis is shown below in Table 9-4.

Table 9-4
RBM and MOC Comparison Against Test Data

The MOC code properly simulates the effects of air, steam, and wave propagation when compared against the test data. The RBM was shown to properly simulate the effects of air and steam by comparison against the MOC code for cases where wave propagation effects do not significantly influence the peak pressure. The RBM was shown to over-predict the test data. It is therefore concluded that the rigid body model is an appropriate tool for conservatively predicting the magnitude and rise time of column closure waterhammers provided the reflection criteria are satisfied.

9.4.4 Rigid Body Model Limitations

The comparison between the rigid body model and previously benchmarked MOC code indicates that the RBM provides an appropriate tool for predicting the pressure pulse magnitude (see Section 9.2.1) and rise time (see Section 9.3.2). Consideration for potential positive reflected waves must be given as described in Section 9.3.4.

Plant conditions that fall within the following limits are bounded by the RBM runs performed and summarized in the User's Manual.

Table 9-5
Rigid Body Model Analysis Limits

Variable	Requirement	Basis
Water Column Size	$Lwo_{RBM} \geq Lwo_{plant}$	The RBM runs bound shorter slug lengths.
Void Length	$Lao_{RBM} \geq Lao_{plant}$	The RBM runs bound shorter void lengths.
Initial Velocity	$V <\sim 20$ ft/sec	The RBM was verified up to 30 ft/sec. Curves are provided for velocity 10, 15, and 20 ft/sec.
Gas Content	$Mgas > 60$ mg $(ID/2)^2$ (ID in inches)	A minimum amount of gas is required to apply the fixed *hA* found in the test data. This amount is related to the square of the pipe diameter.
Void and Interface Temperature	Void Temp ≥ 200°F Void Temp < 200°F	Consider air and steam cushioning. Consider air cushioning only.

10

COLUMN CLOSURE WATERHAMMER – TEST DESCRIPTION AND RESULTS

Column closure waterhammer tests were performed under controlled laboratory conditions which simulated critical components of the transient events. These data were used to develop analysis methods that consider cushioning and to benchmark the analytical models described in the previous two sections.

10.1 Test Configurations 1, 2a and 2b

Several different pipe configurations were used to produce column closure waterhammer data. The configurations are referred to as configuration 1, configuration 2a, and configuration 2b. Descriptions of the test configurations, procedures, and results are provided in this section.

This test piping was designed to produce column closure waterhammer events utilizing a water column driven by compressed air. Two interchangeable test sections were designed to fit into the test piping. The first configuration (configuration 1) featured a test section into which steam was introduced from an outside source, which permitted independent control of the steam and the water conditions. The second configuration (configuration 2) featured a test section in which steam was created by boiling water in a portion of the test pipe. This configuration used the same water which was boiled to subsequently close the steam void. Illustrative drawings are provided in Figure 10-1 and Figure 10-2.

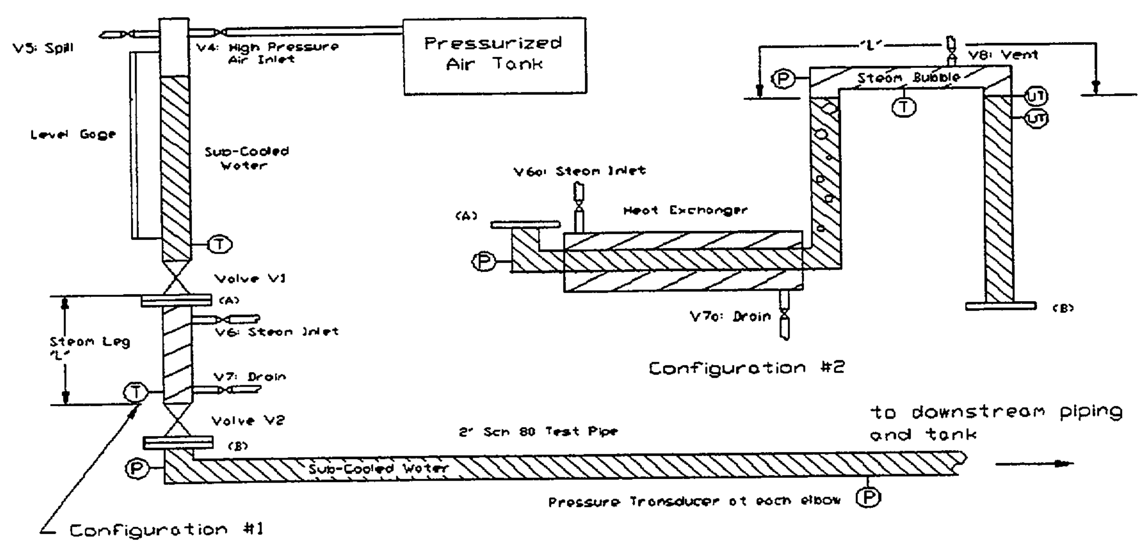

Figure 10-1
Schematic of Configurations 1 and 2 Test Piping

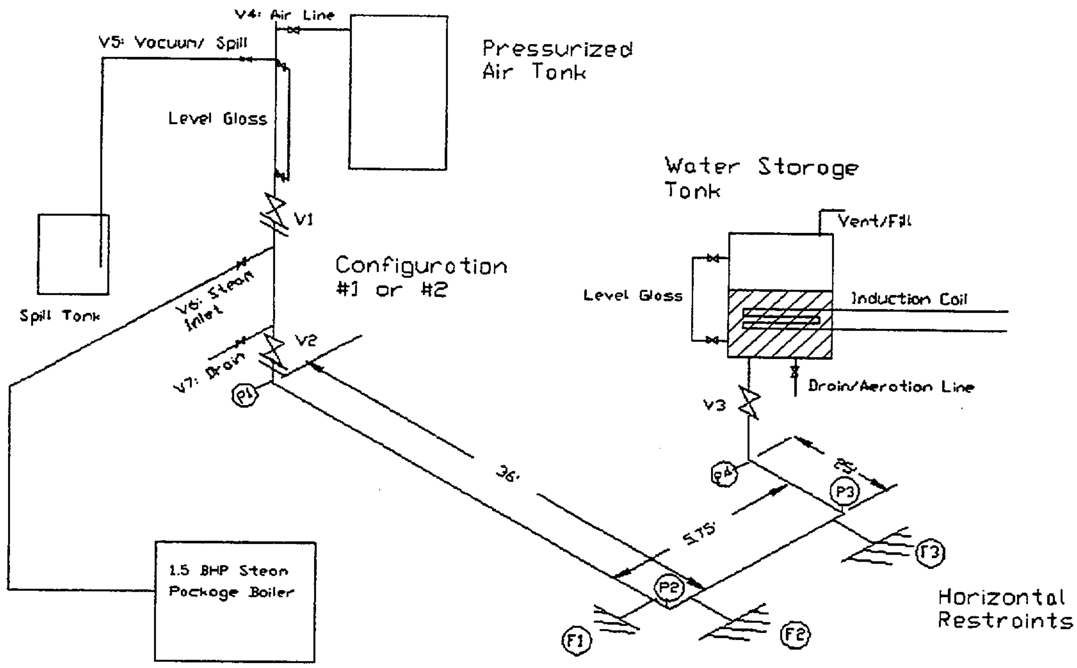

Figure 10-2
Isometric of Test Piping with Configuration 1 Installed

Configuration 1 investigated waterhammer without the mitigating effects of air in the void, since the steam supplied to the void was free of non-condensable gases. The more controlled waterhammers in configuration 1 produced valuable data for evaluation of piping and support responses. Piping structural response is described in Section 13.

Configurations 2a and 2b allowed for the study of the effects of the water conditions in the pipe on the produced waterhammer. The piping in the configuration 2 testing featured a heat exchanger consisting of an 8" pipe jacketed around the 2" test pipe. Configurations 2a and 2b consisted of two test sections, which differed in the size of the heat exchanger and heat-up sequence. The 8" pipe was supplied with steam, and this arrangement induced boiling and void formation in the 2" test pipe. The two configurations were interchangeable in the overall test assembly using flanged connections (A) and (B) as shown in Figure 10-1.

The configuration 2 piping was configured to simulate the conditions introduced in service water systems and FCUs subjected to external heating. In configuration 2 tests, the steam voids are created by boiling water in the pipe and allowing the bubbles to rise. The voids accumulate above the region of heating, typical of power plants. When pump power is restored, the water will refill the pipe and create column closure events.

The piping system consisted primarily of 2" schedule 80 pipe, with a waterhammer producing section isolated by ball valves. Downstream of the waterhammer section, the outlet piping ran approximately 70 feet through a series of elbows to a vented tank.Figure 10-2, the isometric drawing of the test loop, shows the overall layout of the system. Note that the piping downstream of pressure transducer P4 to the tank is not drawn to scale. The long runs of pipe allowed for the pressure wave to fully develop and impact each elbow. The transient forces in the pipe supports were measured, which allowed comparison to analytical prediction methods for support loads.

10.1.1 Configuration 1 Description

A more detailed drawing of the configuration 1 test section is presented in Figure 10-2 and Figure 10-3. Waterhammers were created in configuration 1 by introducing and then collapsing a steam void in the portion of pipe between valves V1 and V2.

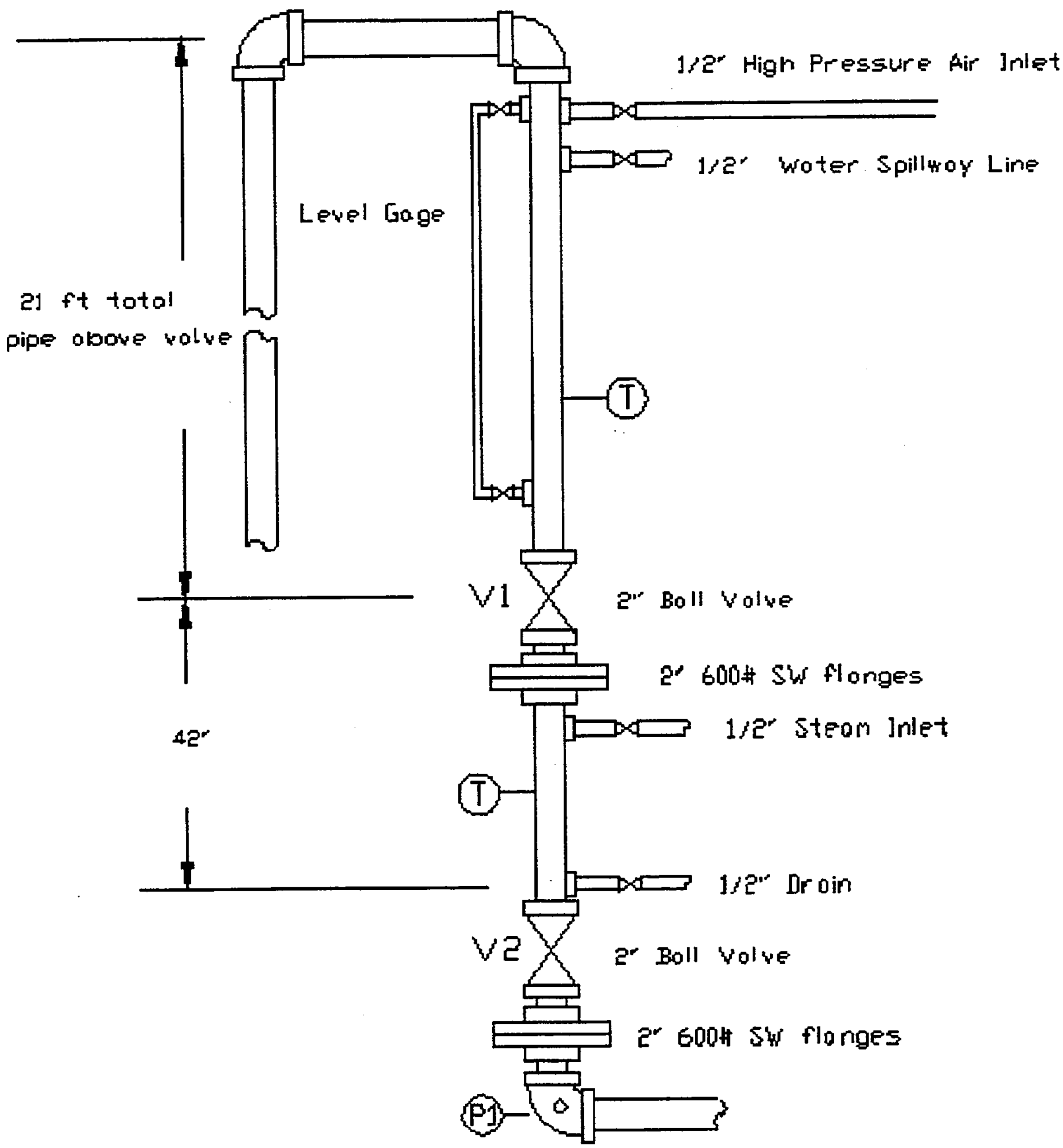

Figure 10-3
Configuration 1 Test Section

The test procedure consisted of filling the column to a specific height as observed in a sight glass, and isolating the test section by closing valves V1 and V2. V1 and V2 were air-driven rapidly opening ball valves (approximately 0.135 sec were required to open the valve). Steam was introduced into the test section by opening a 1/2" inlet and drain for several minutes. The steam was isolated and the test was initiated by opening valve V2 and then opening valve V1 approximately 0.5 sec later. The vertical column of water was driven into the void upon opening V1, and the steam void collapsed. This method produced repeatable, controlled waterhammers.

Steam was provided to the test section using a 1.5 BHP electric steam boiler, set to provide steam at approximately 5 psig. The steam inlet and outlet to the test section were controlled using 1/2" steel ball valves.

10.1.2 Configurations 2a and 2b Description

Steam voids were created in the configurations 2a and 2b piping by boiling the fluid in the pipe. This was accomplished by introducing steam into a heat exchanger jacket around the test pipe. Steam was supplied from a 1.5 BHP boiler, set to approximately 12 psig. Configurations 2a and 2b were inserted into the same test piping used for configuration 1 by replacing the piping between the flanged connections (below V1 and below V2) with either of the new test sections.

The test procedure consisted of filling the column to a specific height observed in the sight glass, venting the test section, and isolating the test section by closing valve V1. Steam was created in the test section by heating the jacket with boiler steam. Boiling was allowed to occur in the test pipe until the level sensors on the downstream leg of the configuration 2 loop showed that the steam void had emptied the pipe past that point. This steaming process took approximately five minutes. The steam void was monitored using the ultrasonic (UT) level gages on the downstream leg of the loop. Due to fluctuation in the water/steam interface level, the void was allowed to condense until the lower of the two level gages indicated the pipe was water solid and the higher was alternating wet/dry. At this point the test was initiated. The test section of pipe was sloped away from valve V1 to cause the steam void to form at the top of the pipe loop. When V1 was opened, the incoming water collapsed the steam void and produced a waterhammer.

Configurations 2a and 2b were similar configurations but had some geometrical differences, including the length of the steam void section ("L" inFigure 10-4). The configuration 2a steam void was approximately 35" in length. The configuration 2b steam void was approximately 108" in length. Configuration 2b also used a longer water column (20 feet upstream of valve V1) and was supplied with driving air pressure using a larger 1" ID hose. The steam void position was monitored in configuration 2b using a sight glass and not ultrasonic level gages.

Another difference in the configurations 2a and 2b testing was the boiling sequence. The 2a system was heated until the steam progressed past the UT level sensors and condensed back to the void length desired. The 2b configuration, utilizing sight glasses to monitor the void, was only boiled until steam void grew to the desired void length. The process used for introducing steam into the configuration 2a void should have increased the amount of air in the void relative to the void size as compared to configuration 2b.

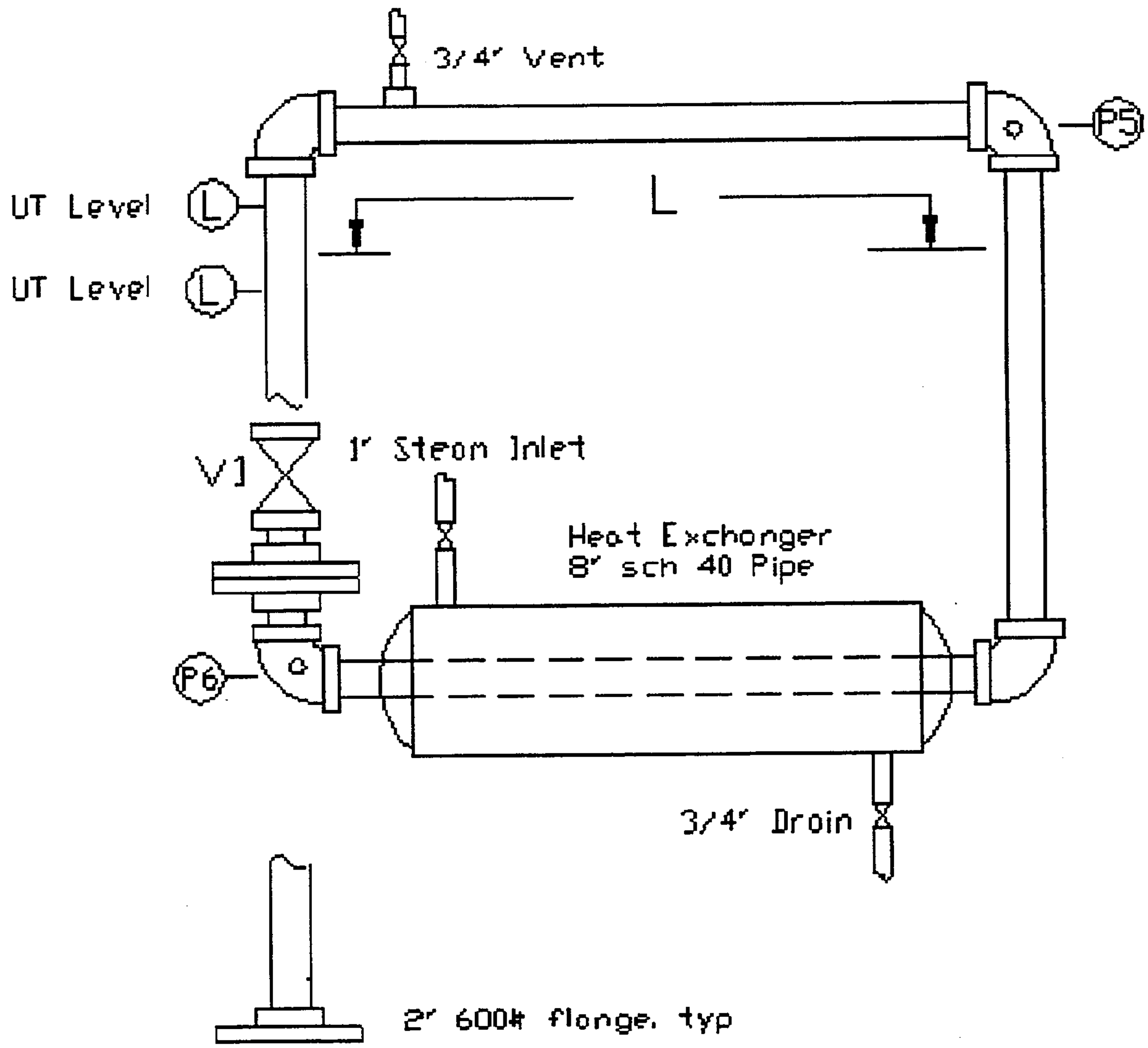

Figure 10-4
Configurations 2a and 2b Test Section

10.1.3 Comparison of the Configurations 1, 2a and 2b Tests

A summary comparison of the three test configurations is presented in Figure 10-5, which is a diagrammatic representation of the test geometry and conditions in one dimension.

The configuration 1 tests used driving pressures of 15, 30 and 45 psig to accelerate water column lengths of 36", 68", 204", and 240" into a pure steam void.

The configuration 2a tests used driving pressures of 30 and 45 psig to accelerate a 108" (36" + 72") water column into a steam void created by boiling a 72" length of water for 3-5 minutes. The resulting 87 mg of air in the void is an average value for a range of deaerated, normal, and aerated water used in the test.

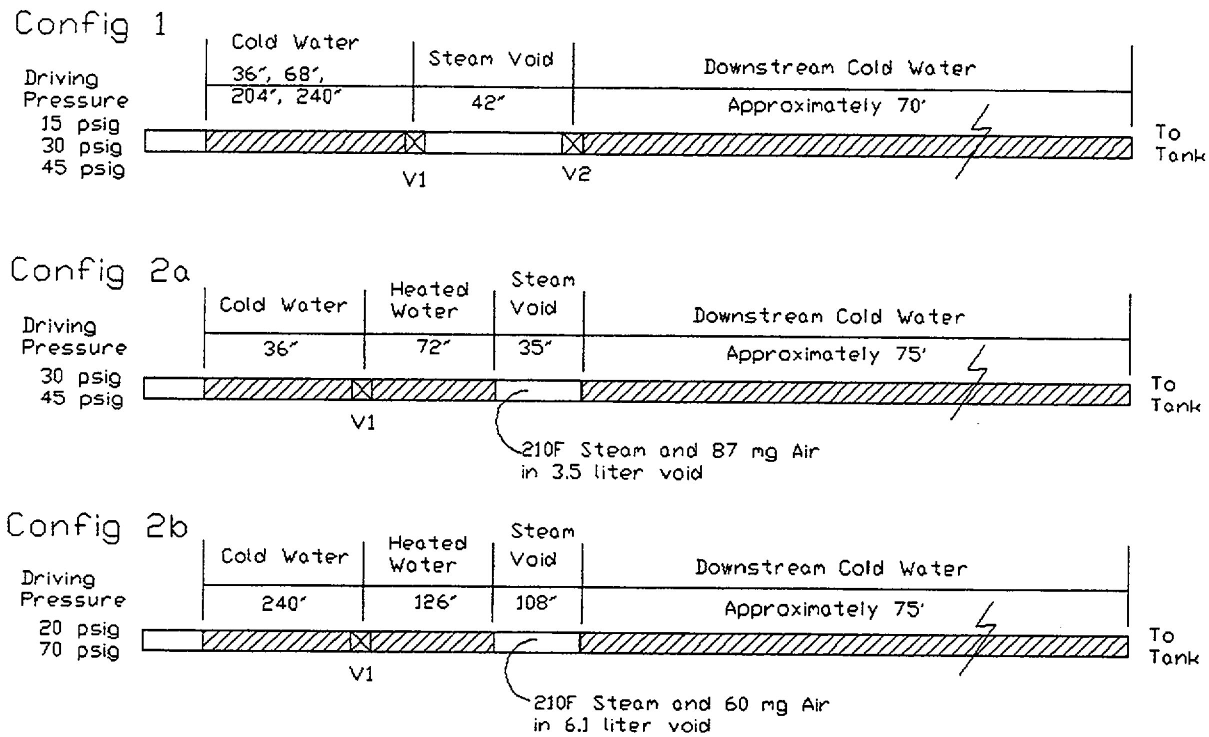

Figure 10-5
Comparison of Configurations 1, 2a, and 2b

The configuration 2b tests used driving pressures of 20 and 70 psig to accelerate a 366" (240" + 126") water column into a steam void created by boiling a 126" length of water for several minutes. The resulting 60 mg of air in the void is an average value for a range of deaerated, normal, and aerated water used in the test.

Test matrices and complete test listings are provided in Sections 10.6 and 10.7.

10.2 Test Equipment

10.2.1 Valves

The main valves controlling the fluid in the test section were operated automatically using piston type air operators. An internal rack and pinion provided the 90° turn motion required to close the valves. These operators featured springs to allow the valve to fail in a predetermined position.

Valves V1 and V2, isolating the top and bottom of the test section, respectively, were designed to operate quickly in specific directions. V1 was set to fail open, with air assist in the opening direction and a dump valve to release cylinder air. This caused the spring force and the air on the piston to open the valve with very little resistance from the air on the "closing" side of the piston. The opening/closing times of the valves were tested as described below.

V2 was set to fail closed, with air assist and a dump valve set to the opposite direction as V1. This provided a safety feature for the test, shutting down the flow in case of loss of power or other interruption. It also served to stop the test after the CCWH had subsided. This was necessary to prevent the air tank from completely emptying the test piping.

Valves V1 and V2 were 2", 1500#, carbon steel ball valves with socket-welded ends. These valves were a full port design to have minimal impact on the fluid flow. The valve positions were controlled using solenoid valves. Other information about the valves used in the test system is presented in the following table.

Table 10-1
Test System Valves

Valve Designation	Purpose	Valve Type	Operation
Valve V1	Isolate top of test section	2" full port, 1500# ball valve	air with spring - fail open
Valve V2	Isolate bottom of test section	2" full port, 1500# ball valve	Air with spring - fail closed
Valve V3	Isolate water tank	2", 600# gate valve	Manual
Valve V4	Air inlet	1/2" 150# ball	Manual
Valve V5	Spill line	1/2" 150# ball	Manual
Valve V6	Steam inlet	1/2" 600# ball	Manual
Valve V7	Steam outlet	1/2" 600# ball	Manual
Valve V6a	Config 2 steam inlet	1/2" 150# ball	Manual
Valve V7a	Config 2 steam outlet	1/2" 150# ball	Manual
Valve V8	Config 2 vent	1/2" 150# ball	Manual

10.2.1.1 Valve Operating Time Testing

In order to measure the opening and closing times of each valve, switches were installed on the valve stem. As a valve began to move, it would open a contact. When the valve reached the end of travel, a second contact was closed. The timing for the valve to act was recorded as the time between the opening of the first contact and the closing of the second. Three tests were performed for each valve. The results are presented in the following table.

Table 10-2
Measured Valve Operating Times

Valve V1	Test 1	Test 2	Test 3	Average
Opening Time (sec)	0.198	0.207	0.206	0.204
Closing Time (sec)	0.672	0.698	0.715	0.695
Valve V2				
Opening Time (sec)	0.132	0.135	0.136	0.134
Closing Time (sec)	0.711	0.706	0.712	0.709

10.2.2 Water Storage/Treatment Tank

The tank at the end of the pipe run provided a free volume to dissipate the waterhammer pressure pulse. The tank was anchored to the floor using Hilti concrete anchors. The tank could be isolated from the test piping by closing valve V3, but this valve was left open during testing. An air line was fitted to the top of the tank to allow it to be pressurized during the filling process.

The 80-gallon water storage tank also provided a means of treating and storing water to fill the piping system, which was important for the testing performed with configuration 2 in which water properties were varied. The tank was equipped with an induction heating coil screwed into a 3" NPT port at approximately 1/3 of the tank height. The heating coil was used to boil the test water to lower the dissolved oxygen level prior to filling the pipe. The tank was also fitted with an air line at the bottom drain port of the tank. This line was used to aerate the water and increase the dissolved oxygen content of the water.

10.2.3 Air Tank/Air Supply System

An air supply manifold was used to provide air to the tanks (air and water), the solenoid valves positioning valves V1 and V2, and the vacuum pump. The air manifold was constructed from 1" copper pipe attached directly to the building service air. This air was supplied at approximately 80 psig. The manifold featured 1/2" ball valves to control the supply of air to the equipment, and 1/2" diameter plastic tubing connected the manifold to the equipment.

An 80-gallon tank (identical to the water tank) was used as an air storage tank. This air volume provided the motive force to accelerate the water column and cause the waterhammer. A sufficient volume was desired to provide a constant accelerating force with no reductions as the column moved. The air tank was instrumented with a 0-100 psig dial gage and with a safety relief valve set to 100 psig. The tank was filled from the air supply header described below. The tank was connected to the test piping with 1/2" plastic air tubing.

Air to position the valves V1 and V2 was controlled using 5-way solenoid valves. These valves featured an inlet port and A and B outlet ports with two corresponding exhaust ports. The air from the manifold was connected to the solenoid supply port, and the A and B ports were connected to the V1 and V2 operators. On the spring return side, the line from the solenoid port passed through the dump valve before entering the valve operator.

Air was also used to pressurize the water storage tank to pump water through the test section to a desired column height. In configuration 1, the water was pushed to a height above the column and excess was spilled over until the desired amount in the tank was used. The level was then set by draining the column through valve V7. In configuration 2, the test section loop was filled and vented and then the level was set in the same manner as configuration 1.

10.3 Test Control Program

A program was written utilizing the LabView software package to automate valve operation and the data acquisition process. The control program output drove relays which provided 120V power to position the solenoid valves.

The control program could be operated in two modes. The first mode featured real time control, during which valves could be positioned and instruments could be read and adjusted. This operating mode was used during the filling of the system and preparation for testing. The second mode of operation was a programmed sequence of steps by which valves were operated and data was collected and written to a file. This automated mode was used during the test to ensure consistent operating conditions.

10.4 Instrumentation

10.4.1 Pressure Transducers

Four pressure transducers were attached to the piping, one at each of the four changes of direction to provide indication of the magnitude of the pressure pulse passing each elbow. These were designated P1 through P4, respectively.

The pressure transducers were 0-1000 psi or 0-3000 psi, internally amplified instruments, manufactured by Sensotec, Inc. The pressure transducers responded at up to 0.088 ms for the 1,000-psi units and 0.037 ms for the 3,000-psi units. The pressure transducer at the first elbow (P1) was replaced during the testing with a 3000-psi instrument since the 1000-psi range was being exceeded during the shorter column lengths and higher driving pressure. The recording frequency of each pressure transducer was 4000 Hz.

10.4.2 Temperature Sensors

Two temperature sensors were employed in each configuration. A thermocouple was used to determine the temperature of the vertical water column above the test section. The second probe was a threaded device, Pipe Plug TC Probe, by Omega Engineering. This temperature probe was screwed into a thread-o-let in the test section. This probe provided the temperature of the steam void. The range of both the thermocouples and the screw in probe were 0-250°F. Temperature was recorded at 4000 Hz.

10.4.3 Level Indicators

The level of the fluid was measured in two locations for configuration 1. These measurements included the level of the water column above the steam leg and the level of water in the downstream tank. These measurements were made using a sight glass. The level of the column of water above the steam leg was important to the test since it controlled the duration of the pressure pulse traveling through the system. The tank level was measured to determine the amount of water replaced in the test section between tests. This helped ensure that each test was not influenced by the parameters measured during the previous test.

The fluid level was measured in an additional location for configuration 2. This level measurement provided information about the length of the steam bubble. This measurement was accomplished using non-penetrating ultrasonic (UT) level sensors. These devices were manufactured by Kay-Ray Sensall and utilize a transmitter and receiver tuned to measure the existence water. The UT sensor produces a sound pulse that passes through the pipe. If water or steam fills the pipe at that location, a logical full or empty signal is returned. Two UT probes spaced 2" apart were used to make this measurement since there was some fluctuation in the water level. The second level gage was considered positive once the first indicated a constant full reading.

10.4.4 Strain Gages

Each pipe restraint was fitted with strain gages to provide data about the load transmitted to the support and the support reaction. Two gages were placed on the threaded rod section of each support and wired in a bridge to eliminate the effects of bending load. Strain measurements were recorded at 4000 Hz.

Pipe supports were calibrated with attached strain gages. This was accomplished by inserting the pinned ends of the struts into a tensile test machine. Using a voltmeter, the response per loading was determined. The struts were calibrated for 1,000 lbf in compression to 4,000 lbf in tension.

10.4.5 Oxygen Meter

The amount of dissolved oxygen dO_2 in the test water was measured using an Extech model 407510 digital dissolved oxygen/temperature meter. The meter measured dissolved oxygen in water from 0 to 19.9 parts per million (ppM) and in air from 0 to 100%. Parts per million (ppM) is equivalent to mg/L.

The dissolved oxygen level was used as a basis for determining total dissolved air in the fluid. It was assumed that the dissolved oxygen remained proportional to the dissolved air in the system. This appeared true except when water was allowed to remain stagnant in the system, and some oxygen was scavenged by corrosion. Therefore, the system was refilled between tests with fresh water as described in the test sequence.

10.4.6 Data Acquisition Equipment

Data was sampled from the various instruments through two multichannel boards. A 32-channel board obtained input from the pressure transducers and strain gages. An 8-channel board obtained input from the thermocouples.

10.5 Test Sequence

The sequence for filling the system and performing the test was important to ensure repeatable, predictable, waterhammer. For both configurations, the system was filled and the boiler was brought up to pressure before testing commenced. The sequence for each configuration is described below. Refer to the schematic drawing in Figure 10-1 for valve designations.

10.5.1 Configuration 1

10.5.1.1 Filling

The configuration 1 piping was filled by opening valves V1, V2, and V7 until water was emitted from the test section drain valve (V7). V7 was shut and water storage tank pressure was then used to pump water up the test column and over into the spill bucket. Approximately 2" to 4" of water were drained from the water storage tank into the test piping between each test. Given the 18" diameter tank and 2" diameter piping, this corresponded to replacing 13 to 27 feet of water in the piping between tests. This reduced the potential for entrained voids from the previous test to influence the current test.

Once the system was filled and flushed, the vacuum line was isolated (V5 closed), and the bottom of test section was isolated (V2 closed).

10.5.1.2 Set Column Height

The column height was adjusted by opening the air supply valve and slowly lowering the water column level by cracking open valve V7. Once the desired column level was reached, valve V1 was shut.

Two measurements were taken at this point in the test. The pressure in the air tank was checked and changed as required. Also, a sample was obtained from the water drained from the test column. This sample was checked for dissolved oxygen content. The process for oxygen monitoring is described in Section 6.3.

10.5.1.3 Steam Void Creation

Steam was introduced into the test section by opening valves V6 and V7. Steam was blown through the test section for 3 minutes prior to each test. The steam valve and drain were shut off in order (V6 then V7) to ensure atmospheric pressure in the test section. During the steaming process, any adjustments required to zero out the pressure transducers or strain gages were performed.

10.5.1.4 Waterhammer Generation

Data collection was started and the test initiated with the opening of valve V2 which produced a relatively stable steam void over water condition. It was estimated that little condensation of the steam occurred for several reasons. First, the test section was insulated with 3/4" fiberglass wrap. Second, the steam was blown through the test section for 3 minutes, allowing the valves and piping to heat up to approximately 212°F to 215°F. Third, the small portion of piping (approximately 1½") between the top of valve V2 and the test section drain was filled with 212°F water which condensed from the steaming process. This water would provide an insulating layer between the subcooled water below valve V2 and the steam above. In any event, the test was left in this condition for a very short period of time (< 0.5 sec).

The second test step was the opening of valve V1, which followed V2 by a period of 500 to 800 milliseconds. This valve opened rapidly, in approximately 0.134 sec. This exposed the steam void to the rapidly accelerating water slug, collapsing the steam. The impact of the water slug on the standing water at valve V2 caused the waterhammer.

The pressure pulse traveled through the piping and was recorded at each elbow pressure transducer (P1 through P4). The support reaction at each pipe restraint was also recorded.

10.5.1.5 Test Shut-Down

The test was stopped by the closure of valve V2 approximately 0.6 to 0.8 sec after V1 opened. This prevented the air tank from emptying the test piping.

It was noted, due to the rapid closure of valve V2 (also approximately 0.128 sec), that a secondary valve closure waterhammer was created. This occurred if valve V2 was closed soon enough after valve V1 opened such that the piping near V2 was still water filled when it closed.

Data recording was stopped 3 seconds after valve V2 was closed.

The test was brought back to the refill position by isolating the air tank (closing valve V4), relieving the pressure through valve V7, and opening valve V2.

10.5.2 Configuration 2a

Configuration 2a differed from configuration 1 in the testing sequence used to create the steam void and initiate column closure.

10.5.2.1 Filling

The configuration 2a piping was filled by adding air to pressurize the water storage tank. Valves V1, V5, and V8 were opened until water was emitted from the test section vent valve (V8). Valve V8 was shut and the pressure was used to push water up the test column and over into the spill bucket. Approximately 3" to 5" of water were drained from the water storage tank into the test piping between each test. Based on the volume of the piping, this corresponded to about 20 to 34 linear feet of fresh water being replaced in the system between tests. This reduced the potential for entrained voids from the previous test to influence the current test.

Once the system was filled and flushed, the spill line was isolated (V5 closed), and the water storage tank was depressurized. A sample was obtained from the water spilled through the vent valve. This sample was checked for dissolved oxygen content.

10.5.2.2 Set Column Height

The column height was adjusted by cracking open the air supply valve which pushed the water back toward the storage tank. Once the desired column level was reached, valve V1 was shut. At this point, the pressure in the air tank was checked and changed as required.

10.5.2.3 Steam Void Creation

The steam void was created in the test pipe by boiling water in the heat exchanger. The steam to the outside of the jacket was introduced by opening valves V6a and V7a. The steam supply was modulated using a steam trap on the drain side of the jacket. Boiling was allowed to occur in the test pipe until the level sensors on the downstream leg of the configuration 2 loop showed that the steam void had emptied the pipe past that point. This steaming process took approximately 5 minutes. The steam was then shut off (V6a closed). During the steaming process, any adjustments required to zero out the pressure transducers or strain gages were performed.

The steam void was then monitored using the UT level gages on the downstream leg of the loop. Due to fluctuation in the water/steam interface level, the void was allowed to condense until the lower of the two level gages indicated the pipe was water solid and the higher was alternating wet/dry. At this point the test was initiated.

10.5.2.4 Waterhammer Generation

Data collection was started and the test initiated with the opening of valve V1. As in configuration 1, this valve opened rapidly, in approximately 0.134 sec. This exposed the steam void to the rapidly accelerating water slug, collapsing the steam. The impact of the water slug on the standing water at the downstream leg of the test loop caused the waterhammer.

The pressure pulse traveled through the piping and was recorded at each elbow pressure transducer (P1 through P4). The support reaction at each pipe restraint was also recorded.

10.5.2.5 Test Shut-Down

The test was stopped by the closure of valve V1 approximately 0.7-0.9 sec after it was opened. This prevented the air tank from emptying the test piping. This valve closed much slower than it opened (approximately 0.709 sec) and the column had surely passed the valve by that point. Since the valve was not water solid, no secondary valve closure waterhammer was created in configuration 2.

Data recording was stopped approximately 2 seconds after valve V1 was closed. The test was brought back to the position to be refilled by isolating the air tank (V4 closed), relieving the pressure through valve V5, and opening valve V1.

10.5.3 Configuration 2b

Configuration 2b differed from configuration 2a in the testing sequence used to create the steam void and initiate column closure.

10.5.3.1 Filling

The configuration 2b piping was filled by adding air to pressurize the water storage tank. Valves V1, V5, and V8 were opened until water was emitted from the test section vent valve (V8). Valve V8 was shut and the pressure was used to push water up the test column and over into the spill bucket. Approximately 3" to 5" of water were drained from the water storage tank into the test piping between each test. Based on the volume of the piping, this corresponded to about 20 to 34 linear feet of fresh water being replaced in the system between tests. This reduced the potential for entrained voids from the previous test to influence the current test.

Once the system was filled and flushed, the spill line was isolated (V5 closed), and the water storage tank was depressurized. A sample was obtained from the water spilled through the vent valve. This sample was checked for dissolved oxygen content.

10.5.3.2 Set Column Height

The column height was adjusted by cracking open the air supply valve which pushed the water back toward the storage tank. Once the desired column level was reached, valve V1 was shut. At this point, the pressure in the air tank was checked and changed as required.

10.5.3.3 Steam Void Creation

The steam void was created in the test pipe by boiling water in the heat exchanger. The steam to the outside of the jacket was introduced by opening valves V6a and V7a. The steam supply was modulated using a steam trap on the drain side of the jacket. Boiling was allowed to occur in the test pipe until the sight glass in the downstream leg of the configuration 2b loop showed that the steam void had emptied the pipe up to that point. This steaming process took approximately 3 to 5 minutes. The steam was then shut off (V6a closed). During the steaming process, any adjustments required to zero out the pressure transducers or strain gages were performed.

At this point, the level glasses were isolated from the test section to prevent damage from the pressure pulse, and the test was initiated.

10.5.3.4 Waterhammer Generation

Data collection was started and the test initiated with the opening of valve V1. As in configuration 1, this valve opened rapidly, in approximately 0.134 sec. This exposed the steam void to the rapidly accelerating water slug, collapsing the steam. The impact of the water slug on the standing water at the downstream leg of the test loop caused the waterhammer.

The pressure pulse traveled through the piping and was recorded at each elbow pressure transducer (P1 through P4). The support reaction at each pipe restraint was also recorded.

10.5.3.5 Test Shut-Down

The test was stopped by the closure of valve V1 approximately 0.7-0.9 sec after it was opened. This prevented the air tank from emptying the test piping. This valve closed much slower than it opened (approximately 0.709 sec) and the column had surely passed the valve by that point. Since the valve was not water solid, no secondary valve closure waterhammer was created in configuration 2b.

Data recording was stopped approximately 2 seconds after valve V1 was closed. The test was brought back to the position to be refilled by isolating the air tank (V4 closed), relieving the pressure through valve V5, and opening valve V1.

10.5.4 Dissolved Oxygen Monitoring

Sampling and testing of the level of dissolved oxygen in the test section for configuration 2 was performed using a nitrogen blanket to prevent contamination of the water sample. To accomplish this, a beaker was filled with nitrogen gas from a gas cylinder. The oxygen meter was switched to measure the dry air quantity of oxygen and the probe was inserted into the beaker. When the amount of oxygen in the beaker was less than 1%, the water sample was drawn into the bottom of the beaker using an extension from the drain. This sample was kept in motion using a magnetic remote stirrer as instructed by the manufacturer of the oxygen meter. The oxygen meter was then switched to measure the dissolved oxygen in the fluid. In this manner, water from the test piping was not inadvertently aerated and an accurate measurement could be made.

10.6 Configuration 1 and 2 Test Matrix

Multiple waterhammer tests were performed. Table 10-3, Table 10-4 and Table 10-5 provide the test configuration matrix showing the key variables changed for each test for configurations 1, 2a and 2b, respectively.

Table 10-3
Configuration 1 Test Matrix

Test Series	Variable	Values	Number of Tests	Total Tests	Intent
1.1	Vary Column Length	36", 68", 204", 240"	> 10 at each length	45	Determine length effects for 30-psig driving pressure
1.2	Vary Driving Pressure	15, 30, 45 psig	> 10 at each length and pressure	85	Repeat 1.1 at various pressures; 45-psig test with the 36" column not performed due to pressure transducer limitations
1.3	Vary Support Stiffness	Remove stiffener plates to reduce support stiffness	Repeat tests from 1.1, 1.2	114	Determine effect of stiffness change on load

Table 10-4
Configuration 2a Test Matrix

Test Series	Variable	Values	No. of Tests	Total	Intent
2.1	Vary Driving Pressure	30, 45 psig	5 at each pressure	10	Determine refill velocity effects* using tap water (normal air content in water)**
2.2	Vary Water Characteristics	Aerated, Deaerated	5 each for aerated, deaerated	20	Determine effect of high and low dissolved O_2 in test water

* Final (cushioned) closure velocity estimated to be 10 to 22 ft/sec for 30 and 45 psig driving pressure, respectively.
** Tap water with no treatment to alter dissolved oxygen content.

Table 10-5
Configuration 2b Test Matrix

Test Series	Variable	Values	No. of Tests	Total	Intent
2.1	Vary Driving Pressure	20, 70 psig	5 at each pressure	10	Determine refill velocity effects* using tap water (normal air content in water)**
2.2	Vary Water Characteristics	Aerated, Deaerated	5 each for aerated, deaerated	20	Determine effect of high and low dissolved O_2 in test water

* Final (cushioned) closure velocity estimated to be 20 to 42 ft/sec for 20 and 70 psig driving pressure, respectively.
** Tap water with no treatment to alter dissolved oxygen content.

10.7 Test Listing

Tables 10-6 through 10-8 provide a listing of each column closure waterhammer test and the conditions for each test. The peak pressure measured is also listed for each test.

In Table 10-6 the test name identifies the test parameters as follows:

F-1 = configuration 1

B = bolted supports, U = unbolted supports (see Chapter 13)

N = normal water tests

36, 68, 204, and 240 = column length (in)

15, 30, 45 = driving pressure

Sequence number

E = CCWH event

Table 10-6
Configuration 1 CCWH Test List

Table 10-6
Configuration 1 CCWH Test List (Continued)

Table 10-6
Configuration 1 CCWH Test List (Continued)

Table 10-6
Configuration 1 CCWH Test List (Continued)

Table 10-6
Configuration 1 CCWH Test List (Continued)

Table 10-6
Configuration 1 CCWH Test List (Continued)

Table 10-6
Configuration 1 CCWH Test List (Continued)

Table 10-6
Configuration 1 CCWH Test List (Continued)

Table 10-6
Configuration 1 CCWH Test List (Continued)

Table 10-6
Configuration 1 CCWH Test List (Continued)

In Table 10-7 the test name identifies the test parameters as follows:

Blank = normal water, A = aerated water, D = deaerated water

36 = column length (in)

30, 45 = driving pressure (psig)

Sequence number

Table 10-7
Configuration 2a CCWH Test List

In Table 10-8 the test name identifies the test parameters as follows:

F-2B = configuration 2b

N = normal water, D = deaerated water, A = aerated water

240 = column length (in)

20, 70 = driving pressure (psig)

Sequence number

E = CCWH event

Table 10-8
Configuration 2b CCWH Test List

10.8 Test Results

This section provides the results of the column closure testing. The pressure magnitude used to characterize the "waterhammer pressure" throughout the configurations 1, 2a and 2b testing was obtained from pressure instrument P1 (see Figure 10-2). Since this was the instrument closest to the location of the column closure, it was least affected by pressure attenuating phenomena such as losses due to friction in the fittings or pipe.

10.8.1 Configuration 1 Test Results

10.8.1.1 Pressure Magnitude

Figure 10-6 shows the response of the waterhammer pressure relative to the calculated closure velocity. The waterhammer pressure is the peak pressure measured in the configuration 1 tests. As expected from the Joukowski equation, the waterhammer pressure rises in a linear manner with increasing closure velocity, calculated using a sonic velocity of 4,600 ft/sec and $k = 0.5$.

The configuration 1 test data shows no cushioning from air and some cushioning from steam at higher closure velocities, when the steam condensation rates cannot keep up with void pressurization. Configuration 1 does not feature a heated layer of water adjacent to the steam void, since the water closing on the steam void was subcooled. Therefore, the test data most closely matches the Joukowski predictions for the low velocity range. The presence of a heated layer adjacent to the void would slow condensation rates and cause steam cushioning at lower closure velocities.

Figure 10-6
Configuration 1 Waterhammer Pressure vs. Closure Velocity

10.8.1.2 Pulse Shape

The test data has shown that the pressure rise is not instantaneous and that a finite rise time should be expected from real pressure pulses. For some very brief pulses, the rise times are large relative to the total duration and cause the pressure pulse to appear triangular in shape. Data for pulse rise times is presented in the next section. For longer pulses, the pressure wave is trapezoidal. The pulse shapes are presented in Figure 10-7.

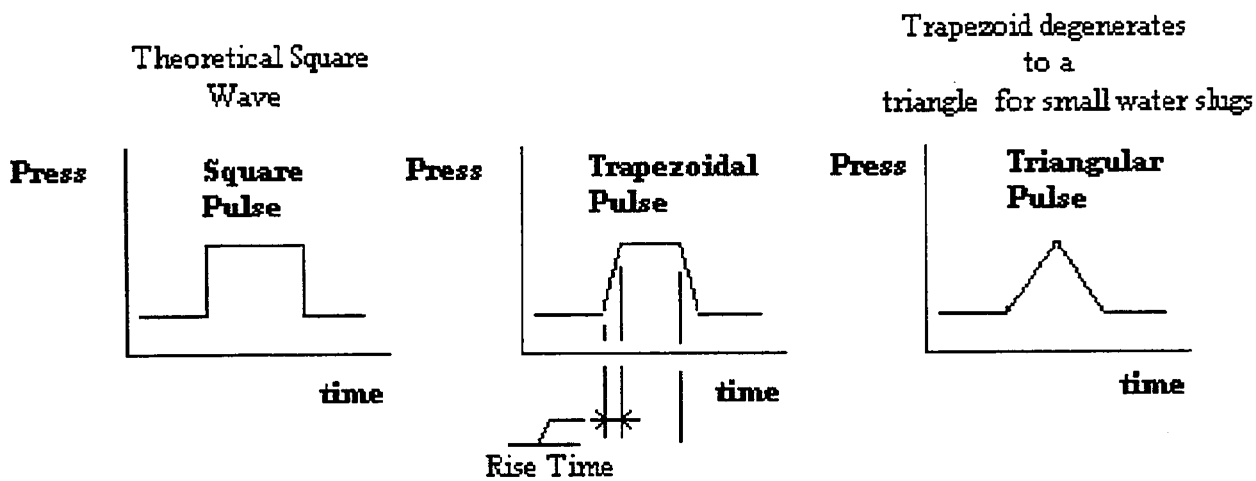

Figure 10-7
Pressure Pulse Shapes

In all cases, the area under the pressure time curve remains equal to the area under the theoretical square wave curve based on an idealized impact without cushioning. This area represents the impulse required to change the momentum of the advancing water column. The addition of finite rise times and broader pulses changes the overall shape, but does not change the area.

10.8.1.3 Rise Time

The rise times of all of the Configuration 1 tests are plotted as a function of predicted impact velocity in Figure 10-8. The rise time is defined as the time between a pressure of 10% of *Pmax* and *Pmax* for the P1 pressure trace.

Figure 10-8
Rise Time vs. Non-Cushioned Closure Velocity

A curve was fit to the rise time data. It was noted that the rise times grew shorter as the closure velocity increased. This is consistent with a physical model in which the rise time is caused by steam and non-condensable pressurization in the void or due to impacting face effects. The faster the advancing column, the less time is available for these effects to influence the waterhammer pressure. A function defining the rise time that fit the data was $t_r = 0.5 \cdot V^{1.3}$. This curve and data are for the configuration 1, 2a, and 2b tests using non-cushioned closure velocities.

10.8.2 Sonic Velocity

Sonic velocity was determined from the test data based on the time required for a pulse to travel from one elbow to another. The time duration from the peak at P1 and P2 over the length of the first piping segment provided an average sonic velocity for configuration 1 of 4,296 ft/sec and for configuration 2 of 4,681 ft/sec. This sonic velocity compares well with the theoretical values calculated previously (4,580 ft/sec using Equation 6-2). The fact that the water between the elbows contains dissolved non-condensables does not affect the sonic velocity. Sonic velocity will only be affected when the dissolved non-condensables are driven from solution and become bubbles.

10.8.3 Configuration 2a and 2b: Effects of Non-Condensables

10.8.3.1 Pressure Magnitude

The configurations 2a and 2b test results for pressure magnitude show the effects of dissolved non-condensables (air) in the test water. Figure 10-9 shows the response of the waterhammer pressure relative to the calculated closure velocity without consideration of void pressurization effects to reduce closure velocity. It can be seen that the data is below the line for predicted waterhammer using the Joukowski equation.

Figure 10-9
Configuration 2a and 2b Peak Pressure vs. Closure Velocity

Dissolved air comes out of solution with the heating and boiling of the water and accumulates in the void. The dissolved air content of the water was measured before each test for configuration 2 by measuring the dissolved oxygen content. This measurement was used to determine the total dissolved air, based on the relative solubility of air and oxygen. Measurements were made in milligrams/liter (mg/L), which is equivalent to parts per million (ppM). These data are listed in Table 10-7 and Table 10-8 for configurations 2a and 2b, respectively.

10.9 Conclusions for CCWH

Non-condensables and/or steam that are in the void can become pressurized as the void closes, and they can slow the reduction in closure velocity of the oncoming water column. Testing has been performed to show the behavior of the void and water column during the CCWH. The reduction in waterhammer pressure magnitudes and pulse characteristics have been measured. The data from the tests described in this section have been used to correlate to analysis models. Analytical models have been developed, correlated to these test results, and used to predict the velocity reduction in plant conditions.

11 LOSS OF OFFSITE POWER VERSUS LOSS OF OFFSITE POWER WITH LOSS OF COOLANT ACCIDENT

This section compares the effects of a LOOP transient with the combined effect of a LOOP/LOCA or MSLB transient for typical piping systems. The intent is to demonstrate that in a plant that has voiding in a LOOP-only event, that the LOOP-only event will be more severe than if the LOOP occurs simultaneously with a LOCA or MSLB.

11.1 Description of LOOP Waterhammer

In open loop plants, voiding can occur in the fan coolers and related piping each time that the service water pumps are shut down. This can occur each time that a LOOP occurs or, more importantly, each time a LOOP test is performed. At many plants, a station blackout test is performed during every refueling outage. Because of the frequency of these events, plant waterhammer experience is important to indicate the impact of the waterhammer following the postulated LOOP. Tests have been conducted by installing pressure transducers and other instrumentation to monitor system response to LOOP tests. These tests have shown that the impact of waterhammer on the piping and supports is relatively minor. In-plant tests are described in Section 5.

In closed loop plants, voiding would not be expected to occur in the fan coolers or any of the system piping when the service water pumps are shut down or when a LOOP occurs.

A column closure waterhammer (CCWH) may occur when system voids are refilled. The filling water closes the voids and impacts stationary water. The waterhammer pressure developed by the impact is primarily dependent upon the closure velocity. Any effects that change the closure velocity will change the magnitude of the waterhammer. Non-condensables and/or steam that are in the void can become pressurized as the void closes, and they can reduce the velocity of the oncoming water column.

11.2 LOOP and LOOP/LOCA in Open Loop System

Figure 2-1 shows a typical open loop service water system. As discussed in Section 5, nine open loop plants have documented the occurrence of column closure waterhammer experience during testing for LOOP. No pressure boundary damage was noted following any of this extensive in-plant testing. Very limited support damage was noted.

When a LOCA or MSLB occurs simultaneously with a LOOP, boiling can occur in the FCUs and release steam and non-condensable gas into the void.

Table 11-1 compares the LOOP-only transient with the combined LOOP/LOCA or MSLB. The added heat in containment from the LOCA or MSLB has a dramatic impact upon the results. This table assumes that similar system configurations will exist for LOOP and LOOP/LOCA transients. For instance, the valve line-ups should be similar and the same number of pumps should start. If the conditions are not similar, the comparison may not be valid.

Table 11-1
LOOP Versus LOOP/LOCA for Open System

	LOOP – Open System	LOOP/LOCA	Comments
FCU Behavior	FCUs would not be a source of heat transfer to system during LOOP.	FCUs provide the primary heat transfer capability for the heat in containment. Boiling is expected in the FCUs.	Significantly different behavior between the LOOP and the LOOP/LOCA.
Void Formation	Voids form in FCUs and high points in system with the drop in system pressure due to LOOP.	Steam voids form in FCUs and high points in system with the drop in system pressure. Boiling in the FCU will produce steam and release non-condensables from the water that will enter the void.	Similar voids form, but the void is expected to be larger during LOOP/LOCA. The voids following LOOP/LOCA will contain steam and significant non-condensables.
Void Closure	Would occur following pump restart.	Would occur following pump restart.	Similar
Closure Velocity	Closure velocity will depend on pump characteristics.	Closure velocity will depend on pump characteristics, but also on air and steam cushioning. Closure velocity will be reduced.	Air and steam cushioning reduce the closure velocity for the LOOP/LOCA case.
Pressure Pulse	Pressure pulse proportional to closure velocity will occur.	Pressure pulse will occur but as a result of a lower closure velocity.	Air and steam cushioning reduce the closure velocity and pressure pulse for the LOOP/LOCA case.
Loads (on pipe supports)	Proportional to pressure pulse magnitude and duration of pulse.	Proportional to pressure pulse magnitude and duration of pulse.	Similar, but expected to be less severe with LOOP/LOCA due to smaller pressure magnitude/.
Pressure Boundary	Failure of the pressure boundary will depend on available energy.	Failure of the pressure boundary will depend on available energy.	LOOP/LOCA case will have less energy in the pressure transient.

- A brief summary of the results and conclusions that were reached with respect to the waterhammer and two-phase flow issues, including problems that were identified along with corrective actions that were taken. If corrective actions are planned but have not been completed, confirm that the affected systems remain operable and provide the schedule for completing any remaining corrective actions.

Licensees are reminded that their evaluations and responses to address the GL 96-06 issues may be subject to future NRC audit and inspection activities.

4 CONCLUSIONS

As discussed in Section 3 of this evaluation, we consider the use of EPRI Report TR-113594, Volumes 1 and 2, to be acceptable for performing evaluations to address the GL 96-06 waterhammer concerns. Licensees who choose to use this report may respond to the plant-specific RAIs that were issued as discussed in Section 3.3 of this evaluation. NRC approval of the EPRI methodology is limited to use by licensees for addressing the GL 96-06 waterhammer issue, and does not extend to any other regulatory applications.

5 REFERENCES

1. M. G. Izenson, P. H. Rothe and, G. B. Wallis, "Diagnosis of Condensation-Induced Waterhammer," NUREG/CR-5220 Vol. 1, October 1988.

2. P. Griffith, "Screening Reactor Steam/Water Piping Systems for Water Hammer," NUREG/CR-6519, Massachusetts Institute of Technology, September 1997.

3. W. Zielke, H-D Perko and A. Keller, "Gas Release in Transient Pipe Flow," Proc. 6th International Conference on Pressure Surges, BHRA, Cambridge, England October 4-6, 1989.

4. E. B. Wylie and V. L. Streeter, "Fluid Transients in Systems," Prentice-Hall, Inc., 1993.

B
EPRI CORRESPONDENCE TO NRC

EPRI Correspondence to NRC:

July 10, 2001	"Resolution of Generic Letter GL96-06 Waterhammer Issues" EPRI Report 113594 - V1 & V2, Revised Sections
August 9, 2001	Response to Questions on Generic Letter 96-06
September 17, 2001	Additional Responses to Questions on Generic Letter 96-06
February 1, 2002	Response to ACRS Comments (letter dated 10/23/01) on the EPRI Report on Resolution of NRC GL96-06 Waterhammer Issues

July 10, 2001

Document Control Desk
U.S. Nuclear Regulatory Commission
11555 Rockville Pike
Rockville, MD 20852

Attention: Mr. Jim Tatum

Subject: "Resolution of Generic Letter 96-06 Waterhammer Issues", EPRI Report TR-113594-V1 & V2, Revised Sections

Enclosed are twelve (12) copies of the revised sections of the document "Resolution of Generic Letter 96-06 Waterhammer Issues", EPRI Interim Report TR-113594--V1 & V2, December 2000. Specifically, Section 5.2.2 and 5.2.3 of Volume 1 (User's Manual) and Sections 6 and 8 of Volume 2 (the Technical Basis Report) are enclosed. The other sections of the report are essentially unchanged from the earlier transmittal and will only have editorial changes made prior to final submittal.

This information is being submitted as a means of exchanging information with the NRC for the purpose of supporting industry resolution of GL 96-06 Waterhammer Issues. The specific modifications to the sections noted were made to address issues raised by the ACRS Thermal Hydraulic Subcommittee at our meeting on January 16, 2001. The questions specifically raised were:

1. Limit of test apparatus for determination of air release fraction.

2. Determination of the "h" in the "hA" term (this was backed out of the test data; perhaps a Table listing the various values of "h" for the tests would be useful).

3. Scale-up of the test data (the suggestion here was to conduct some sort of sensitivity study).

The report sections that are modified include the results of additional air-release testing that has been performed to determine the amount of air released during the GL96-06 transient. The test methods and results are documented in the modification to the Volume 2 Section 6. The modified method to calculate air release for a specific plant application is provided in Volume 1 Section 5.2.3.

The "h" values for the test data are documented in the revised Volume 2 Section 8. A sensitivity study of both the Method of Characteristics (MOC) and Rigid Body Model (RBM) to the "h" values was performed and is documented in the revised Volume 2 Section 8. Additional work also was performed on scaling for pipe diameter (see Section 8.3.6).

Please note that the enclosed document contains proprietary information. Therefore, a letter requesting the report be withheld from public disclosure and an affidavit describing the basis for withholding this information is provided as Attachment 1.

We will plan to meet with the NRR Staff and the ACRS on August 23, 2001 to discuss the material that is attached. If you have any questions on the enclosed document or the general subject it addresses, please call me at 919-546-7959 or Avtar Singh at 650-855-2384.

Sincerely,

Avtar Singh for V Wagoner

Vaughn Wagoner
Carolina Power & Light Company
Chairman, EPRI Waterhammer Project Utility Advisory Group

August 9, 2001

James Tatum
U.S. Nuclear Regulatory Commission
11555 Rockville Pike, M/S O-11A11
Rockville, MD 20852

Attention: Mr. Jim Tatum

SUBJECT: Response to Questions on Generic Letter 96-06

Enclosed are responses to questions raised on the document "Resolution of Generic Letter 96-06 Waterhammer Issues", EPRI Interim Report TR-113594--V1 & V2, December 2000. We have previously transmitted revisions to Section 5.2.2 and 5.2.3 of Volume 1 (User's Manual) and Sections 6 and 8 of Volume 2 (the Technical Basis Report). The other sections of the report are essentially unchanged from the earlier transmittal and will only have editorial changes made prior to final submittal. The attachment to this letter includes responses to specific questions raised by the NRC. This information will be addressed as applicable in the final revision to the Technical Basis Report.

The enclosed document does not contain any proprietary information.

If you have any questions on the enclosed information or the general subject it addresses, please call me at 919-546-7959 or Avtar Singh at 650-855-2384.

Sincerely,

Avtar Singh for

Vaughn Wagoner
Carolina Power & Light Company
Chairman, EPRI Waterhammer Project Utility Advisory Group

Attachment

Questions from Walt Jensen and Jim Tatum (NRR staff):

1. **The relationship of pressure rise time to impact velocity is given only for test configuration No. 1 which did not include air in the steam void. Please provide a comparison of the pressure rise time relationship with the data from test configuration 2 which did include air.**

   Response:

   The individual rise times for the Configuration 2a and 2b tests have been calculated. This data is provided in Figure 10-8, attached. This figure also includes the Configuration 1 test results. The comparison shows that the rise times for Configuration 2a and 2b tests are similar to the rise times for Configuration 1 when the closure velocities are similar.

2. **Please provide figure 10-9 which was missing from the "Technical Basis Report".**

   Response:

   A copy of Figure 10-9 is attached.

3. **We understand that burst tests have been performed for representative fan cooler tubing and piping which showed failure only at very elevated pressures. Please provide documentation for these tests.**

   Response:

   The burst test data discussed during the January 16, 2001 meeting is industry data that had been previously developed by EPRI. A copy of EPRI report TR-108812, dated December, 1997, describing the burst test program has been provided.

4. **The NRC staff shares the same concerns as the ACRS Subcommittee on T/H's regarding noncondensable gas generation during system draining and steam condensation during column closure. In responding to the ACRS T/H subcommittee on this issue, please also address configuration differences that exist between the test apparatus and the actual plant. For example, the heat exchanger tubes in the FCUs are generally horizontal, while the test apparatus modeled a vertical configuration. It would seem that there could be significant differences in the test results if steam bubbles are rising through a vertical tube (as in the test apparatus) vs. the plant configuration where the steam bubbles form in the tube and must expand to a vertical header that is usually at the high point (but could also be at the low point) of the system. It is not clear how the test results apply to the actual plant configuration.**

Attachment

Response:

Additional testing has been performed to determine the amount of air released during the transient. The test results and a modified approach to evaluating air release are documented in the TBR Section 6 and User's Manual (UM) Section 5.2.3, respectively.

Section 6.3.2 of the revised TBR described the test configuration and compared the test configuration and conditions to the prototypical configurations and conditions in nuclear plant applications. Specifically, the additional air release testing utilized a horizontal tube attached to a vertical header. Tests were run both with the header full and with the header empty to simulate a variety of plant conditions. These tests were more prototypical of actual plant geometry and conditions.

Questions from Gary Hammer (NRR staff):

1. **The rigid body model involves defining the waterhammer pulse as a trapezoid function having a recommended rise time. However, the recommended method for choosing rise times does not appear to be conservative when considering the steepest part of the pressure-time data plots. Also, the pulse duration is recommended to be lengthened by a factor to preserve the area under the trapezoid shape. However, this also does not appear to be conservative since it could result in less structural response than for the actually expected duration.**

Response:

The characterization of the pressure pulse as a trapezoid was selected to simplify the complexity of the actual pressure pulses that were seen in the tests. The trapezoidal model used to characterize the pressure pulse was developed to reflect fundamental theory, capture the pulse magnitude, rise time, and duration to simplify the transient pressure response into a set of defined pressure time (P-T) points for use in a structural calculation.

The selection of the pulse was described in Section 9.2 and 9.3 of the TBR. The adequacy of the trapezoidal representation was evaluated and the results were reported in Section 13.5 of the TBR.

The effectiveness of the trapezoid model was tested by comparing the response of an ANSYS model with loading from the idealized trapezoids and loading with actual pressure-time histories to the measured force response from the tests. Support loads at three locations were measured in the tests. A set of 44 test measured pressure traces from the tests was used as the "actual" pressure-time input. The test traces were accurately input to ANSYS in detail. These pulses were also characterized as trapezoids using the methods recommended in the User's Manual and then used to load the ANSYS model. The results of these two load sets (idealized trapezoid versus the actual pressure history) compared to the support forces measured in the tests is provided below (Figure 13-7 of

Attachment

the TBR). Most data fell above the "predicted = measured" line at 45° in the figure. The points that fell below the 45° line were a small percentage of the total and these points were located close to the line.

Figure 13-8 in the TBR, also provided below, showed the results for the trapezoidal characterization of the pulses for all tests analyzed using the same ANSYS model. These force responses are plotted versus the measured force data for all three restraints (F1, F2, and F3). The 45° dashed line (predicted = measured) represents exact matching of the measured response. This plot further demonstrates the accuracy of the trapezoidal modeling technique as a means of predicting real support forces.

These two comparisons show that both the actual pressure trace and the trapezoidal representation provide accurate methods to capture the response of the structure when compared to the test data. Figures 13-7 and 13-8 further show that the "curve fit" for the trapezoidal pulses provide a prediction of a higher support load than the actual pressure pulse. This indicates that on average, the trapezoidal pressure pulse is more conservative. The statistical nature of the testing, particularly for events like waterhammer, does provide a small number of calculated loads that are lower than the test results. The number of calculated points that fall below the test data is considered to be typical of what would be expected for this number of tests for a phenomena that has as much scatter as waterhammer testing.

On average, the analysis with the actual pressure time loading is conservative versus the test data by approximately 15% (percentage calculated at a load of 1,000 pounds) and the analysis with the trapezoidal pressure time loading is conservative versus the test data by approximately 30%. The trends from Figure 13-8 are the same.

The margins that exist in the calculation of the pressure magnitude and in the design and qualification of the supports is considered adequate with this trapezoidal representation to assure that a conservative basis for qualification of supports is provided. The trapezoidal representation gives higher loads than the actual pressure time curve.

The question also asked about the "lengthening" of the pressure pulse. The pulse duration will change as the pressure magnitude is cushioned to satisfy conservation of momentum. This accurately represents how the pressure pulse changes with cushioning. This is discussed in Section 9.2.2 of the Technical Basis Report. Calculation of the pulse duration is provided in the User's Manual, Section 5.3.5. The pressure pulse duration to be used is calculated based on the time of reflection. There is no recommendation to increase pressure pulse duration beyond this value.

Attachment

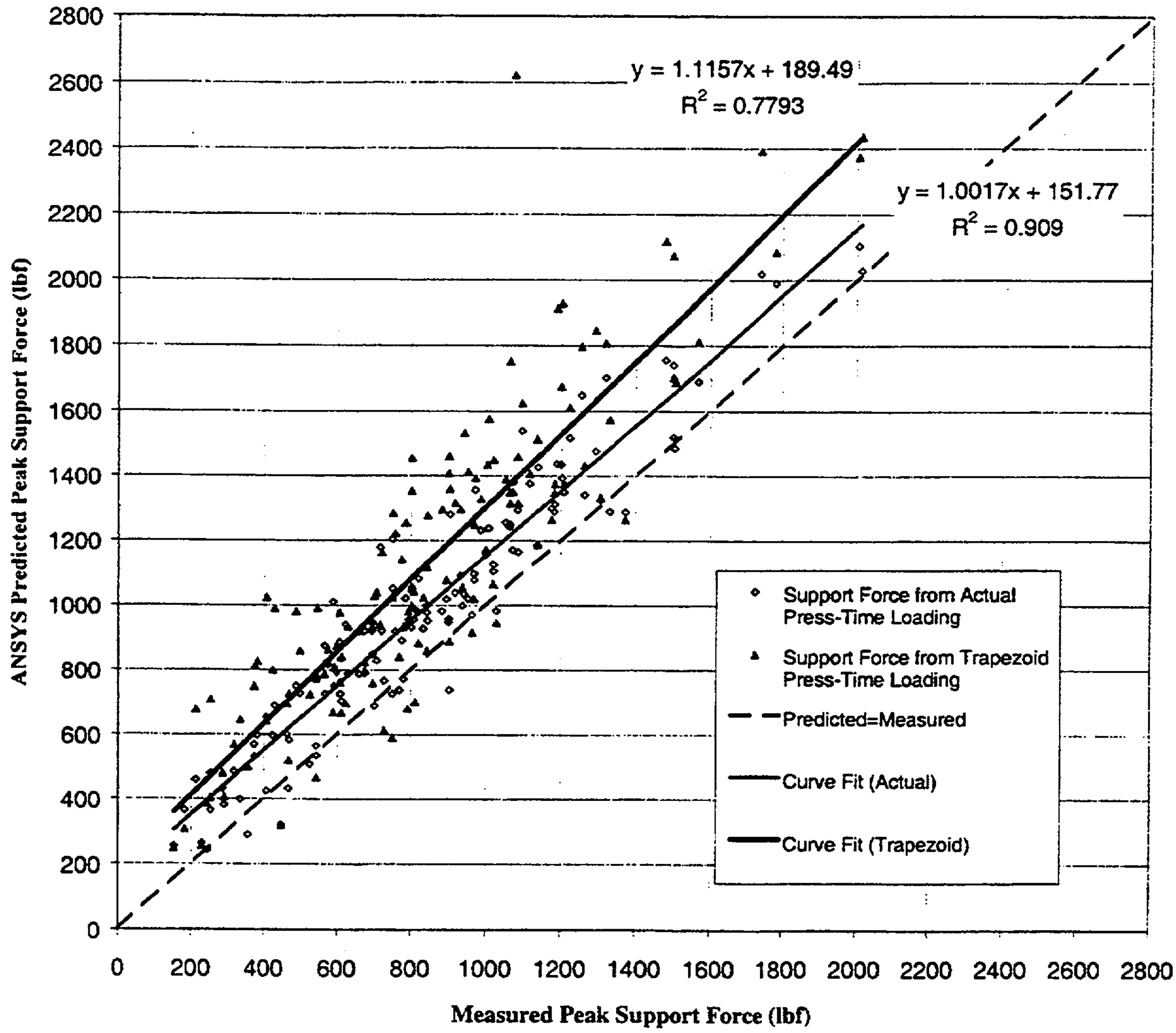

Figure 13-7: Trapezoid Characterization/Actual Data Comparison (44 Tests)

Attachment

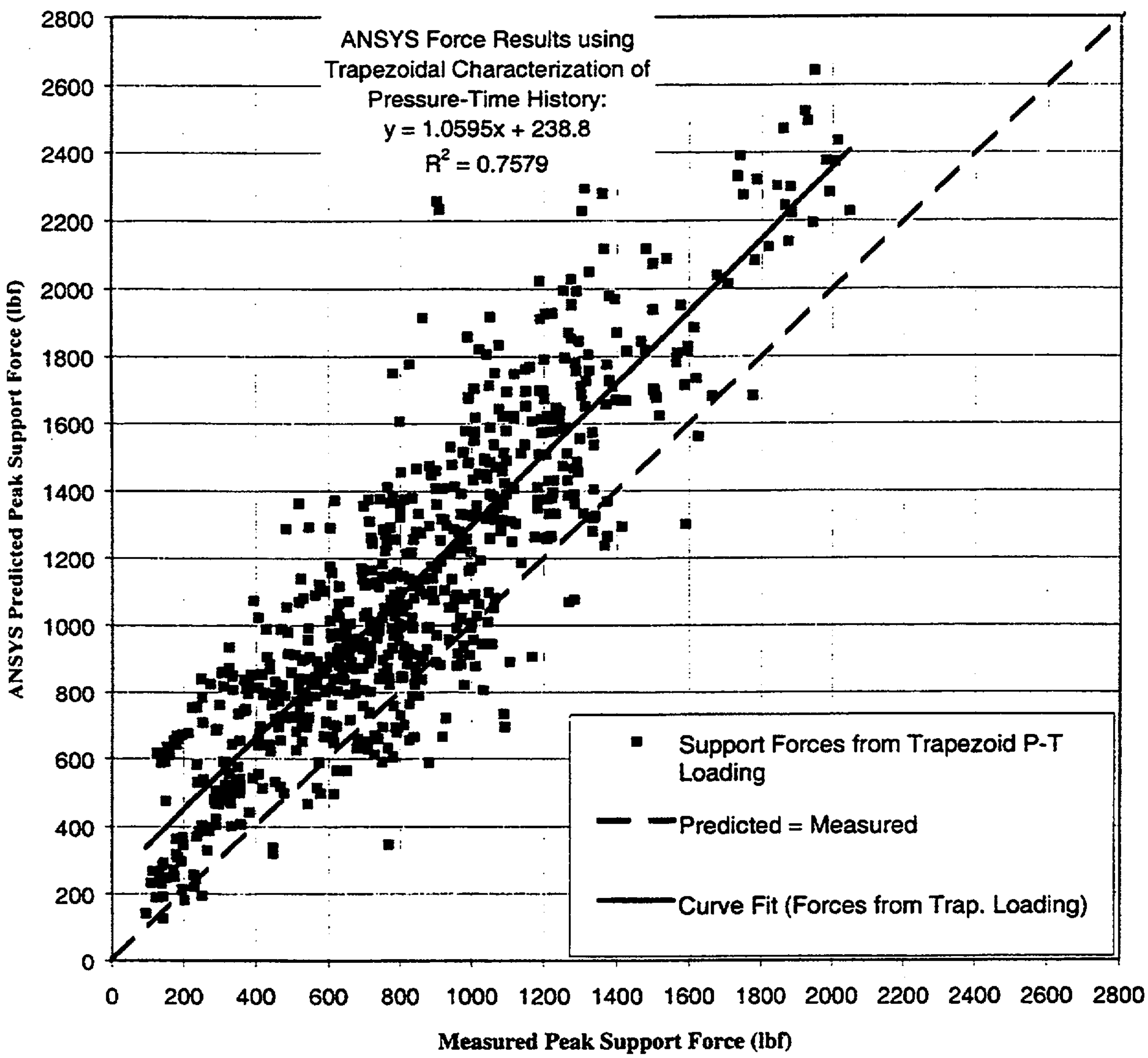

Figure 13-8: Trapezoid Characterization (All Tests)

2. **The report recommends using only one waterhammer pulse in evaluating system piping. However, waterhammer pressure loads are composed of several reversing cyclic pulses (Examples are shown in Figures 5-3 and 7-3). Figure 13-8 indicates that for the test configuration, the use of a single trapezoidal pulse is conservative in most cases evaluated. However, there are a few cases shown where this method is not conservative. Also, the structural and forcing function frequencies for plant piping configurations will differ from the tests. Therefore, a longer pressure history involving several cycles**

Attachment

should be included in analysis of plant piping systems since this could result in additional energy being added to the structures.

<u>Response:</u>

The column closure event is essentially a single pulse phenomenon. Any subsequent pressure pulse after the initial pressure rise is caused by reflected waves passing through the system. The reflected waves will be significantly smaller in magnitude than the initial pulse.

To investigate the accuracy of using a single pulse, a single degree of freedom model was selected as typical of a single segment of piping that experiences an axial load caused by a passing pressure wave. This model was loaded with a repeating, decaying pressure pulse that occurs at the <u>precise</u> natural frequency of the structure. This was compared to a single pressure pulse load of the same initial duration. The degree of decay from the first peak to the second peak was approximately 75% as would be expected with a reflected wave and as was seen in Figure 5-3 of the TBR. The two loads are provided in the following figures.

Single Pulse Loading:

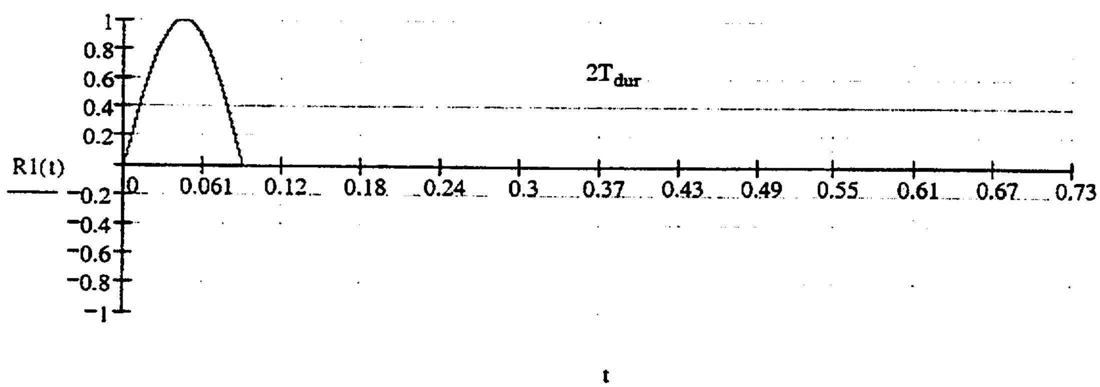

Repeated Pulse Loading:

Attachment

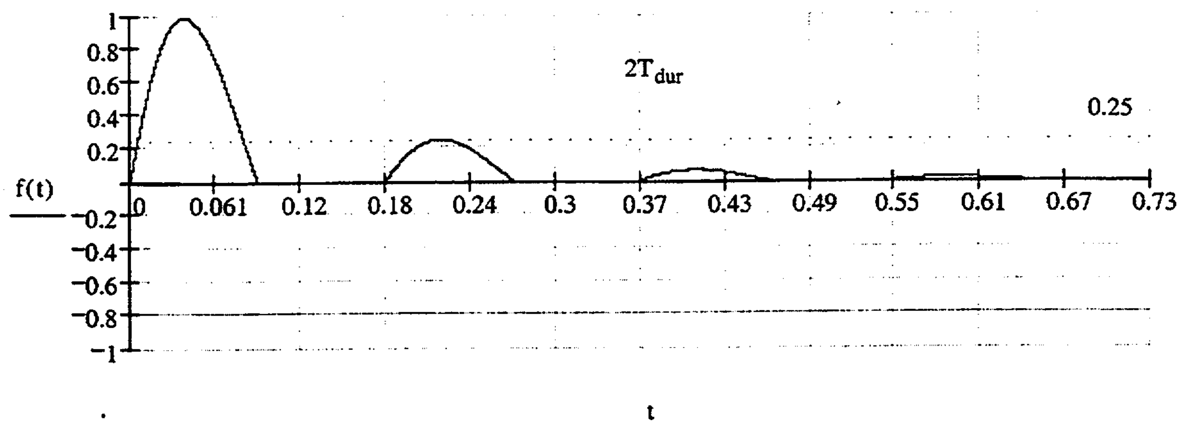

Using 2% damping, the resulting displacements for the multiple loading are within 10% of that produced by a single load. This was for the case where the loading frequency was precisely equal to the natural frequency of the system.

The response of a complex system is dependent not on the response of a single axial segment, but on the combined response of many segments to a passing pressure wave. Further, the load in any individual support is a combination of loads from many parts of a piping system. The likelihood of any individual segment having the precise natural frequency of repeated loading is very low. The likelihood of multiple segments contributing to the loading of a support and having the precise natural frequency as a repeated loading is much lower. Even a small difference between the natural frequency and the driving frequency will dramatically change the response to multiple loading. In other words, the repeated smaller loads do not have the potential to significantly affect the structural response in actual systems.

As shown for the trapezoidal load, the margins that exist in the calculation of the pressure magnitude and in the design and qualification of the supports is considered adequate to allow a single pulse to be used to assure that a conservative basis for qualification of supports is provided.

3. **The report outlines a simple method of incorporating Poisson coupling and junction coupling type fluid-structure interaction based on a study of a very simple configuration. There are significant uncertainties involved in making such predictions, and if fluid-structure interaction is to be considered in attenuating the waterhammer loads, it should be based on a more detailed plant-specific analysis.**

Response:

The analytical evaluation of potential pulse amplification by fluid structural interaction (FSI) is based on the detailed methods defined by Wood as described in reference 33 of the TBR. It was further investigated in references 34 through 38 as described in the TBR.

Attachment

The simplified method of attenuation described in TBR Section 12.4 is not provided for generic plant analysis. It is used to show that the attenuation, being cumulative, will quickly surpass any potential amplification due to FSI. This analysis is used as a basis for the recommendation that the potential amplification from FSI can be conservatively ignored.

At the discretion of the individual licensee(s), fluid structure interaction may be used only if both attenuation and amplification are employed. The degree to which attenuation or amplification dominates fluid structure interaction will be a function of the stiffness of a piping system and its supporting elements. These are plant specific elements, and thus should be addressed in the plant specific responses to the generic letter.

4. **The report does not indicate the structural damping value used in the comparison of analyzed loads vs measured loads. This information needs to be provided as part of the basis for the comparison.**

Response:

The damping used in the analysis for comparison to test data was 0.1% of critical damping. Specific damping values to be used would be plant-specific and would be in accordance with the plant's licensing documents.

Attachment

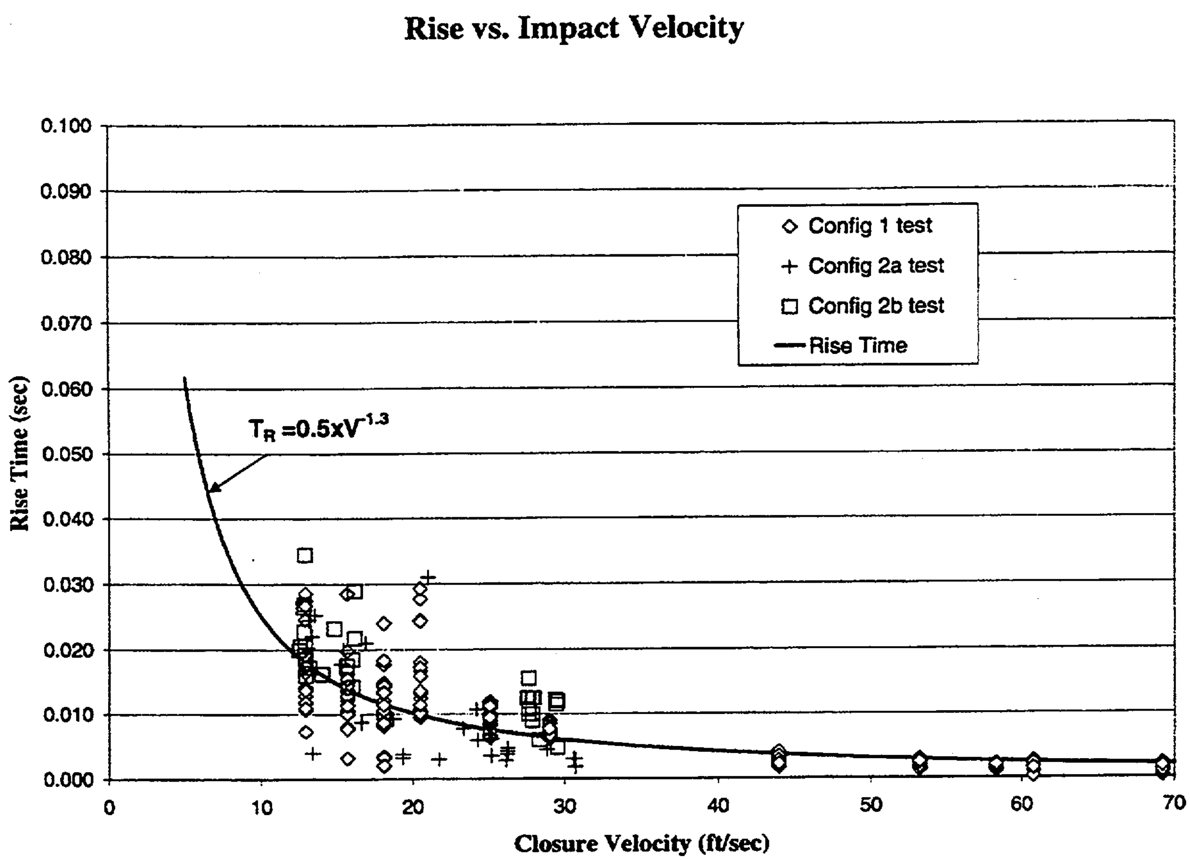

Figure 10-8: Rise Time vs. Impact Velocity – Configuration 1, 2a, and 2b

Attachment

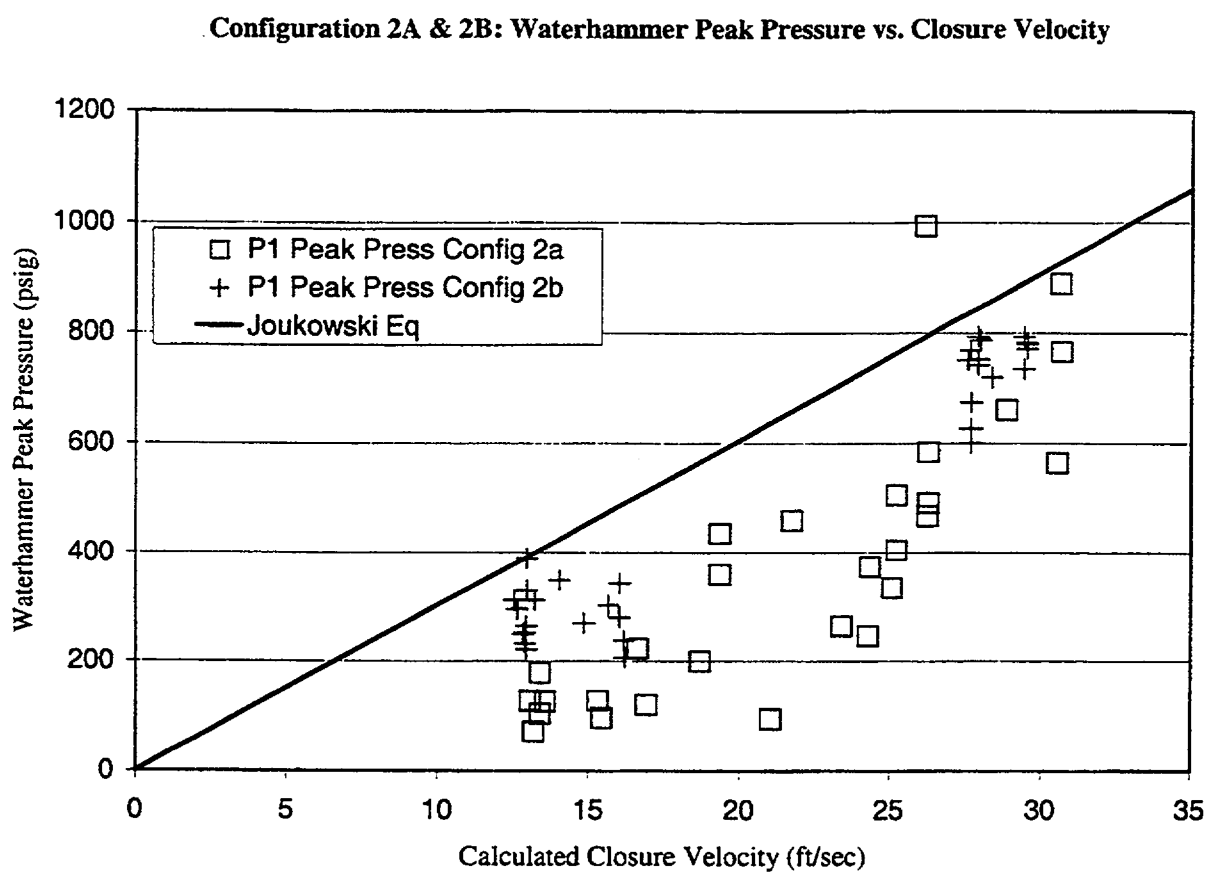

Figure 10-9: Configuration 2a and 2b Peak Pressure vs. Closure Velocity

ELECTRIFY THE WORLD

EPRI

September 17, 2001

Document Control Desk
U.S. Nuclear Regulatory Commission
11555 Rockville Pike
Rockville, MD 20852

Attention: Mr. Jim Tatum

Reference: Letter from Mr. Vaughn Wagoner to Mr. Jim Tatum, Response to Questions on Generic Letter 96-06, August 9, 2001

SUBJECT: Additional Response to Questions on Generic Letter 96-06

Enclosed are additional responses and clarification to our previous letter that responded to questions raised on the document "Resolution of Generic Letter 96-06 Waterhammer Issues", EPRI Interim Report TR-113594--V1 & V2, December 2000. The attachment to this letter includes responses to specific questions raised by the NRC. This information will be added to the final revision of the Technical Basis Report.

Please note that the enclosed document does not contain any proprietary information.

If you have any questions on the enclosed information or the general subject it addresses, please call me at 919-546-7959 or Avtar Singh at 650-855-2384.

Sincerely,

Avtar Singh for

Vaughn Wagoner
Carolina Power & Light Company
Chairman, EPRI Waterhammer Project Utility Advisory Group

Attachment

1. **The relationship of pressure rise time to impact velocity is given only for test configuration No. 1 which did not include air in the steam void. Please provide a comparison of the pressure rise time relationship with the data from test configuration 2 which did include air.**

Response:

The individual rise times for the Configuration 2a and 2b tests have been calculated. This data is provided in Figure 10-8 in the referenced letter. That figure utilized calculated "cushioned" velocity for the abscissa. The ordinate is test data; the abscissa is calculated. The rise time test data has also been plotted against the "uncushioned velocity". A figure showing the rise time versus the "uncushioned" velocity is attached to this letter and is referred to as Figure 10-8a. The uncushioned velocity is a parameter that is much more accurately calculated since it is dependent only on the system hydraulics and not the dynamics of void closure. The uncushioned velocity is readily known for the plant configurations. Note that in Figure 10-8a the rise time equation generally falls on or under the Configuration 2 test results. This is conservative since using a shorter rise time produces higher differential pressures across a pipe segment, and therefore, higher loads. Configuration 2b best represents the plant configuration as it has a longer column that test 2a. Referring to Figure 10-8a, it can be seen that the Configuration 2b test results are all conservative (have longer rise times) relative to the rise time equation recommended for use.

2. **For all the air release tests, the system pressure was decreased to approximately 7.4 psia (15" Hg). We cannot determine how much of the air release was due to the depressurization and how much was due to heat addition. Would the data apply to plants that have closed containment cooling systems and don't depressurize on LOOP?**

Response:

The amount of air released due to depressurization alone, without the agitation and increased nucleation sites developed during boiling, was investigated as part of this project. Research performed by Schweitzer et. al. and Zielke et. al. was reported in the TBR, Section 6.1. Figure 6-1 shows that the amount of dissolved gas released due to depressurization alone reaches a maximum value of approximately 0.031 gm/m^3 during the 30 second transient. The testing performed in the development of the data used to create Figure 6-1 was based on an agitated sample of water that was super-saturated with gas. The agitation was caused either by flow of the water through a pipe or through simple shaking. No boiling occurred in these tests.

Tests performed as part of the TBR development showed that water in the tubes, when exposed to boiling, would release approximately 50% of their dissolved non-condensable gas. Solubility curves were presented (revised TBR sections, Figure 6-7) that show the concentration of dissolved gas in saturated water to be approximately 20 mg/L or 20 gm/m^3. If 50% of the gas is released, the non-condensable gas mass is 10 gm/m^3.

Attachment

Therefore, the effect of pressure alone is approximately 0.3% of the mass released by boiling.

Since pressure alone accounts for little gas release, the effect of applying the data to closed cooling water systems where boiling occurs is expected to be insignificant.

3. **The header air content was determined to be reduced by at least 25%. How much of the air reduction was from de-aerating of the original header water and how much of the reduction was from mixing with the water from the test section that was discharged into the header?**

<u>**Response:**</u>

The water that was selected to be a conservative representative was water that was in the moisture separator region of the test. This water was carried with steam that was being expelled from the tube out of the header region into the moisture separator region. This water had the least amount of air released and had the least amount of mixing in the header. Very little of the air that was released was due to mixing with water from the tube that could have occurred in the header region.

4. **EPRI provided a theoretical argument that pressure in a gas volume between closing water columns is independent of pipe area and the heat transfer coefficient is not a function of pipe diameter. The argument appears correct provided the void shape remains cylindrical so that the heat transfer area does not change shape with piping diameter. Would the heat transfer area change shape for pipe sizes larger than the 2 inch size in the CCWH tests?**

<u>**Response:**</u>

Several potential physical phenomena could account for a change in surface area, but they can be shown to not occur or they are not credible reasons for making the test data unconservative.

First, the flow area could be postulated to slope away from its assumed planar shape. Calculations show that the "keep-full" velocity for piping is related to the Froude number (TBR Equation 7-1). For pipes up to 18" diameter, the keep-full velocity is between 4 and 7 ft/sec. Since the refill velocity to close a void will be greater than this, the pipe will not fill in a stratified manner, and the shape will remain nearly planar as assumed.

Second, the surface roughness of the exposed water in the closing column could be postulated to increase and thereby increase the surface area. Surface roughness is related by Taylor instability as primarily a function of acceleration (or deceleration), and not of pipe diameter (see TBR section 8.3.3). The tests performed as a part of the TBR preparation were run for closure velocities ranging from 10 to 45 ft/sec. The actual closure velocities in the plant are on the order of 15 to 20 ft/second. The higher tested

Attachment

closure velocity would lead to increased deceleration and increased surface roughness compared to the plant. Therefore, the water surface area available for condensation of steam would be larger in the tests than in the plant configuration, relative to the pipe diameter. As described in the TBR, the water surface area change per unit flow area due to surface roughness is pipe diameter independent. Because of the larger relative water surface area in the tests, the steam condensation rate in the plant configuration will be *lower* than those derived from the tests. This would provide more cushioning in the plant than measured in the tests.

5. **CIWH tests were performed at low pressures, less than 15 psig. The TBR states that the report's conclusions should not be utilized above 15 psig. The UM states that the results can be utilized up to 20 psig. What will be the basis for approving analyses for plants where CIWH might occur above 15 psig?**

Response:

The mechanism of the occurrence of condensation induced waterhammer (CIWH) was investigated in detail following the receipt of the test data. No mechanism exists that would result in a change of the behavior of the CIWH in a system that has a pressure that is five psia higher than that tested. The TBR concluded that the CIWH event would not impact the integrity of the system. This conclusion is not different for a modest increase in the system pressure from 15 to 20 psig.

6. **EPRI stated that the comparison of analyzed vs. test data loads was based on a structural damping value of 0.1%. A better comparison would be for typically assumed damping values (2-3%).**

Response:

The calculated responses shown in the predicted to measured support load comparisons provided in TBR Figures 13-7 and 13-8 were made from the results of a structural model with 0.1% damping. The analytical model was loaded by trapezoidal idealizations of the pressure pulses. These calculated loads were compared to actual support load data from the tests.

To determine the effect of increasing the damping to 2%, a single degree of freedom (SDOF) model was made for each pipe segment in the test, using measured geometry and structural frequencies. This is an appropriate model as there was very little participation between the legs of the test model. These SDOF models were loaded with forces of equivalent rise time and duration as developed by the tests and previously used. The resulting dynamic load factors decreased 1.9% to 7.7% with the increased damping. The magnitude of the change depended upon the pulse duration, specific pipe leg being loaded, and stiffness of that pipe leg. Translating these results to Figures 13-7 and 13-8, it can be seen that lowering the predicted forces 1.9% to 7.7% would not significantly impact the comparison between the measured and calculated forces. The conclusion that

Attachment

the trapezoidal representation of the pulse is an appropriate modeling method would not change.

7. **The air release experiment was performed at a pressure of approximately ½ atmosphere.**

   a. **What would be the expected amount of air released for other (especially increased) initial pressure conditions?**
   b. **For the actual plant situation, wouldn't pressure be expected to actually increase and not remain at ½ atmosphere? What effect would this have on the amount of air that is released?**

   Response:

   The pressure change had very little to do with the amount of air released as this is a secondary effect in comparison to boiling (see response to question 2). If boiling does not occur but a pressure reduction did occur, no credit would be taken for air release. The pressure in the test was selected to assure that there was very little residual air in the test fixture prior to the initiation of the test and so that boiling would occur quickly following the initiation of the test. Typically, open loop plants will have pressures that are initially lower than ½ atmosphere and then the pressures will increase to a pressure that is on the order of 1 atmosphere at the time that the pumps are restarted. Closed loop plants will typically have a higher initial pressure (around atmospheric) and the pressure will increase during the event. The test configuration is approximately in the middle of the ranges of pressure expected. Given the small impact of pressure on air release, the amount of air would be independent of the precise pressures reached in the plants.

9. **If the fan coolers are at a low point and the water in the supply and return headers maintain enough pressure on the water in the fan cooler tubes, boiling will not occur and no credit is allowed for air release. Now suppose that the height of water in the supply and return headers is slightly reduced to the point where nucleate boiling occurs in the fan cooler tubes. How much air would be released? Continuing with this thought, as the height of water is gradually decreased, what amount of air would be released for the various boiling intensities that are experienced?**

   Response:

   Credit for air will not be taken unless the water is exposed to temperatures above the boiling point corresponding to the pressure. All the water does not boil, but it has to be exposed to boiling that occurs in the region for the air to be removed. In order to assure that the water is exposed to boiling, a condition will be added to the TBR and the User's Manual that will eliminate credit for air release unless the temperature of the tubes reaches a temperature that is 10°F above the temperature at which boiling would occur. This will assure that the water in the tubes is exposed to boiling and that air release due to "air stripping due to boiling" will occur.

Attachment

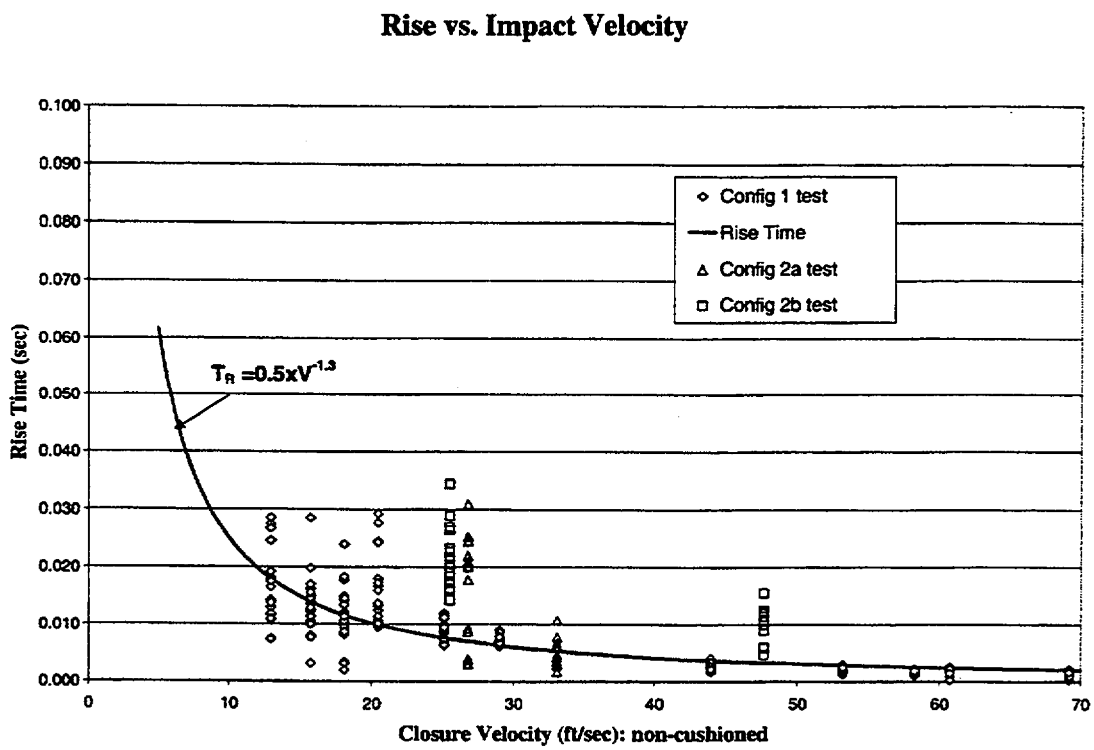

Figure 10-8a: Rise Time vs. Non-cushioned Impact Velocity

ELECTRIFY THE WORLD

EPRI

February 1, 2002

Document Control Desk
U.S. Nuclear Regulatory Commission
11555 Rockville Pike
Rockville, MD 20852

Attention: Mr. Jim Tatum

SUBJECT: Response to ACRS Comments (letter dated 10/23/01) on the EPRI Report on Resolution of NRC GL96-06 Waterhammer Issues

Dear Mr. Tatum:

EPRI has reviewed the input from the ACRS Thermal Hydraulics Subcommittee and Full Committee relative to Generic Letter 96-06 waterhammer issues as provided in the subject letter. We would like to provide some additional information on the specific issues that are raised in the ACRS letter, and we would also like to provide, as suggested in the letter, a perspective on the risk associated with the use of the methods recommended by the EPRI reports.

ACRS Comments

Many of the ACRS comments address the complexity associated with plant-specific evaluation of heat transfer in the fan coolers and the hydraulics of the voiding and draining process. The application of the EPRI work to plant-specific scenarios and configurations depends upon the plant-specific definition and subsequent evaluation of the plant-specific scenarios and configurations. Although the plants are generally similar in the design and performance of these systems, the plant specific differences require that individual, plant specific analyses be performed to evaluate the behavior of the fan cooler, the draining characteristics, and several other system related parameters. These specific plant calculations must be performed and reviewed on a plant-by-plant basis. The scope of the EPRI Technical Basis Report (TBR) was to provide methodology for evaluation of waterhammer loads at the time of final refill and column closure following pump restart.

The EPRI User's Manual (UM) provided plant specific analysis steps in Figure 2-1 and describes the application in Section 2.2. The following text that was extracted from the User's Manual describes the requirement for plant specific evaluation for heat transfer in the fan cooler, system voiding, and system refill.

Model System Hydraulics: The flow, pressure, and potential paths for water to move and voids to form in the service water system should be determined for the duration of the transient. This will specifically include the time from the loss of power to the time of closure of the void. The system hydraulic model should include the following sub-tasks.

a) **Determine Fan Cooler Unit Performance:** The heat transfer across the coolers and the contribution this heat makes to the generation of steam voids should be determined. This effort should be performed on an individual plant basis – specific guidance is not provided in this User's Manual.

b) **Determine System Voiding:** Using the FCU heat input, piping elevation and system resistances, the system pressure and voiding should be determined. This effort should be performed on an individual plant basis – specific guidance is not provided in this User's Manual.

c) **Determine System Refill**: The flow rates and velocities of the refilling water should be determined from the pump curves and system hydraulic model. Determine anticipated location(s) of closure. This effort should be performed on an individual plant basis – specific guidance is not provided in this User's Manual.

On some issues, such as consideration of single active failure, guidance was provided in the User's Manual to assist in the development of a plant specific analysis.

Once the specific plant analysis was complete, the EPRI User's Manual and Technical Basis Report (TBR) would then be used to provide methodology for the determination of waterhammer loads at the time of final refill and column closure following pump restart. Limitations of application of the EPRI methodology to a specific plant were also provided. In Section 5.3.2 of the User's Manual, for example, limitations on column length, void length, water velocity, gas content, and void and interface temperature were provided. If these limits are not met by the results of the specific plant analysis, the results presented in the EPRI User's Manual are not applicable.

This is a complex problem that requires the analysis of system hydraulics, fan cooler boiling, void formation, and steam and gas behavior within the system. The EPRI project does not provide this analysis for the plants nor does it recommend methods to perform this analysis. These issues are the responsibility of the plant analysts.

The User's Manual provides guidance for the calculation of waterhammer characteristics after the pumps restart and final closure of the columns occurs. This is where cushioning for steam and other non-condensables in the void is calculated. The User's Manual also provides a basis for determining some of the final closure input (such as the amount of gas release) and methods for applying these dynamic pressures to a piping system to calculate loads in the pipe supports and stresses in the piping.

Risk Consideration

Given that we have not come to a conclusion with the ACRS on the conservatism of the technical approach presented in the User's Manual and the Technical Basis Report, a consideration of the risk associated with the events and the results that will be achieved if the report methods are used may be important. If the methods proposed in the EPRI Reports do not significantly increase the risk of unacceptable plant performance nor lead to an unacceptable risk to the plant, it is proposed that the methods of the EPRI report may be safely implemented without compromising the integrity or safety of the piping for plant application.

In order to assess the risk to the plant of application of the EPRI method, a review of the "progression" of events that could lead to an unacceptable condition should be performed. For the purposes of this evaluation, the "unacceptable condition" following a LOOP/LOCA event will be defined as a breach of the service water system pressure boundary. The events are as follows:

1. **Occurrence of a LOCA or MSLB** – The probabilities of occurrence of LOCA and MSLB events are provided in NUREG/CR-5750. From that document, the mean frequency of occurrence of a large LOCA is $5 \cdot 10^{-6}$/year, a medium LOCA is $4 \cdot 10^{-5}$/year, and a MSLB is $1 \cdot 10^{-3}$/year. The LOCA probabilities are represented in NUREG/CR-5750 as "reasonable but conservative" estimates of the frequency of occurrence.

2. **Occurrence of a LOOP following a LOCA or MSLB** – Studies provided in NUREG/CR-6538 and subsequent NRC work indicate that the dependent probability of a Loss of Offsite Power event following a LOCA event is approximately $1.4 \cdot 10^{-2}$/demand.

3. **Occurrence of a Simultaneous LOCA/LOOP Event** – The required design basis consideration is for the simultaneous occurrence of a LOCA or MSLB and a LOOP. The frequency of the combined event depends upon the probability of the LOCA and the MSLB and the dependent probability of the LOOP given that the LOCA has occurred. Using the values defined in each of the NUREGs referenced above gives a probability of the combined event on the order of $1.5 \cdot 10^{-5}$/year. For our purposes here, the value of probability of the design basis event (LOCA or MSLB occurring simultaneously with a LOOP) will be taken as 10^{-5}/year. With best estimate probabilities, this event likelihood of occurrence could be expected to be even lower.

4. **Void Formation** - If we have a LOCA/LOOP event, a void will form in an open loop plant with certainty. In a closed loop plant, void formation will depend on the specific plant characteristics and a void may or may not form. If a void does not form, a waterhammer will not occur.

5. **Pump Restart** – The pumps will restart with certainty and the velocity of the fluid in the pipe, immediately prior to closing the void, will be defined by the pressure in the void, the piping geometry, and the pump characteristics. This uncushioned closure velocity can be

reliably calculated. This velocity will not be higher than the rate at which the pumps, once restarted, can pump water. The calculation of the water velocity prior to closure is a plant specific analysis that can be conservatively performed.

6. **Column Closure** - The water columns will refill the void and the velocity at closure cannot be larger than the largest calculated differential velocity for the upstream and downstream water columns.

7. **Maximum Waterhammer Pressure** - An upper bound on the water hammer pressure can be calculated by the Joukowski relationship with the uncushioned closure velocity that corresponds to the pipe in which the closure will occur. The waterhammer pressure cannot be larger. With a probability of one, the waterhammer pressure will be equal to or less than the Joukowski pressure. The actual waterhammer pressure that will occur is stochastic and will have a wide variation. This variation is due to variations in the void distribution in the system immediately prior to final closure. This variation appears in all the integral system level experiments. The variation in the test data has been reviewed and, in the velocity range of interest, it varies from 50% to 100% of the maximum (for example, in the Configuration 2a tests, at a velocity of approximately 25 feet per second, the maximum pressure measured from the test was approximately 400 psig, the minimum pressure was approximately 200 psig, the Joukowski pressure for this velocity of closure is 775 psig -- see Figure 10-9 in the TBR). The variation in the test data that has been seen as part of the EPRI project is typical of many other waterhammer tests that have been previously performed and it indicates that it is unlikely that the Joukowski pressure will be attained given the scatter in the results of measured waterhammers compared to those predicted. It is assumed in the EPRI reports that the largest (Joukowski) pressure is attained for the calculated cushioned velocity, although it is very likely that the pressure less than the maximum seen in a test will be experienced.

8. **Cushioned Waterhammer** - With the cushioning that is predicted to occur due to gas and steam, the cushioned velocity will be on the order of approximately 30% to 40% lower than the maximum velocity (see User's Manual appendix – this depends on many parameters, including the amount of gas and steam). For closed loop plants, this value may be only 10-15%. The waterhammer that is predicted, then, will be on the order of 30% to 40% less than the pressure calculated by Joukowski, as the relationship between pressure and velocity is linear. If the cushioning did not occur, the waterhammer pressure and the stresses in the piping would be equivalent to the uncushioned waterhammer that would not have the 30% to 40% adjustment. There are two ways to consider the impact of this potentially higher stress:

   - The first is to consider actual plant performance. The occurrence of the waterhammer following a LOOP event – either simulated in a test or real – is known to have occurred many times in the industry. The waterhammer following a LOOP-only event is not cushioned by gas and steam in the void. The total number of occurrences of LOOP-only events are estimated to be on the order of at least several hundred, based on a review of the available plant data. These occurrences have all been in open loop plants and are more severe than a waterhammer that would occur following a LOOP/LOCA event.

Without any cushioning, the LOOP waterhammer is more severe than that following a LOOP/LOCA. No piping failures have occurred in any of these events. This would indicate that the probability of failure for a more severe waterhammer (an uncushioned waterhammer) is of the order of 10^{-2} or lower.

- The other method is to take the ASME Code limits and to calculate the probability of failure if the code limits were to be exceeded by approximately 40%. For the purpose of this evaluation, it will be assumed that the piping system is designed so that all the ASME code stresses in the piping were at the faulted condition limit when the cushioned waterhammer occurred – that is, the EPRI methodology is used and that the pipe was designed up to the code acceptable limit for that load. To determine probability of failure, an assumed stress distribution is used around a stress that is 40% larger than the faulted allowable ($2.4S_h$) and compared to the actual tested material strengths for A106-Gr B piping. Based on the actual margins available in the ASME code (see NUREG/CR-2137), the probability of the stress exceeding the strength can be shown to be on the order of 10^{-4} or less.

For the purpose of continuing the "event progression", a probability of failure in the pipe if the cushioned waterhammer were exceeded will be taken to be on the order of 10^{-2}. It is probably much less likely.

9. **Likelihood of an Unacceptable Event** - Given the low probability (10^{-5}/year) of the initiating events and the low probability (10^{-2}) of piping failure, the use of the methodology in the User's Manual and the Technical Basis Report will lead to a likelihood of an unacceptable event that is on the order of 10^{-7}. Again, for the purposes of this evaluation, the "unacceptable event" following a LOOP/LOCA event is taken as a breach of the service water system pressure boundary. The probability of 10^{-7} for this event is below the threshold for significant risk to the plant. Use of the methods in the User's Manual, therefore, will not compromise the safety of the plant for the systems within the bound provided in the User's Manual and Technical Basis Report. The methodology should be accepted as recommended in the report.

The most important consideration in the behavior of the waterhammer following pump restart is that there is an upper bound on the waterhammer pressure that can be attained -- the waterhammer without cushioning -- and that the waterhammer without cushioning has occurred many times in simulated LOOP events. The methods proposed in the EPRI TBR use the physics of gas compression to calculate a reduced closure velocity and waterhammer magnitude. The change in risk introduced by the use of these methods is not significant and the methods do not lead to an unacceptable plant risk following a LOOP/LOCA event. Hence, from the Risk-informed perspective, the methods proposed in the submitted EPRI TBR and UM are adequate for plant-specific application for resolution of the Generic Letter 96-06 issues.

The methods provided in NUREG 5220 were considered acceptable for conservatively analyzing waterhammer events. The NUREG uses the Joukowski relationship with the uncushioned velocity. NUREG-5220 acknowledges that the calculated results using their methods could be 2-10 times higher than reality. All seem to agree that if a void forms following a LOOP/LOCA event, it will have non-condensable gas and some steam in it, and that some cushioning will occur. The emphasis of the work that was performed by EPRI is to define the amount of cushioning that would be expected. The cushioning calculated will provide, in general, between zero and approximately 40% velocity reduction and subsequent pressure reduction. The risk discussion of this letter shows that given the low probability of the events, the limited energy available from this event, and the low probability of pipe failure, that the methodology proposed in the User's Manual is reasonable for those cases that fit within the parameters of the User's Manual and Technical Basis Report.

We hope the information provided herein is helpful. If you have any questions on the enclosed information or the general subject it addresses, please call me at 919-546-7959 or Avtar Singh at 650-855-2384.

Sincerely,

Avtar Singh for

Vaughn Wagoner
Carolina Power & Light Company
Chairman, EPRI Waterhammer Project Utility Advisory Group

Target:
Nuclear Power

About EPRI

EPRI creates science and technology solutions for the global energy and energy services industry. U.S. electric utilities established the Electric Power Research Institute in 1973 as a nonprofit research consortium for the benefit of utility members, their customers, and society. Now known simply as EPRI, the company provides a wide range of innovative products and services to more than 1000 energy-related organizations in 40 countries. EPRI's multidisciplinary team of scientists and engineers draws on a worldwide network of technical and business expertise to help solve today's toughest energy and environmental problems.

EPRI. Electrify the World

1003097

EPRI • 3412 Hillview Avenue, Palo Alto, California 94304 • PO Box 10412, Palo Alto, California 94303 • USA
800.313.3774 • 650.855.2121 • askepri@epri.com • www.epri.com